Fabrication of diamond nanostructures and investigation of the imbedded NV centers

Dissertation

zur Erlangung des akademischen Grades eines Doktors der Naturwissenschaften (Dr. rer. nat.)

vorgelegt im Fachbereich 10 - Mathematik & Naturwissenschaften der Universität Kassel

vorgelegt von: Emil Petkov

Tag der Disputation: 11 Dezember 2014

Gutachter: Priv.- Doz. Dr. Cyril Popov

Prof. Dr. Egbert Oesterschulze

Prüfer: Prof. Dr. Arno Ehresmann

Prof. Dr. Martin Garcia

Kassel, 2014

INA Institute of Nanostructure Technologies and Analytics

UNIKASSEL VERSITÄT

CONTENTS

SUMMARY

Diamond is a material with many exceptional properties making it a promising candidate for applications in diverse fields of science and technology. In the last decade diamond has emerged as a unique platform for novel applications, e.g. in quantum information technology (QIT) or in magnetometry on a nanoscale, using one of the most common luminescent defects in its lattice, namely the nitrogen–vacancy (NV) color centers which emit in the visible range with an absolute photostability at room temperature. The creation of NV center in diamond can be accomplished by ion implantation followed by annealing to enhance migration of the vacancies towards the substitutional N atoms in the diamond lattice. In order to exploit the outstanding properties of the NV centers by increasing both the photon emission yield and the collection efficiency of the emitted photons, the NV centers should be embedded in an optical cavity, e.g. in all-diamond devices like nanopillars, photonic crystals, microrings, etc.

In the present work we have investigated NV centers in diamond nanocrystallites and nanopillars, formed during the growth process. Single nanocrystallites and nanocrystalline diamond (NCD) films, from which the nanopillars were etched, were grown by hot filament chemical vapor deposition (HFCVD). For comparison, also ultrananocrystalline diamond (UNCD) films were prepared by microwave plasma assisted chemical vapor deposition (MWCVD). The resulting films have been thoroughly characterized concerning their morphology and structure by scanning electron microscopy (SEM), and concerning their crystalline properties by X-ray diffraction (XRD). The composition was analyzed by X-ray photoelectron spectroscopy (XPS), whereas XPS and Raman spectroscopy were applied to get information on the bonding structure of the films. The influence of the substrate temperature on the properties of the NCD and UNCD films was investigated to address the possibility for integration of diamond films with temperature-sensitive materials, like III-V semiconductors, low-melting metals, polymers, etc. The comparative investigation revealed that if diamond films are to be deposited at rather low temperatures (below 600–700 °C), UNCD is a superior choice as compared to

NCD films as their properties do not degrade to the same extent as that of NCD films. For the deposition of high-quality NCD films substrate temperatures in the range of 850 – 900 °C are required.

One-dimensional diamond nanostructures (diamond nanopillars) have been fabricated using NCD and UNCD films as a starting material, and electron beam lithography (EBL) and reactive ion etching in an inductively coupled O_2 plasma (ICP-RIE) as processing techniques. In a first step, the etch rates have been determined as a function of four major plasma parameters, namely the ICP power, the RF power applied to the substrate holder, the pressure, and the oxygen flow rate. These parameters have been varied in wide ranges. In order to get insight into the mechanisms of the etching process, etching experiments have been performed with unpatterned NCD and UNCD films by varying the process times using rather short intervals. The differences observed are due to the different natures of the diamond films: the NCD films are composed of diamond nanocrystallites of up to several hundreds nanometers growing from the substrate surface, while the UNCD films consist of diamond crystallites with a size up to 10 nm embedded in an amorphous phase. Finally, EBL has been applied prior to the etching with gold as a hard mask to obtain nanopillars with diameters from 50 nm to 1 µm.

The optical characterization of the NCD and UNCD pillars by fluorescence mapping and photoluminescence spectroscopy revealed the presence of NV centers in both types of pillars. The NCD pillars contain the desired NV^- centers, while the UNCD pillars contain only NV^0 centers which can be attributed to the relatively high content of —active" surface electron traps per NV in such small crystallites. The results clearly indicate nanostructures based on NCD with embedded NV centers as perspective candidates for applications in QIT.

ZUSAMMENFASSUNG

Diamant ist ein Material mit vielen außerordentlichen Eigenschaften, die ihn zu einem äußerst vielversprechenden Kandidaten für Anwendungen in Wissenschaft und Technik machen. In den letzten Jahren wurde Diamant häufig als einzigartige Plattform für neue Anwendungen beispielsweise in der Quanteninformationstechnologie (QIT) oder in der Magnetometrie im Nanometermaßstab eingesetzt, wobei einer der wichtigsten lumineszierenden Gitterdefekte im Diamantgitter eingesetzt wird. Dabei handelt es sich um die sogenannten Stickstoff/Fehlenstellen-Farbzentren (NV-Zentren), die im sichtbaren Bereich mit einer absoluten Photostabilität bei Raumtemperatur emittieren. NV-Zentren in Diamant können durch Ionenimplantation erzeugt werden, gefolgt von einer Temperaturbehandlung, um eine Wanderung von Fehlstellen zu den substitutionellen Stickstoffatomen im Diamantgitter hervorzurufen. Um die außerordentlichen Eigenschaften der NV-Zentren ausnutzen zu können, ist eine Optimierung der Photonenemissionsausbeute und der Effizienz der Photonenerfassung erforderlich. Dazu sollten die NV-Zentren in eine optische Kavität eingebaut sein, am besten in nur aus Diamant bestehenden Strukturen wie Nanosäulen, photonischen Kristallen oder Mikroringen.

In dieser Arbeit wurden NV-Zentren in Diamantnanokristalliten und –nanosäulen untersucht, die während des Wachstumsprozesses erzeugt wurden. Einzelne Diamantnanokristallite und nanokristalline Diamantschichten (NCD), aus denen Nanosäulen geätzt wurden, wurden mithilfe der Hot Filament Chemical Vapour Deposition (HFCVD) abgeschieden. Zu Vergleichszwecken wurden auch ultrananokristalline Diamantschichten (UNCD) mittels Mikrowellen-CVD (MWCVD) hergestellt. Die Filme wurden sorgfältig mithilfe der Raster-Elektronenmikroskopie (SEM) in Bezug auf ihre Morphologie und mit Röntgenbeugung (XRD) in Bezug auf ihre kristallinen Eigenschaften untersucht. Zur Untersuchung der Zusammensetzung wurde die Röntgen-Photoelektronenspektroskopie (XPS) eingesetzt. XPS-Messungen und die Ramanspektroskopie gaben Aufschlüsse über die Bindungsstruktur der Filme. Um die Möglichkeit einer Integration dieser

Diamantschichten mit temperaturempfindlichen Materialien wie III/V-Halbleitern, Metallen mit niedrigem Schmelzpunkt oder Polymeren zu untersuchen, wurde der Einfluss der Substrattemperatur ermittelt. Eine vergleichende Untersuchung ergab, dass für eine Niedertemperaturabscheidung (unter 600–700 °C) UNCD-Filme die bessere Wahl darstellen, da ihre Qualität nicht in dem Maß abnimmt wie die von NCD-Schichten. Für die Abscheidung von qualitativ hochwertigen NCD-Schichten sind Temperaturen von 850 – 900 °C erforderlich.

Eindimensionale NCD- und UNCD-Diamantnanostrukturen wurden ,mithilfe der Elektronenstrahllithographie (EBL) und reaktivem Ionenätzen in einem induktiv gekoppelten O_2-Plasma (ICP-RIE) hergestellt. Zur Vorbereitung wurden zunächst die Ätzraten in Abhängigkeit von den vier wichtigsten Parametern ermittelt, der ICP-Leistung, der an den Substrathalter angelegte RF-Leistung, dem Druck und der Sauerstoffflussrate. Dabei wurden diese Parameter in weiten Bereichen variiert. Weitere Erkenntnisse über die Ätzmechanismen wurden durch Ätzexperiment mit unstrukturierten NCD- und UNCD-Schichten erhalten, die in sehr kurzen aufeinander folgenden Zeitintervallen durchgeführt wurden. Die dabei gefundenen Unterschiede beruhen auf den Unterschieden zwischen den beiden Arten von Filmen: NCD-Filme bestehen aus Kristalliten mit mehreren hundert Nanometer Durchmesser, deren Wachstum auf der Substratoberfläche beginnt. Im Gegensatz dazu bestehen UNCD-Schichten aus Diamant-Nanokristalliten mit Größen bis zu 10 nm, die in eine amorphe Kohlenstoffschicht eingebaut sind. Mittels der EBL konnten mithilfe von Gold-Ätzmasken Nanosäulen mit Durchmessern von 50 nm bis zu 1 µm hergestellt werden.

Eine optische Charakterisierung der NCD- und UNCD-Nanosäulen erfolgte mithilfe von Fluorenzenz-Mapping und Photomumineszenz-Spektroskopie. Diese Messungen ergaben, dass in beiden Arten von Säulen NV-Zentren vorhanden sind. Allerdings wurden nur in NCD-Säulen die gewünschten NV^--Zentren gefunden, in UNCD-Säulen hingegen nur NV^0-Zentren. Dies ist auf den realtiv hohen Gehalt an Oberflächen-Elektronentraps in derartig kleinen Strukturen zurückzuführen. Die Ergebnisse dieser Arbeit zeigen, dass NCD-Nanostrukturen mit eingebauten NV-Zentren Anwendung in der QIT finden können.

1. INTRODUCTION

Due to its outstanding properties diamond has become a very attractive candidate for different fields of application. Its unique mechanical properties, like extreme hardness, high Young modulus, scratch resistance and low friction coefficient combined with inertness to aggressive, abrasive environments determine the use of diamond as coating material used in various technologies. Examples for diamond-coated tools are drill bits, cutting tools, even precision tools like chirurgical scalpels. Due to its high wear resistance diamond is used for production of heavily wearing units like gear mechanisms, axles, etc. The mechanical properties of diamond combined with its biocompatibility make it ideal material for coating of protheses and implants. Due to its optical properties diamond is used for production of lenses, IR and X-ray windows in different optical devices. Possessing the highest thermal conductivity of all materials diamond is implemented as heat spreader in diverse high-power opto-electronic devices. The outstanding electrical properties of diamond combined with the chemical inertness, biocompatibility and low adsorption find applications for electrodes, electro-chemical detectors and bio-chemical sensors.

Diamond in the form of thin films is of benefit for applications in the electronics, tribology and optics. Thin films can be prepared by different techniques retaining the outstanding properties of bulk diamond and adding properties, like extended surface-area-to-volume ratio, ultra smooth surface, etc. The chemical vapor deposition (CVD) is the most commonly used technique to synthesize diamond films. Since more than three decades this method has been developed in order to increase the diamond growth rate and quality using different energy sources and chemical systems. The hot filament CVD (HFCVD) technique (the technique used in the current work) is used for deposition of poly-, nano- and ultrananocrystalline diamond films because of its cheapness and easiness of application.

In the last decade diamond has attracted the attention of scientists as a unique platform for quantum information technology (QIT) based on the properties of one of the most common luminescence diamond lattice defects that emit in the visible range with absolute photostability at room temperature, namely the nitrogen-vacancy (NV)

centers. In its negatively charged state (NV−) the electronic spin can be easily initialized and manipulated, e.g. with microwaves, and read out, showing long spin decoherence times T_2 reaching the millisecond range at room temperature.

The creation of NV centers in diamond can be accomplished by ion implantation either starting from nitrogen-rich native type Ib diamond implanting, e.g., gallium, carbon, or helium to generate vacancies, or from nitrogen-poor type IIa diamond implanting nitrogen ions which additionally create vacancies along their tracks. In both cases, subsequent annealing above 600 ^{0}C is required to enhance the migrations of the vacancies toward the substitutional N sites in the diamond lattice and hence the formation of NV centers. In this work another method for incorporation of NV centers in diamond is proposed. The centers are created during the diamond growth in the HFCVD chamber, relaying on the nitrogen background pressure in the chamber and the high temperature needed for the growth.

To enhance further the photon emission yield and the collection efficiency of the emitted photons, the NV centers should be coupled to optical resonators, e.g. to diamond nanopillars, photonic crystals, microrings , etc.

As with almost all nanostructures, two different strategies have been proposed in the literature to prepare diamond nanostructures: (a) top-down techniques, in which the structures are created by suitable etching techniques from pre-grown diamond films of different nature and (b) bottom-up techniques. In the case of top-down techniques, almost exclusively ion assisted plasma techniques, such as reactive ion etching (RIE) have been used. They can also be divided into two groups with respect to the chemistry employed – the first one is based on hydrogen mixtures and the second one uses O_2 (implemented in this work) and O_2-based mixtures (O_2/Ar, O_2/CF_4).

In the present work nanocrystalline diamond films (NCD) prepared by HFCVD were etched with the aim to create one-dimensional diamond nanostructures by means of RIE. Electron beam lithography was used to define the diameters of the pillars varied between 1000 and 50 nm. After establishing the etch mechanisms of the nano- and ultrananodiamond films (used for comparison), the influence of the basic etching parameters on the shape of the pillars and on their properties in view of the application in quantum information technology, the incorporation of NV centers and their optical properties was imvestigated.

2. DIAMOND

Diamond is one of the allotropic forms of carbon. In this chapter the different modifications of carbon, like graphite, fullerene and diamond will be introduced. Further the structure, different properties and possible applications, of diamond will be dismissed in details.

2.1. Crystalline modifications of carbon

Carbon is the fourth most abundant element in the universe, after hydrogen, helium and oxygen. However, the latter three elements are gasses, so carbon becomes the most abundant solid in the universe [1]. It is present in all known life forms, and in the human body carbon is the second most abundant element by mass (about 18.5%) after oxygen [2].

Carbon is the sixth element in the periodic system. The carbon atoms have $1s^2 2s^2 2p^2$ electron configuration, which allows the valence electrons to form either sp^3-, sp^2- or sp-hybridization. Because of its tendency to build chains with similar atoms, (object of the Organic Chemistry) currently there are known millions of hydrocarbons, while the different carbon modifications are subject of the Inorganic Chemistry.

The most famous carbon modifications are graphite and diamond. Their physical and chemical properties are however completely different - the diamond is the hardest known material, insulator and optically transparent, the graphite, which at normal conditions is the thermodynamically stable configuration, is soft and electrically conductive [3]. This can be ascribed to the different hybridization, bonding and structure.

The diamond is more thermodynamically stable than the graphite at temperatures higher than 1300 °C and pressures greater than 40×10^3 bar (Fig. 1).

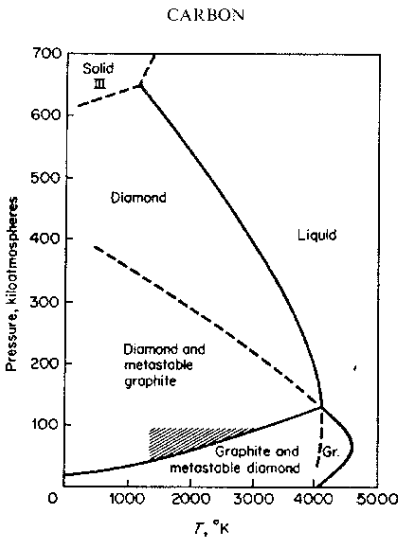

Fig. 1: Carbon phase diagram [4]

At a temperature of 298 K and a pressure of 1 atmosphere, the standard Gibbs free energy of formation of diamond differs by only 2.9 $kJ.mol^{-1}$ from that of graphite. There is no easy rearrangement mechanism by which diamond can convert into graphite. The energetic activation barrier for conversion is very high and the conversion is therefore kinetically unfavourable. Hence, diamond will remain in a meta-stable state at room temperature and pressure without converting into graphite [5].

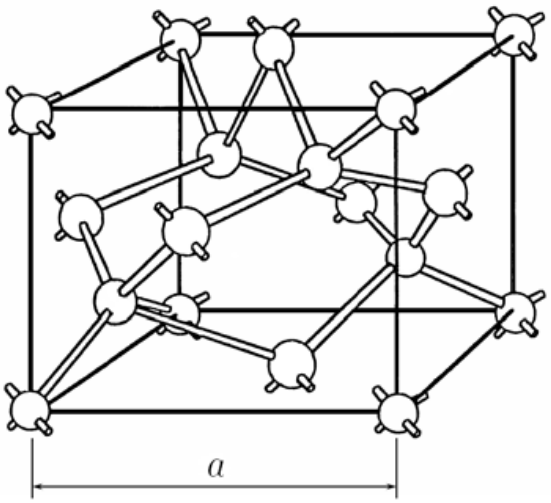

Fig. 2: Crystal structure of diamond (lattice constant a= 0.356 nm [6])

In diamond the sp^3-hybridized carbon atoms are placed in a face centered cubic lattice with a bond length of 0.154 nm and a lattice constant a = 0.356 nm. In the diamond lattice each carbon atom is bonded to other four by σ bonds set at an angle

of 109° to each other (Fig. 2). The σ bond is highly energetic and is responsible, together with the tight tetrahedral structure, for the outstanding diamond properties [6].

Due to this compact structure diamond possesses the highest atomic number density ($1.77x10^{23}$ atoms.cm^{-3}) among all substances which leads also to the extremely high density of diamond – 3.514 g.cm^{-3}.

Graphite consists of parallel sheets of sp^2 carbon atoms, each sheet containing hexagonal arrays of carbon atoms. Each atom is connected to three nearest neighbors within the sheets by three sp^2 hybridized orbitals, that separate them by a distance of 0.141 nm. The fourth valence electron of the carbon, which is not involved in the hybridization, builds distributed π bonding, which gives rise to delocalized electrons that make graphite electrically conducting. The sheets are held together by weak van der Waals forces and are separated from each other by a distance of 0.335 nm (Fig. 3a). This long distance between the sheets determines the extreme softness of the graphite.

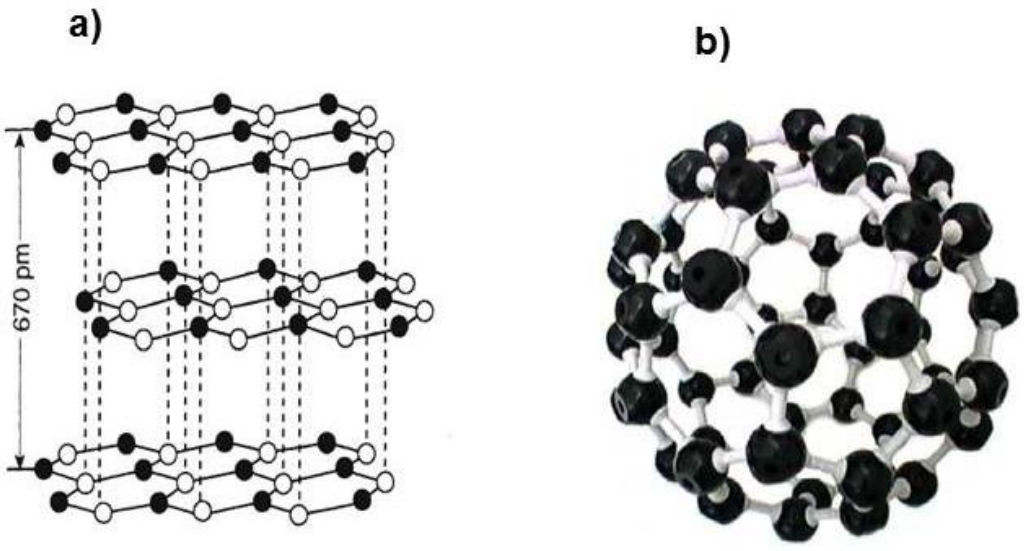

Fig. 3: Crystal structure of: a) graphite [7] and b) fullerene [8]

Another stable form of carbon are fullerenes. Discovered by Kroto et al. [6] bucky-ball fullerene is a sixty atoms molecule, containing pentagonal and hexagonal rings in which no two pentagons share an edge (Fig. 3b). The structure of C_{60} is a truncated icosahedron, which resembles an association football ball of the type made of twenty

hexagons and twelve pentagons, with a carbon atom at the vertices of each polygon and a bond along each polygon edge. The C_{60} molecule has two bond lengths. The 6:6 ring bonds (between two hexagons) can be considered "double bonds" and are shorter than the 6:5 bonds (between a hexagon and a pentagon), where the average bond length is 0.14 nm.

The van der Waals diameter of a C_{60} molecule is about 1.1 nm, the nucleus to nucleus diameter of a C_{60} molecule is about 0.71 nm.

2.2. Properties of diamond

Mechanical properties

The extraordinary mechanical properties of diamond are ascribed to its lattice structure and bonding nature. Diamond is the hardest known natural material with a hardness of 90 GPa, a high tensile strength (1.2 GPa) and a compressive strength (110 GPa) [9]. Due to this hardness diamond performs inelastic on strain till breakage. The breaking resistance of diamond is about 2500 MPa and so outclasses all other materials, like e.g. germanium (90 MPa). It possesses the highest hardness of any bulk material. The huge atomic number density and short bonding length explain the lowest compressibility ($1.7x10^{-7}$ $cm^2.kg^{-1}$) of all up to now known materials [10]. Another extreme mechanical property is the stiffness, which is expressed by the high value of Young‘s modulus (E=1050 GPa). The extreme rigidity of the diamond structure explains many of the unique properties which make it pre-eminent as a gem stone, an industrial tool and a material for solid state research. Materials with high hardness are usually brittle and in this respect diamond is no exception. A well-known, a well-orientated blow can cleave a diamond along a (111) plane with the expenditure of very low energy [11]. The dominance of (111) cleavage can be explained by either the lowest bond density in this direction, or caused by faulted growth (incorporation of impurity) which induce lower strength and energy for fracture on these planes [12].

Due to its outstanding mechanical properties diamond can find application in each field, where excellent wear resistance is needed. Combined with its chemical stability it makes diamond a perfect material for protection layer in raw chemical environment

(e.g. wall protection material for chemical reactor [13]). Further diamond is used for coating of tools (sometimes there is an interlayer between the tool surface and the diamond for better adhesion and protection from delamination). Examples for diamond-coated tools are drilling and cutting tools, like saw blades or drill bits for rock. Combining the mechanical properties of diamond with its biocompability one can use it for applications in the medical engineering - e.g. for coating of protheses and implants. There is very low erosion on the produced parts and diamond causes no defense reaction of the surrounding tissue [14].

Thermal properties

Due to its atomic number density diamond possesses the highest heat capacity c_v of all solid state materials by temperatures above the Debye temperature. However, because of the high value of Debye temperature (1860 K), diamond has very low molar heat capacity at room temperature – 6.185 $J.mol^{-1}K^{-1}$[15].

Diamond has the highest heat conductivity and its maximal value is 175 $W.cm^{-1}.K^{-1}$ at 65 K. Even at room temperature its thermal conductivity is roughly four times superior to that of copper, which is supposed to be a very good heat conductor. In contrast to metals where the heat conductivity is a result of motion of free electrons, in non-metals like diamond the phonons are „responsible" for the heat transfer. Diamond with its very strong and tight lattice and possessing the highest photon velocity (17000 $m.s^{-1}$) [16] of all solid materials, is an excellent material for heat transfer via phonons, which lead to extreme high heat conductivity. Naturally the heat conductivity of polycrystalline diamond decreased in comparison with that of monocrystalline diamond, because the heat resistance at the grain boundaries is determined by phonon scattering processes, but even in this case the reported value of 20 $W.cm^{-1}.K^{-1}$ is amazing [17].

The thermal expansion coefficient of diamond is relatively low 1×10^{-6} K^{-1}, which combined with its mechanical hardness can be used for fabrication of X-ray lithography masks [3]. Diamond is also a suitable material for thermal management applications. The use of diamond as a heat sink for integrated circuits has the potential to allow closer packing of components and lower operating temperatures.

Diamond is currently used as a heat sink for specific applications, such as power transistors, semiconductor laser diodes, microwave diodes and small microwave integrated circuits [18,19].

Electronic properties

When it is free of any defects and dopants, diamond is a very good insulator. Its huge band gap (E_g= 5.45 eV) does not allow the creation of charge carriers via thermal excitation; even at a temperature of 700 K the band gap is still around 5.35 eV.

The band structure of diamond, as shown in Fig.4, was calculated for the very first time by J. Chelikowsky and S. Louie [20]. The maximum of the valence band is by $\vec{k}$=0 at Γ-point, but the minimum of the conduction band does not stand direct above it. It means that diamond is an indirect semiconductor with a large band gap. This leads to the very poor conductivity of diamond, because the value for thermal energy at room temperature E=kT~0.025 eV makes the probability of thermal excitation negligible.

The huge band gap of diamond determines also the low intrinsic carrier concentration (10^{-27} cm^{-3}); only at temperatures above 1000 °C this value will become significant due to its temperature dependence. The high specific resistance of 10^{16} Ω.cm is similarly explained by the band gap. It can be notably decreased by doping the diamond and providing in this way presence of impurity atoms for enhancement of electrical conductivity. The most common dopants are boron, which has an acceptor level at 0.37 eV above the valence band, and nitrogen, which has a donor level at 1.7 eV below the conduction band minimum. Another important parameter is the carrier mobility, respectively electron and hole mobility. Since they have different effective masses, they will have also different mobility: the electron mobility is 1800 $cm^2 .V^{-1}.s^{-1}$ and the hole mobility 2100 $cm^2 .V^{-1}.s^{-1}$.

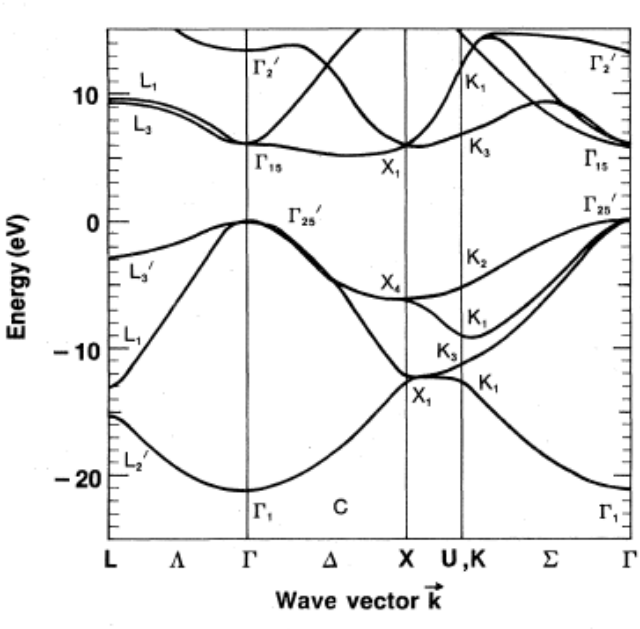

Fig. 4: Band structure of diamond [20]

The carrier mobilities of diamond are very high with only electron mobility of GaAs exceeding those values. High carrier mobility is desirable for fast-response and high-frequency electronic devices. Combined with the highest breakdown field strength and excellent thermal conductivity it makes diamond a perfect candidate for development of electronic devices with superior performance regarding power efficiency, power density, high frequency properties, power loss and cooling [21]. It can be also used for production of sensors [22], electrodes and field emission displays [23].

Optical Properties

Due to the wide band gap, diamond is transparent for the spectral range from the deep UV to far IR (from 220 nm to 100 μm) (Fig. 5). The brilliance of a diamond crystal is owing to its high refractive index. With a value of about 2.4 it is the highest of any transparent substances for visible light [24].

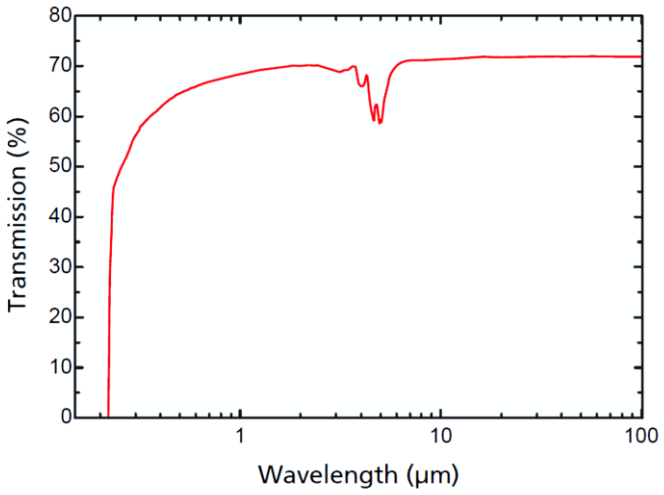

Fig. 5: Transmission spectrum of CVD diamond [24]

The absorption begins first below 220 nm, however there are different ways for enhancement of light absorbing: using the lattice oscillations, or the existence of defects. Impurities or sp^2-carbon can be used as additional levels in the band gap, so that radiation with higher wavelengths can be absorbed. The absorption in the visible spectral range causes characteristical color, depending on type of defects, e.g. yellow/green for nitrogen doped or blue for boron doped.

Because of its optical properties, diamond finds application in optical components, particularly as a free-standing plate for use as an infrared window in harsh environments. Conventional IR materials, especially in the 8–12 μm wavelength range (such as ZnS, ZnSe and Ge), suffer the disadvantage of being brittle and easily damaged. Diamond, with its high transparency, durability and resistance to thermal shock, is an ideal material for such applications [18].

Combining its optical properties with high thermal conductivity, hardness, wear resistance and chemical inertness, diamond is the material of choice for high power lasers, spacecraft and fiber optic backbones. Windows, lenses, prisms and beam-splitters made of diamond are nowadays commercially available [24].

3. COLOR CENTERS IN DIAMOND

In this chapter a short overview of the different types of defects in the diamond crystal lattice will be given. The major criteria for the classification of diamond will be introduced, followed by the description of the color centers, which exist in the diamond lattice, including a vast introduction of the most common defect – the nitrogen-vacancy (NV) color center.

3.1. Crystallographic defects

An ideal crystalline solid has a periodic structure that is based on the chemical properties of its constituent atoms. However, the real crystals are not perfect. Any distortion or violation of regularity in the crystal atomic arrangement can be considered as a crystal lattice defect - it could be an extra or missing atom in the crystal lattice or an impurity. The presence of defects in a real crystal distinguishes it from an ideal crystal lattice and some properties of a real crystal are determined by its defect structure [26]. The defects can determine the color of the crystal, its electric conductivity, and they can also introduce modifications in the lattice vibrations.

There are some different ways (and reasons) for the appearance of the defect - e.g. defects from fundamental physical laws, defects from natural minerals, defects from crystal growth or defects from strain [27]. There are several categorizations of the defects. One of the common classifications is based on the dimension of the defect structure. Defects may be classified into four groups; point defects (0D), line defects (1D), planar defects (2D), and volume defects (3D). Some examples are given in Table 2.

Table 2.Examples of defects with different dimensionality

point defects	line defects	planar defects	volume defects
Vacancies	Edge dislocations	Stacking faults	Precipitates,
Self-interstitials	Screw dislocations	Grain boundaries	Voids
Impurities	Mixed dislocations	Twin boundaries	

- ***Point defects***

The simplest types of point defects in a crystal are as follows: interstitial atoms are atoms occupying positions between the equilibrium positions of ideal lattice atoms; vacancies are lattice sites where atoms are absent; and substitutional impurities are atoms, located on a lattice site, i.e. replacing the native atom.

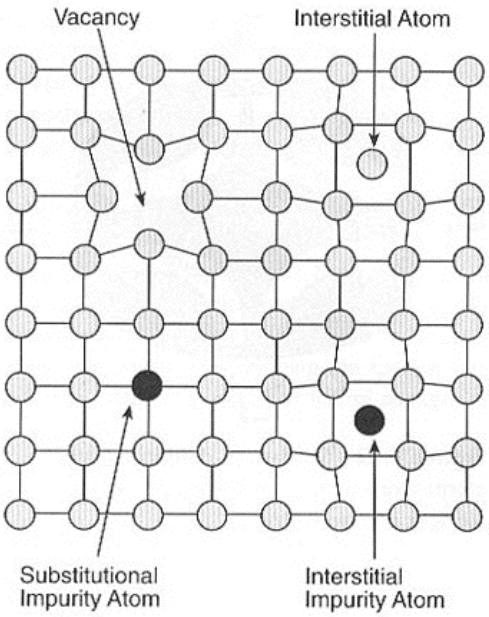

Fig. 6 Various types of point defects

There is a thermodynamical equilibrium between the crystal and the defect concentration. The number of defects is increasing with the temperature and the type is depending on the structure of the crystal, the geometry and the bonding environment. Many properties of the crystal are based on existence of defects. They enable the diffusion in the crystal and are responsible for the conductivity. The solid

states reactions are ascribed to the defects; when temperature is increased, the reaction is started due to the diffusion of the atoms. The reaction rate is significant lower than by gasses and liquids, but it is increasing with the temperature, since the defect concentration and the diffusion are rising as well [28].

- ***Line defects***

Dislocations are linear defects; they are lines through the crystal along which the crystallographic registry is lost. Their principle role in the microstructure is to control the yield strength and subsequent plastic deformation of crystalline solids at ordinary temperatures. Dislocations also participate in the growth of crystals and in the structures of interfaces between crystals [29].

They are characterized by the Burgers vector (*b*) [30] that represents the magnitude and direction of the lattice distortion in a crystal lattice. Edge dislocations (Fig. 7a) occur when an extra plane is inserted. The dislocation line is at the end of the plane. In an edge dislocation, the Burgers vector is perpendicular to the dislocation line. Screw dislocations (Fig. 7b) result when displacing planes relative to each other through shear appear. In this case, the Burgers vector is parallel to the dislocation line. If the dislocation line is neither perpendicular, nor parallel to the Burgers vector, it is called a segment of mixed type.

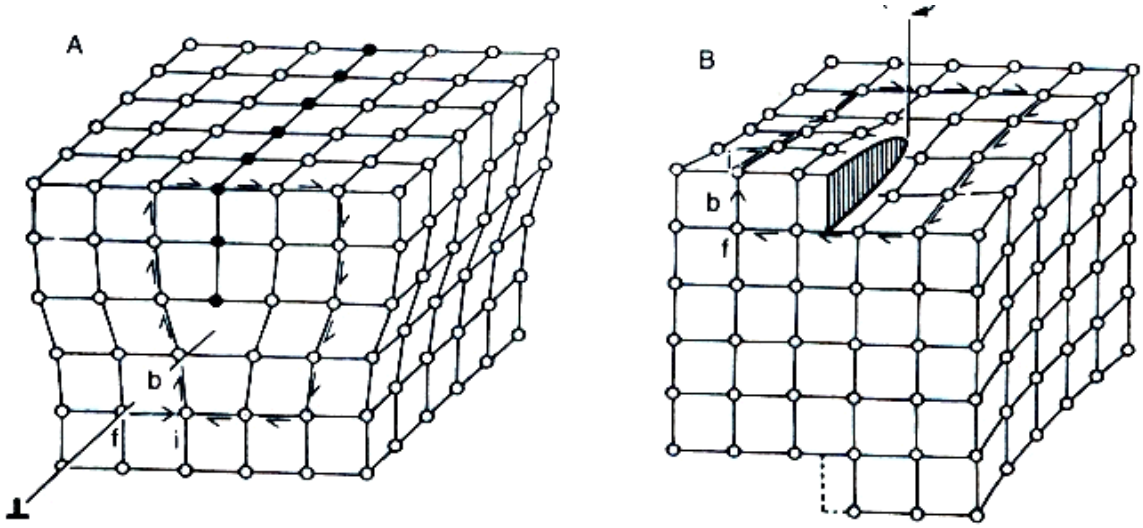

Fig. 7: Types of dislocations: a) edge, b) screw dislocation

Dislocations more commonly originate during plastic deformation, during solidification, and as a consequence of thermal stresses that result from rapid cooling. An edge dislocation arises when there is a slight mismatch in the orientation of adjacent parts of the growing crystal. A screw dislocation allows easy crystal growth because additional atoms can be added to the ‗step' ofthe screw.

- ***Planar defects***

A planar defect is a discontinuity of the perfect crystal structure across a plane; they are represented by stacking faults and grain boundaries.

Stacking fault is a change in the stacking sequence of the atom planes. It can occur in a number of crystal structures, but it is easiest to see how they occur in close packed structures.

A grain boundary (Fig. 8) is a general planar defect that separates regions of different crystalline orientation (i.e. grains) within a polycrystalline solid. The atoms in the grain boundary will not be in perfect crystalline arrangement. Grain boundaries are usually the result of uneven growth when the solid is crystallizing.

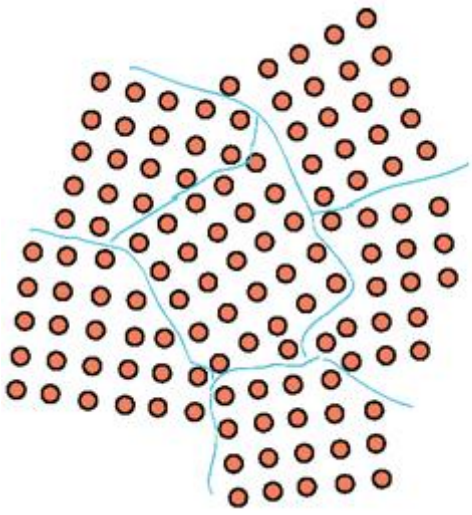

Fig. 8: Grain boundaries

- ***Volume defects***

Voids are small regions where there are no atoms, and can be thought of as clusters of vacancies. Impurities can cluster together to form small regions of a different phase. These are often called precipitates.

3.2. Classification of diamond

Pure diamond crystal is colorless and an excellent insulator. Its electrical conductivity and absorption in the visible range are ascribed to the defects in the diamond lattice. There is a huge variety of defects in diamond. They can be divided into two groups: intrinsic defects (including vacancies and interstitial atoms as well as extended structural defects such as dislocations) and impurity-related defects (foreign atoms like nitrogen or boron, or even complexes of larger atoms).

The classification of diamond, due to the presence of different impurity atoms is described in detail in [31]. Nowadays diamonds can be mainly classified into four types: Ia, IIa, Ib, and IIb [32] (see Table 3).

Type I

Type I diamonds contain nitrogen. Approximately 98% of all diamonds are of this type. We can divide type I diamonds in two groups:

Type Ia

If the nitrogen atoms are clustered together within the carbon lattice, then the diamond is said to be a type Ia diamond. Ia diamond contains the highest concentration of nitrogen (up to 3000 ppm). The most common aggregations, which are present in diamond are A-center and B-center. The A-center consists of a pair of substitutional nitrogen atoms in the nearest neighborhood, while the B-center occurs as a complex of four substitutional nitrogen atoms surrounding a lattice vacancy. Because these diamonds absorb blue light, they can have a pale yellow or brown color. 98% of natural diamonds are type Ia.

Type Ib

Ib diamond contains up to 600 ppm nitrogen and the nitrogen is dominantly in single-substitutional form. High Pressure High Temperature (HPHT) or Chemical Vapour Deposition (CVD) diamonds can be counted in this class. These diamonds absorb

green light as well as blue light, and have a darker color than type Ia diamonds. Depending on the precise concentration and spread of the nitrogen atoms, these diamonds can appear deep yellow, orange, brown or greenish. Less than 0.1% of diamonds belong to type Ib.

Type II

Type II are diamonds that contain no or very few nitrogen atoms (~ 1 ppm) or boron atoms.

Type IIa

These diamonds can be considered as the purest ones - they contain no or negligible amounts of impurities (less than a few ppm nitrogen) and are usually colorless. An imperfection appears when the carbon tetrahedrons that built up the diamond were twisted and bent out of shape while the diamond rose to the surface of the earth. An imperfect carbon lattice will make the diamond absorb some light, which will give it a yellow, brown or even pink or red color. 1-2% of diamonds belong to type IIa.

Type IIb

These diamonds contain no nitrogen – the most common impurity is boron, which absorbs red, orange and yellow light. These diamonds therefore usually appear to be blue, although they can also be grey or nearly colorless. All naturally blue diamonds belong to type IIb, which makes up 0.1% of all diamonds.

Table 3. Classification of diamond

Type	Impurity	Amount	Color
I a	Nitrogen (aggregate)	200-3000 ppm	yellow, brown
I b	Nitrogen (on atomic place)	< 600 ppm	yellow , orange, brown
II a	Nitrogen	< 1-2 ppm	yellow, brown, pink
II b	Boron		blue

3.3. Color centers in diamond

A color center is an optically active point defect in a crystal lattice and it can absorb and emit electromagnetic radiation. Due to its discrete level in the band gap of the

surrounding material, it can be described as an artificial atom, which is trapped into a transparent matrix [33]. The biggest advantage of the color centers, compared to the single atoms (or ions), which act as single photon emitting source, is their solid state environment that allows investigation at room temperature. It reduces the cost for the experimental work. In addition, the solid state matrix brings excellent photostability of the color center, compared to other single emitters, like organic molecules. The property that makes the color centers very attractive for application in the Quantum Information Technology (QIT) is the very long decoherehce time, which is a consequence of the stability of the host material.

More than 100 electronic optical centers have been detected in the absorption and/or luminescence of diamond. Half of them are believed to be impurity related. A vast majority of these centers are due to nitrogen. No other impurity exhibits in diamond such a great variety of optical centers as does nitrogen [34].

3.3.1. Nitrogen-Vacancy Color Center

The nitrogen-vacancy (NV) color center in diamond is one of the most common luminescent defects in its lattice and an important physical system for emergent quantum technologies, including quantum metrology, information processing and communications, as well as for various nanotechnologies, such as biological and subdiffraction limit imaging [35], and for tests of entanglement in quantum mechanics [36].

The nitrogen-vacancy (NV) color center consists of a substitutional nitrogen atom adjacent to a vacancy (a missing carbon atom) into the diamond lattice. Three dangling bonds are reaching into the vacancy from the remaining neighboring carbon sites. With the two unbound atoms of the nitrogen this forms a five electron system, called neutral NV center (NV°).

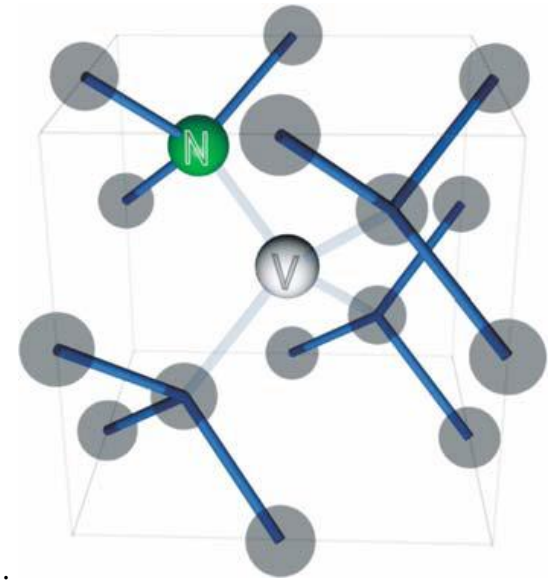

Fig. 9: Schematic representation of NV center [37]

In its negative state (NV^-), the nitrogen-vacancy defect has six electrons, adding an extra charge from the diamond lattice. The identifying features of NV^- and NV° are their optical zero phonon lines (ZPLs) at 1.945 eV (637 nm) and 2.156 eV (575 nm) [38], respectively, and associated vibrational bands that extend from their ZPLs to higher/ lower energy in absorption/emission.

The detection of single negatively charged NV^- color centers in 1997 [39] marks a critical point in the evolution of diamond based quantum technologies. It is a very promising candidate for application in the quantum information field: it possess strong optical transition with absolute photostability at room temperature [40] and shows the longest spin decoherence time in solid-state systems at room temperature (T_2 = 1.8 ms) [41]. Additionally NV centers can be easily prepared, manipulated and read out by optical pumping. The two unpaired of its six electrons build a spin triplet S = 1 in both ground ($^3A_2$) and excited ($^3E_2$) states, described with the sub-levels: m_s = 0 and ±1 with zero-field splitting of 2.88 GHz [42].

The m_s = 0 and ±1 sublevels of this ground state can be chosen to function as a qubit state, and coherent rotations between the two sublevels may be induced by applying microwave radiation tuned to the energy splitting between them [43]. The biggest advantage of NV^- center is the easiness of optical detection using differing fluorescence of the m_s = 0 and ±1 spin projections. If the color center populates m_s = 0 ground state and it is excited with green laser light (λ = 532 nm), after the

radiative decay from the excited state it shows high fluorescence intensity and lands direct to the ground state $m_s = 0$ under photon emission [44] (Fig. 10). However, the optical transition from $m_s = \pm 1$ is not spin conserving. It undergoes a non-radiative decay via a singlet state and lands on the ground state $m_s = 0$. This leads to rapid spin polarization according to recent researches [45].

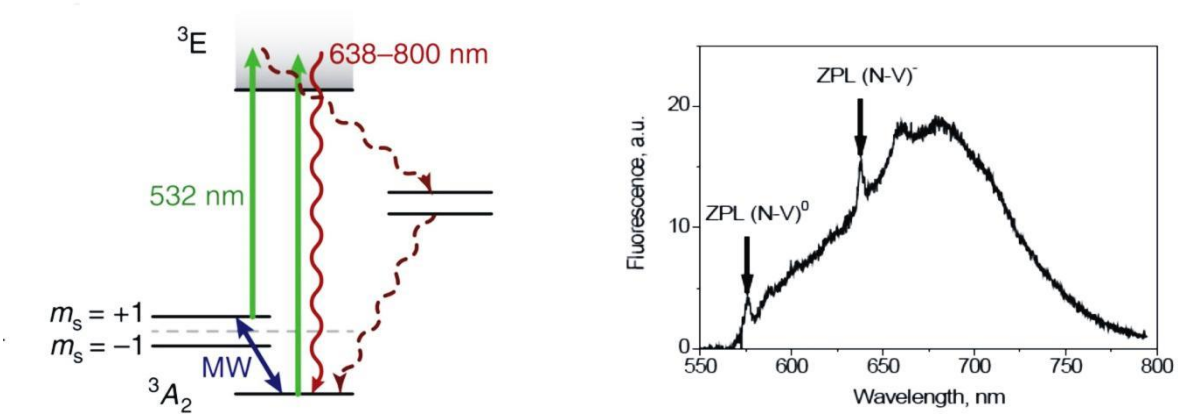

Fig. 10: Energy level scheme of nitrogen-vacancy center and photoluminescence spectrum of NV^o and NV^-

The main disadvantage of the NV center is that from the very large emission only 4% of the photons are emitted into ZPL and the remaining photons relax into the phonon sidebands.

There are several different ways for the fabrication of NV centers. Single NV centers are usually found in any natural diamond sample [46] because nitrogen is always present (as a major impurity in diamond) and over the ages vacancies migrated to some of these nitrogen atoms forming NV centers. In the artificial diamonds (HTHP- and CVD thin films) they must be created. The first possibility is ion implantation, followed by thermal annealing (to make the vacancies, created during the implantation, „move—and combine with the nitrogen atoms) [47, 48], another opportunity is to make use of electron irradiation, also followed by thermal annealing [49]. In both cases the sample is heated to temperatures over 600 °C and dwelt for several hours. The last „route—for fabrication of nitrogen-vacancy centers, used in the present work is the creation of NV centers during the diamond growth in the chemical vapor deposition (CVD) set up. This simple method makes use of the background nitrogen content in the CVD chamber for incorporation into the diamond layer. During the growth there are some inevitable growth faults, which lead to formation of

vacancies. The temperature needed for diamond growth is over 800 °C, so the requirement for vacancy migration is also fulfilled.

3.3.2. Other color centers in diamond

Like mentioned before, there are more than 100 color centers in diamond, some of them studied for use in the abovementioned application fields. Probably the most important, investigated and used defect in the diamond lattice after the NV center is the silicon-vacancy (SiV) color center. It consist of an interstitial silicon atom and a lattice vacancy arranged in a so-called „split-vacancy configuration", where a substitutional silicon atom relaxes its position towards a neighboring vacancy [50] (Fig. 11a). The SiV color center possessing a strong narrow ZPL at 1.681 eV (738 nm) (Fig. 11b) was first observed in 1981 by Vavilov et al. in cathodoluminescence (CL) investigations of CVD homoepitaxial diamond layers and polycrystalline diamond films [51].

The emission is mainly concentrated in zero-phonon lines as narrow as 0.7 nm. This is the biggest advantage of the SiV color center over the NV centers with a large phonon side-band (over 100 nm) making them very promising candidates for narrow-band, bright single-photon sources [53].

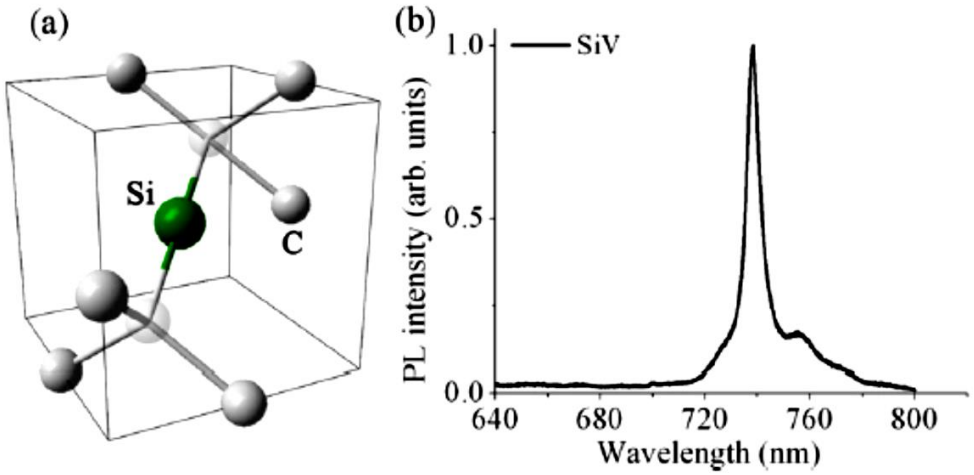

Fig. 11: a) Crystallographic model and b) room temperature PL spectrum of SiV color center in diamond [52]

A further advantage is their emission in the near infrared at 738 nm in a spectral region where the background fluorescence of the surrounding diamond material is weak.

Another extraordinary property of the SiV center is the short luminescence lifetime. It was measured to be 4 ns at 5 K and 2.7 ns at room temperature in homoepitaxial CVD diamond film and about 1 ns nearly independent of temperature in a polycrystalline CVD diamond film [54]. Single photon count rates up to 4.8 Mcps at saturation make the SiV centers the brightest diamond-based single photon sources to date [55].

Another well-known color center is the so called the nickel–nitrogen complex (NE8) center. It consists of four nitrogen atoms adjacent to a nickel atom (Fig. 12a). The NE8 center has recently attracted a lot of attention because of its spectral and temporal parameters that seem more attractive for applications in fiber optics of quantum communication systems than those of the NV^- and SiV centers [56]. Strong emission at room temperature, 2 ns short lifetime and seemingly narrow spectra emission range concentrated mainly in ZPL = 800 nm (Fig. 12b) have been considered as the advantages of the NE8 center.

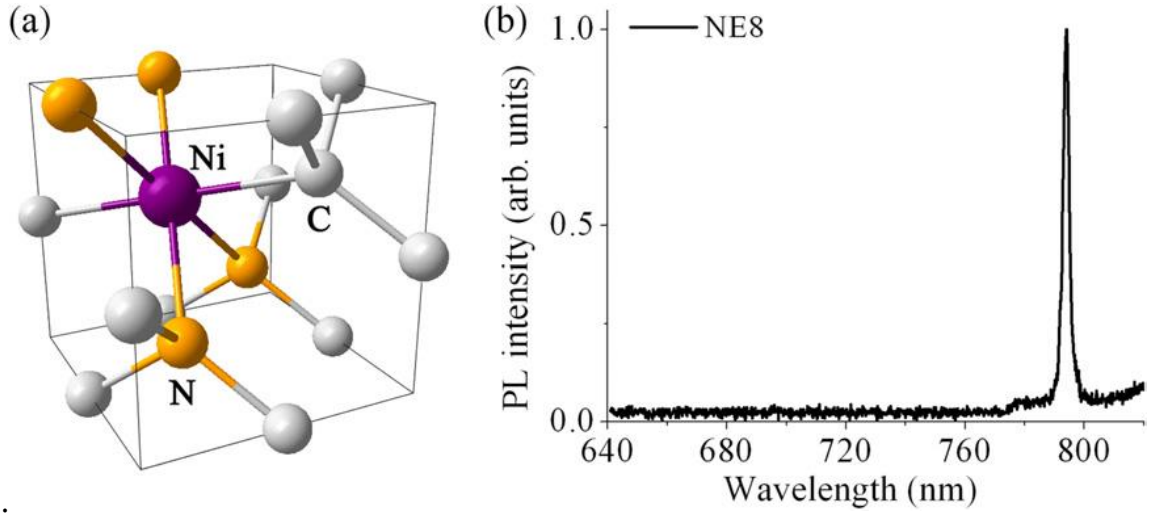

.

Fig. 12: a) Crystallographic model and b) room temperature PL spectrum of NE 8 color center [52]

4. FABRICATION OF SYNTHETIC DIAMOND

The history of the artificial diamond fabrication will be presented in this chapter. The two main methods, namely the high-pressure high-temperature (HPHT) technique and the chemical vapor deposition (CVD) method will be introduced. Further the growth mechanism of the crystalline diamond films will be explained and the classification according to their impcrystallinityand their morphology will be presented.

4.1. High-pressure high-temperature (HPHT) technique

The knowledge of the conditions under which natural diamond is formed deep underground suggested that diamond could be synthesized by heating carbon under extreme pressure. There are several high-pressure based technologies for diamond fabrication, that were developed at the beginning of the last century, but the first reported artificial diamonds are created by the Swedish firm ASEA (Allemana Svenska Elektrika Aktiebolaget) in 1953. The first diamond was produced from a mixture of cementite (Fe_3C) and graphite, using tantalum as a catalyst, by a working pressure between 8 and 9 GPa and a temperature over 2000 °C [57]. Almost two years later General Electrics in the United States produced successfully synthetic diamond. In this process, a mixture of graphite and troilite (FeS) was compressed in a hydraulic press to 5 GPa, heated to over 1600 °C in the presence of a suitable metal catalyst, and left until diamond crystallized [58].

Generally speaking the production of HPHT diamond is based on graphite as „carbon deliverer—and different metals (Ni, Co, Fe), which are used as catalyst to achieve higher growth rates. Graphite and metal plates are stacked in the reaction chamber and at high pressure and high temperature the diamond crystallite begins to grow from the graphite-metal melt. The HPHT growth process offers a significant degree of control over the quality and geometry of diamond obtained. Diamonds produced by this method are used for production of drill bits, cutting and polishing tools, and also for polishing pastes [59].

4.2. Chemical vapor deposition (CVD) method

In addition to the physical method for producing diamond in the region where it is the thermodynamically stable form of carbon (Fig. 13), there is also a chemical method for fabrication of diamond in the region, where it is meta-stable.

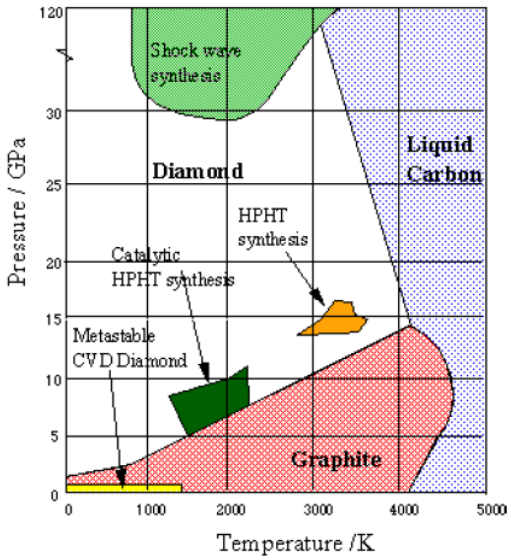

Fig. 13: Phase diagram of carbon with P- and T-regions for different diamond synthesis techniques [60]

Simultaneously to the HPHT method (in the early fifties) the low pressure technique (called CVD) started to attract interest. First in the former USSR Deryagin proposed the growth of diamond at low pressure through thermal decomposition of carbon tetraiodide [61]. Diamonds were synthesized using CBr_4 or CI_4 at temperatures ranging from 800 to 1000 °C and pressures of approximately $4x10^{-4}$ Pa. The first successful documented attempt to grow diamond at low pressures was made by William G. Eversole of the Union Carbide Corporation (USA) in 1952. But this new method had a major disadvantage of much lower growth rates (compared to the HPHT technique) since graphite was co-deposited with diamond leading to impure mixed phases [18]. This problem was solved in the early 70s by introducing atomic hydrogen into the reaction chamber. As established by Angus et al. [62], the atomic hydrogen etches preferentially the graphite phase rather than the diamond. This leads to higher growth rates and allows the nucleation of new diamond crystallites on

non-diamond substrates. The next significant step in the development of CVD diamond took place in Japan. A team led by Nobuo Setaka at the National Institute for Research in Inorganic Materials (NIRIM), Tsukuba, developed methods for the rapid growth of diamond at low pressures. They reported a deposition of diamond films on various substrates at 850 °C and pressure in the range of $4x10^3$ and $5x10^3$ Pa using different CVD techniques (hot filament, radio frequency, microwave plasma CVD) [63].

Basically all types of CVD techniques consist of activation of the gas mixture of hydrocarbons and hydrogen for creation of carbon-containing reactive radicals and atomic hydrogen. The latter is used to suppress the growth of sp^2-bonded carbon and to make possible the growth of diamond crystallites outside of the region, where diamond is thermodynamically stable [15]. Being in the region where diamond is metastable compared to graphite implies that the synthesis of diamond under CVD conditions is driven by the kinetics and not by the thermodynamics [64]. The main difference between all CVD techniques is the way that the gas mixtures are activated. Nowadays well-established methods are the Hot Filament CVD (HFCVD) [65], where tungsten or tantalum filaments are electrically heated for the gas decomposition; Microwave-plasma CVD (MPCVD) [66], where a plasma is generated by microwave radiation; Direct Current arc CVD (DCCVD) [67], where a DC plasma is produced from gas phase and the flame CVD technique [68], where combustion of acetylene in oxygen is used for reaching of higher gas temperature.

The major advantage of the CVD diamond growth compared to the HPHT method is obviously the much lower equipment and energy costs and the advantage of the HPHT growth process is the significant control over the quality and geometry of diamond obtained.

- ***Plasma-enhanced methods***

First the plasma-enhanced methods will be addressed. Plasma-assisted CVD uses carbon-containing species mixed in low concentration with hydrogen. The plasma is generated either by various forms of discharges or by induction heating. The role of the plasma is to generate active species (atomic hydrogen and carbon precursors for

the growth of diamond). The atomic hydrogen is produced by electron impact dissociation of molecular hydrogen [69] and as carbon deliverer methane is the most commonly used, but also other hydrocarbons like acetylene can be implemented. The two most common types of MWCVD reactors are the ASTEX-type (Fig. 14a) and the NIRIM-type (Fig. 14b) reactor

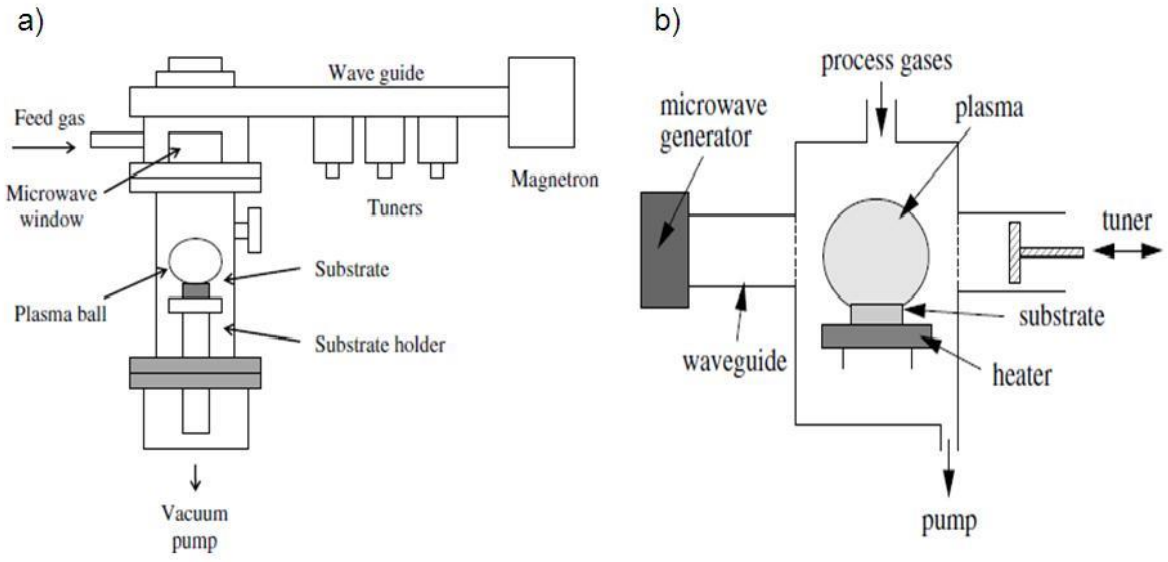

Fig. 14: A schematic diagram of microwave-assisted CVD set up: a) „ASTEX" type [70] and b) „NIRIM" type [18]

In the NIRIM-type reactor [71], a quartz discharge tube is inserted through the side of a fundamental mode rectangular waveguide appropriate for the propagation of 2.45 GHz microwaves. The arrangement is such that the electric field maximum is centered in the middle of the discharge tube, creating stable plasma in that position. The exact position of the plasma can be altered by tuning using a sliding short in the waveguide. The substrate is introduced from the bottom of the discharge tube using a dielectric rod to prevent microwave leakage to the outside. The biggest disadvantage of this type of reactor is the limitation of the substrate size (2-3 cm^2) and the power (below 1.5 kW). Another drawback is the possible contamination of the growing film via etched material from the chamber walls.

The other common type of microwave reactor (Fig. 14a) was designed in the late 1980s [72], and was then commercialized by Applied Science and Technology, Inc. (ASTEX). In this reactor, the microwaves are coupled into a water-cooled metal

cavity through a quartz window, using an antenna which converts the TE10 microwave mode in the waveguide to the TM01 mode in the cavity. The inner chamber diameter is chosen so that only one microwave radial mode can be sustained in the cavity at 2.45 GHz. Substrates as large as 10 cm in diameter can be coated by positioning them on a heated stage beneath the plasma ball. Microwave powers of up to 5 kW can be used in such systems giving growth rates well in excess of 10 $\mu m.h^{-1}$. This method of diamond growth has a number of distinct advantages over the other methods.

Other plasma assisted CVD techniques that are not so frequently used, but should be mentioned are RF-CVD and DC-CVD. In contrast to the microwave deposition (using a discharge at 2.45 GHz) the RF-CVD is a lower frequency process (discharges typically at 13.5 MHz), which leads to lower plasma density and lower energy electrons (Fig. 15a). The achieved lower concentration on active species combined with the impurity problems (caused by sputtering of material from electrodes and chamber walls) make the RF-CVD set up not the first choice for diamond growth [73].

The DC-CVD, called also ‚arc jet', is a generic expression for a high pressure direct-current plasma discharge in which convection plays a significant role in transport processes. Its major benefit is the simplicity of the set up (Fig. 15b). Electrical energy is converted to thermal and kinetic energy of a flowing gas mixture by an electric arc discharge. Like other CVD methods, a major constituent of the gas mixture is hydrogen, while methane is most often introduced into the plasma jet as a source of carbon. The plasma is directed to the substrate at a pressure of 1 bar and very high gas temperature of the thermal plasma (5000 K) is achieved, which leads to very high active species concentration, consequently to very high growth rates. The biggest disadvantage of this process is the small deposition area (5x5 mm^2) [74] and poor homogeneity of thickness and quality of the films [75].

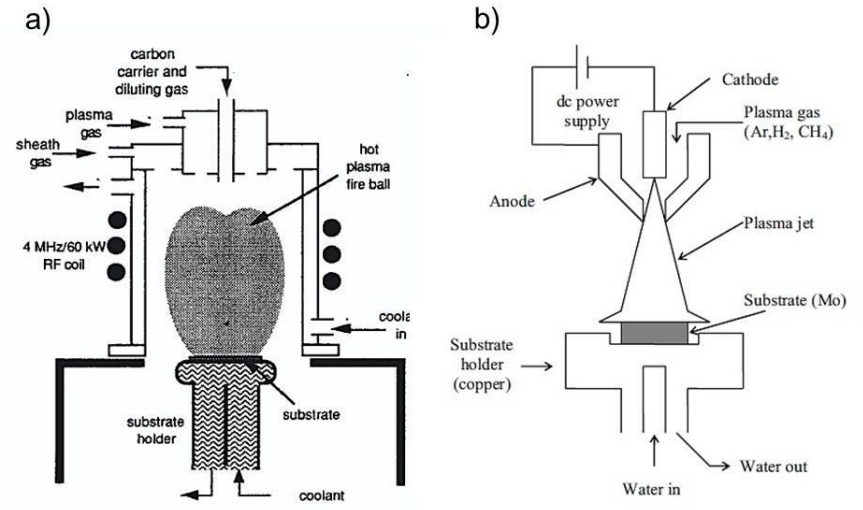

Fig. 15: A schematic diagram of: a) RF-CVD set up [73] and b) DC-CVD set up [70]

- ***Thermal assisted CVD***

This method is based on the thermal decomposition of carbon containing species. The most popular and used technique is the HFCVD. In this method, single diamond crystallites or diamond films are deposited on a heated substrate from a mixture of methane and hydrogen, dissociated by high-melting-point metal (in most cases tungsten) filaments placed close to the substrate. The filament temperature may reach around 2200 °C during this process. The main role of the hot filaments is to dissociate the molecular hydrogen and the methane. Additionally during the diamond deposition the tungsten filament reacts with the methane and undergoes carburization. This results in the consumption of carbon from the methane, which leads to a specific incubation time needed for the nucleation of diamond films. Therefore the carburization process should be performed before the beginning of diamond growth [15].

The gas temperature in the chamber is lower than by the plasma-assisted CVD set ups and consequently less atomic hydrogen and reactive carbon species are produced. The low gas species concentrations give relatively low growth rates compared with the plasma methods. Another disadvantage is the sensitivity of the

filaments to oxidizing or corrosive gasses, which causes limitation of the variety of the used gas mixtures. It is also very hard to avoid contamination coming from the filaments.

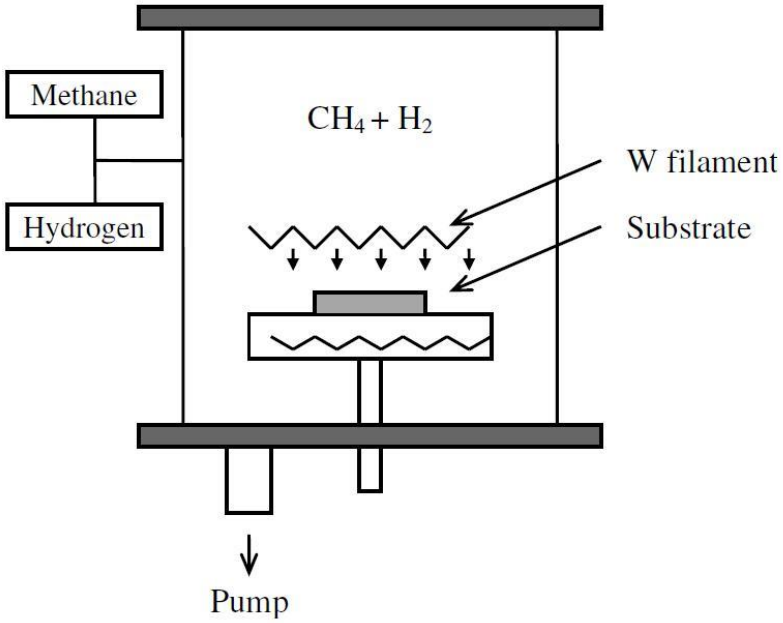

Fig. 16: A schematic diagram of a HFCVD set up [70]

Despite these drawbacks, hot-filament assisted deposition has remained popular because of its low capital cost and simplicity. Also, hot-filament reactors are directly scalable to large sizes and can be used to coat complex shapes and internal surfaces, while the plasma-assisted reactors (with higher growth rates) are more often used for production of thick diamond films. A hot filament reactor has superior uniformity compared to the MW and DC reactors. It brings a uniform temperature across the deposition area, while microwave reactors and DC torches create a sphere or plume of energy that is hotter at the center than at the edge [65]. This is ascribed to the much easier process control of the HFCVD.

The last type of thermal-assisted CVD is combustion CVD (CCVD). Diamond synthesis with this technique was first reported by Hirose and Mitsuizumi (1988). They used a conventional atmospheric pressure premixed C_2H_2-O_2 brazing torch and have obtained a high quality polycrystalline film, deposited on a small area (<10 mm^2) with very high growth rate (about 100 $\mu m.h^{-1}$). Beside the high growth rate another advantage of the process is its simplicity, but there are many drawbacks like

the small deposition area, problems with the thermal management and non-uniformity of the films.

A summary of the major features of different CVD techniques is presented in Table 4.

Table 4. Present status of low pressure CVD methods [69]

Method	Rate, $\mu m.h^{-1}$	Area, cm^2	Advantages	Drawbacks
Microwave plasma	0.1	100	Quality, stability	Area, contamination
RF plasma	180	3	Rate, quality	Area, stability, homogeneity
DC plasma jet	900	2	Rate, quality	Contamination, stability, homogeneity
Hot filament	0.5-8	250	Simple, large area	Contamination, stability
Combustion flame	30-100	2	Simple	Area, stability

4.3. Growth mechanism of diamond

The growth of the CVD diamond is fascinating and exciting from many perspectives. The first important question is how it is possible to synthesize diamond by relatively low temperatures and pressures, although it is thermodynamically metastable at these conditions. One must understand what are the chemical processes which lead to diamond versus graphite or amorphous carbon growth. Since diamond is not thermodynamically stable, the process should be kinetically favorable. At room temperature is graphite 2.9 $kJmol^{-1}$ more stable than diamond, which corresponds to not so big difference in the bonding energy (~0.03 eV) per carbon atom. The difference in the thermal energy of the atoms is also negligible, so the energy barrier should not be an obstacle. The only thing that must be granted is that the first deposited atoms are sp^3-hybidized carbon.

The growth process is divided in two steps: nucleation phase and growth phase. It begins when the reactive species from the carbon precursor in the gas phase nucleate onto the surface. Most of them exhibit a sp^2-hybridization and the dangling bonds of the carbon atom tend to build π bonds with another carbon atom, which leads to reconstruction of the surface and graphite building. Simultaneously atomic hydrogen is formed due to the gas excitation. It is the most critical component in the gas phase mixture, and indeed the one that drives the whole chemical system. The atomic hydrogen is very reactive and terminates very quickly the surface, converting the sp^2-bonded carbon to sp^3. The atomic H is known to etch graphitic sp^2 carbon many times faster than the diamond-like sp^3 carbon. Thus, the H atoms serve to remove back to the gas phase any graphitic clusters that may form on the surface, while leaving the diamond clusters behind. The atomic hydrogen reacts also with neutral species, e.g. CH_4 to create reactive radicals, such as CH_3, which can be attached to suitable surface sites. In addition, H atoms annihilate long-chained hydrocarbons, breaking them up into smaller pieces. This prevents the build-up of polymers or large ring structures in the gas phase, which might ultimately deposit onto the growing surface and inhibit diamond growth [18]. The sp^3 carbon clusters are more stable than sp^2 since the hydrogen-carbon bond is stronger than carbon-carbon bond (resp. 416 $kJ.mol^{-1}$ (H-C bond) and 348 $kJ.mol^{-1}$ (C-C bond)). This fact leads to the next problem - after the whole surface is hydrogenated, the carbon radicals can not remove the hydrogen atoms from the diamond surface. Once again the atomic hydrogen is the answer of the problem - if a H atom lands on the surface, it can recombine with a hydrogen atom from terminated diamond surface (which is thermodynamically favorable, since H-H bond is very strong - 436 $kJ.mol^{-1}$), leaving a free place, which could be occupied by a carbon atom or a carbon-containing radical. However this is very unlikely, because the carbon content in the gas phase is very low compared to the hydrogen. According to literature, for the integration of one carbon atom in the diamond layer 10000 H atoms have to be produced [76]. The diamond growth process is schematically presented in Fig. 17.

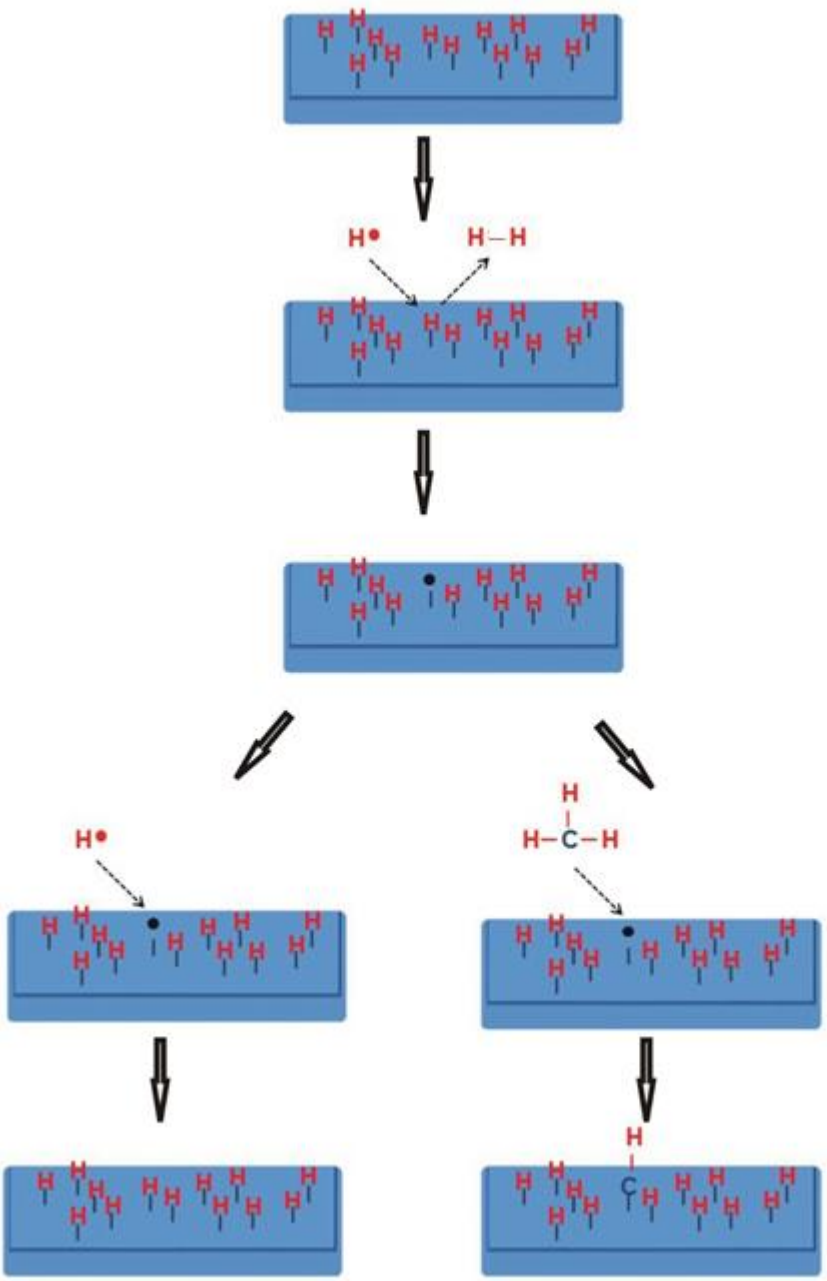

Fig. 17: Schematic presentation of diamond growth

The deposited carbon clusters grow laterally and in height, till the formation of the so called —critical size—Since this moment the energy barrier for the conversion of sp^3-bonded carbon into graphite is too high, which makes it impossible. This is also the end of the nucleation phase. The growth phase consists of the following attachment of carbon-containing components to the nucleation centers that are growing in all directions till the building of closed film on the surface.

Very important for the diamond growth is also the choice of substrate. It can be metal or non-metal. The best possible substrate is diamond, which allows a homoepitaxial growth. The growing diamond film matches to the crystallographic orientation and so high quality diamond layers with well-defined arrangement are produced. However diamond is very expensive material, that is why other materials are used as substrates. They should fulfill some conditions: firstly, the substrate must have a melting point (at the process pressure) higher than the temperature required for diamond growth. Another criterion is that the substrate material should have a thermal expansion coefficient comparable with that of diamond. Also good match of the lattice constant between the substrate material and diamond is needed to avoid strain during the growth. The substrate materials used for diamond deposition may be classified into three major groups in terms of carbon–substrate interactions. According to these interactions, the materials can be classified as such with (1) little or no carbon solubility or reaction, (2) strong carbon dissolving and weak carbide formation and (3) strong carbide formation. The materials from the first group do not form a carbide layer, and so any diamond layer will not adhere well to the surface. This can be used as one method to make free-standing diamond films, as the films will often readily delaminate after deposition. Typical examples are some metals (Au, Ag, Cu) and also some non-metals (Ge, sapphire, aluminium oxide). When the materials are strong carbon dissolving (group 2), there is a considerable amount of carbon diffusing into the substrate during diamond growth. The substrate acts as a carbon sink, and the deposited carbon dissolves into its surface, forming a solid solution. This can result in large quantities of carbon being transported into the bulk, rather than remaining at the surface where it can promote diamond nucleation. This class of materials includes some metals such as Pt, Pd, Rh, Fe and Ni. Materials with strong carbide formation include metals such as Ti, Nb, Ta, Cr, Mo, W and some rare earth metals. B and Si are also materials that form carbide layers, like other Si compounds such as SiO_2, quartz and Si_3N_4. Carbide materials (for instance SiC, WC and TiC) are also particularly suitable for diamond deposition.

The most used foreign substrate for diamond growth is silicon. The growth process is basically suppressed by the big difference in surface energy of diamond compared to silicon (6 $J.cm^{-2}$ to 1.5 $J.cm^{-2}$ respectively) and the relatively low sticking coefficient of gaseous precursors on silicon. These two facts explain the low nucleation densities

of around 10^4–10^5 cm^{-2} [77] on unpretreated silicon substrate. For formation of closed diamond layer a nucleation density of at least 10^8 cm^{-2} [15] is required. For the fulfillment of this condition an extra nucleation enhancement step is introduced. There are three most used techniques for this step: mechanical abrasive method, ultrasonically particle treatment and bias enhanced nucleation. The first method (using a mechanical scratching of the substrate with a diamond paste/powder) accomplishes a nucleation density up to 10^{10} cm^{-2} [78]. The main idea of this nucleation enhancement is the embedding of small residual diamond particles in the substrate, the smaller diamond particles are used, the higher nucleation densities and better uniformity are achieved. Further the nucleation enhancement by scratching can be generally attributed to: seeding effect, minimization of interfacial energy on a sharp convex surface, breaking of a number of surface bonds or the presence of a number of dangling bonds at sharp edges and the rapid carbon saturation (fast carbide formation) at sharp edges [69]. Ultrasonic treatment of substrates has been shown to enhance nucleation densities to 10^{11} cm^{-2} [79]. This is a gentler method, where the substrate is simply immersed in an ultrasonic bath, with the diamond powder (or diamond slurry) properly dispersed in an organic solvent like e.g. methanol. It causes similar damage to the substrate as with abrasion processes and also embed diamond fragments, but contrary to abrasion techniques, the nucleation density actually increases with the particle size, presumably due to very small diamond particles having insufficient momentum to damage the substrate or embed diamond fragments [80]. The last method (bias enhanced nucleation (BEN)) also achieves a nucleation density over 10^{10} cm^{-2} [81]. The major advantage of this technique is that it can be performed in-situ. During BEN, the substrate, which must be conductive, is negatively biased by around 100–250 V DC with respect to the (grounded) chamber or a second internal electrode. This process is generally carried out under rather methane rich (4–10% in hydrogen) conditions as compared to the diamond growth [82]. The applied electric field increases the ionization degree of the neutral gas molecules, the energy of the ions and the surface ion bombardment rate. During the bombardment, the ionic species alter the surface and create surface structures that act as seeds for the growth.

4.4. Diamond films

In chapter 3.2. the synthetic diamonds have been divided according to their impurity content, another classification possibility is according to the crystallinity of the diamond films. They can be seen as single crystalline or polycrystalline. The single crystalline diamonds can be obtained only if a diamond substrate is taken and used for the diamond growth. The polycrystalline diamond films are formed whenever growth occurs on non-diamond substrate (after a pretreatment) and can be divided into polycrystalline, nanocrystalline and ultrananocrystalline CVD diamonds.

- ***Single crystalline diamonds***

Besides the natural diamonds which are single crystalline, as mentioned above single crystalline diamond can be produced by HPHT technique or by CVD method. They are characterized by well-defined orientation of the crystal lattice and continuous surface structure with dominantly (100)-surfaces observed, but also (111)-surfaces and in very rare cases (110)-surfaces. The morphology of the diamond layer is determined by the ratio of the growth rates in (100) and (111) directions. It is expressed through the so-called growth parameter or α-parameter :

$$\alpha = \sqrt{3}\frac{v_{100}}{v_{111}} \ ,$$

where v_{100} and v_{111} are the growth velocities in the (100) and (111) directions, respectively. For lower values of α (i.e. α = 1), the crystallites are growing in cubic form, for higher values (α = 3) in octahedral forms. The crystal form depends strongly on the growth parameter (Fig. 18). Higher carbon concentrations in the gas phase in the chamber lead to higher α-parameter, while an increase of the substrate temperature or a decrease of the pressure lead to decreased growth parameter and to cubic crystals.

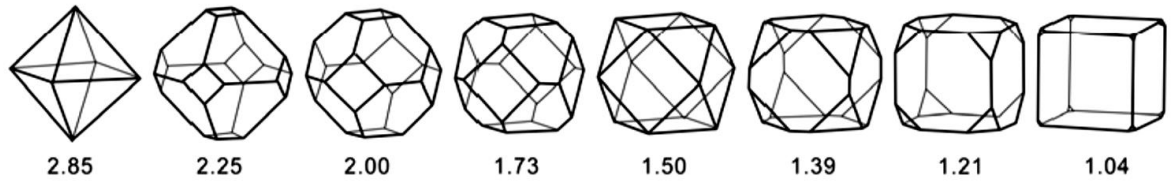

Fig. 18: Dependence of the crystal form from the growth parameter.

- ***Polycrystalline diamond films (PCD)***

Unlike single crystalline diamond films PCD do not have continuous structure and well-defined orientation (Fig. 19a). They consist of smaller single crystallites in most cases several micrometers, which show faceted structure and are merged together with a grain boundary material; the grain boundaries may contain non-diamond carbon phases, such as sp^2 bonded and/or graphitic amorphous carbon. Their preferred crystallographic orientations are (100) and (111) like for the single crystalline diamonds. The orientation of the crystallites is influenced by the growth parameter. Only those crystallite nuclei, which exhibit the highest growth rate vertical to substrate surface, can survive. These crystallites suppress the nuclei with different orientations, so that at the end of the growth there are only crystallites with equal orientation.

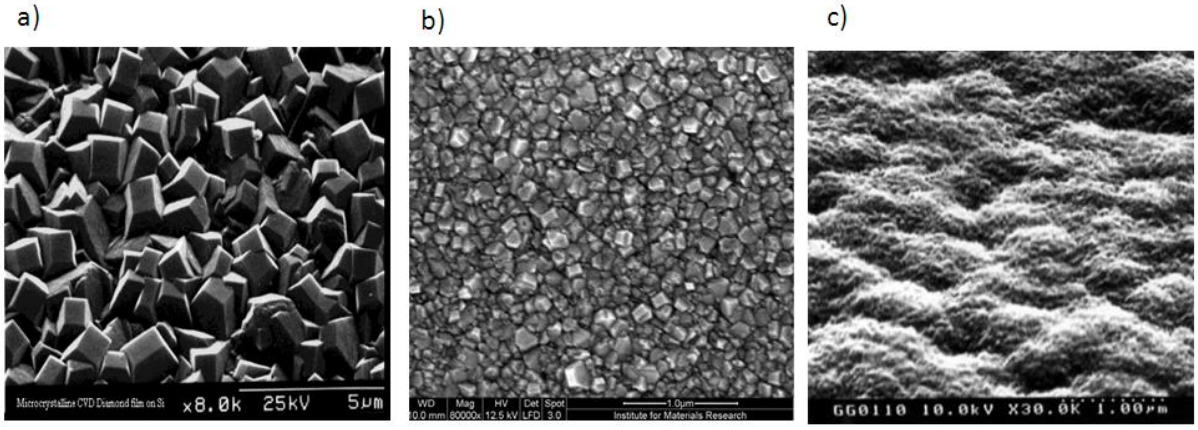

Fig. 19: SEM pictures of: a) PCD, b) NCD, c) UNCD films

The polycrystalline diamond shows different properties since these are the combination of the properties of the diamond grains and of the grain boundaries.

- ***Nano- and ultrananocrystalline diamond films***

Nanocrystalline diamonds (NCD) are form of polycrystalline diamonds in which the initial seeds are of nanometer dimensions resulting in extremely high nucleation density (between 10^{10} cm^{-2} and 10^{12} cm^{-2}) [83]. The grain size of NCD material is usually below 100 nm (but can reach several hundert nanometers (Fig. 19b), however grain sizes and a film thickness of about 30 nm are nowadays possible [84]. An UNCD film consists of small diamond crystallites (with size below 10 nm) embedded in an amorphous carbon matrix. It has an impact on all of the physical properties of the film, like lowering the density, the hardness, but it has also a positive influence, like improvement of the roughness, which is very important for applications in many technological fields. The easy trick how to obtain a nanocrystalline diamond film instead of a polycrystalline one is to change the very well-defined process parameter window by selecting one or more parameters outside it in an appropriate way [86]. The NCD films are grown a hydrogen-rich environment with small percentage of methane; in contrast the UNCD layers are grown in hydrogen-poor gas mixtures, where the methane (with higher concentration, compared to the CH_4 percentage for NCD growth) is diluted in argon or nitrogen.

The main differences between the polycrystalline and the nanocrystalline films are based on the growth process, not on the nucleation step [86]. As it can be seen from Fig. 19c UNCD (unlike NCD which has a facet columnar structure) has spherulitically shape. The conditions that have to be fulfilled for such a spherulitic growth are a low density of primary nucleation and a high rate of secondary nucleation. In Fig. 20 the differences in the NCD and UNCD growth are schematically shown. Both, NCD and UNCD growth start from individual nucleation sites. In the case of NCD, well-faceted single crystallites are observed while in UNCD deposition, ballas- or „cauliflower‘- like structures grow. The very difference between both cases is the rate of secondary nucleation, which is low for poly- and nano- but very high for ultrananocrystalline diamond film growth. This high rate of secondary nucleation also reflects in the substructure of the nodules (cauliflower structure).

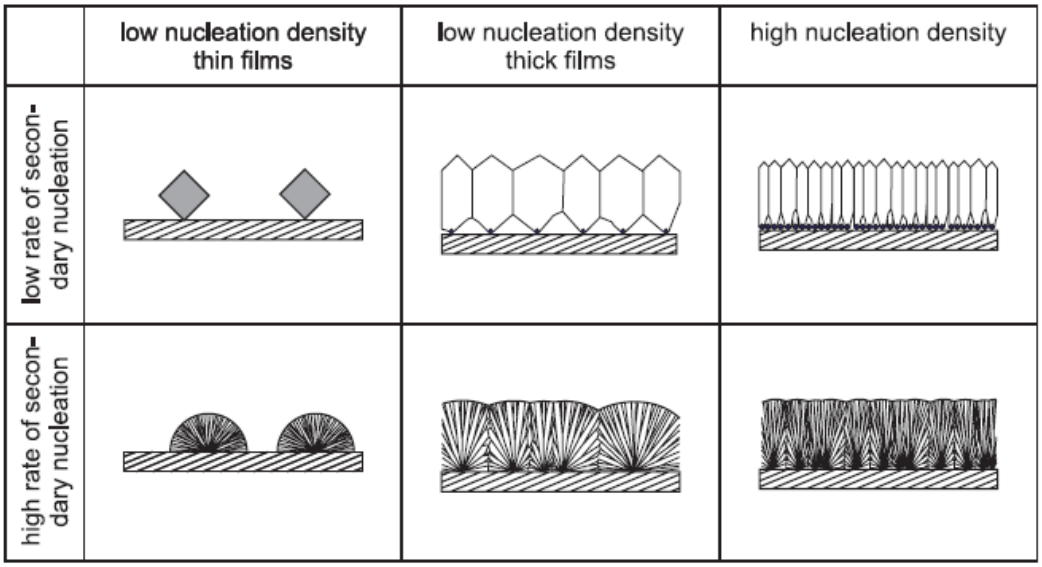

Fig. 20: Schematic drawing of diamond growth in dependence of the primary nucleation density and the rate of secondary nucleation [85]

Another striking difference is the fact that with the thickness the grain size of NCD increases. The effect of grain enlargement represents a form of van der Drift growth and the whole process can be described as „ surviving of the largest". In contrast UNCD shows no columnar structure and the grain size stays constant during the growth. This is due the high renucleation rate of hydrogen-poor environment, leading to continuous nucleation of new crystals and thus limiting the grain size. One advantage of this surface is that the surface roughness is independent of film thickness, as unlike in case of NCD. The biggest disadvantage of this material is that it really consists of two phases: the grain material and the grain boundaries [87].

5. STRUCTURING OF NANOCRYSTALLINE DIAMOND FILMS

In this chapter a short overview of the etch processes will be given. In details the physical background of the process steps used in this work for fabrication of diamond nanostructures will be explained and a literature search of current works on diamond etching will be presented.

5.1. Lithographical processes

Lithography is used for structuring of films or substrates via selective material removal. It is defined as the process of transferring shapes or patterns onto substrates or materials. The lithography process consists of the following steps:

- Surface preparation - includes the cleaning and drying of the surface;
- Resist Spin Coating - a thin layer of resist material is spin-coated on the surface of the sample;
- Soft Bake (Prebake) - used to evaporate the resist solvent and to increase the density of the resist after spin coating;
- Alignment and exposure - the sample is aligned and designated locations of the resist are exposed to light, electron beam and others, resulting in change of the resist properties;
- Development – removing of exposed or unexposed resist from the sample.

Depending on the exposure type there are the following lithography techniques:

- Optical lithography;
- Electron beam lithography (EBL);
- Ion beam lithography;
- X-ray lithography.

5. STRUCTURING OF NANOCRYSTALLINE DIAMOND FILMS

The most important and used technique is the optical lithography. It consists of transferring geometric patterns from a photo mask to the light-sensitive photoresist on a substrate, using an ultraviolet light. A major advantage of photolithography is the ability to fabricate many devices at once (i.e. in parallel), making possible the production of very complex structures in a relatively short time. A fundamental limitation of photolithography is the diffraction, which limits the size of the features that can be made to approximately the wavelength of the light used (>100 nm).

The ion beam lithography makes use of accelerated ions, which transfer directly the pattern on a substrate. The advantages of this technique are the higher resolution (below 100 nm) and the fact that due to bigger mass of the ions compared to the electrons (used by EBL) the back scattering (so-called proximity effect) is negligible. A drawback is the low penetration depth, because the energy is transferred via scattering to the whole material.

X-ray lithography uses x-rays to transfer a geometric pattern from a mask to a light-sensitive photoresist on the substrate. It is similar to the photolithography technique, but overcomes its diffraction limits. X-ray lithography allows the fabrication of structures with size down to 30 nm [88]. A major disadvantage of X-ray lithography is the necessity of a X-ray mask, because its production is quite expensive.

Electron Beam Lithography (EBL) will be introduced much more comprehensive, since it is the technique used in this work. Electron beam lithography is a modern technology that uses a beam of electrons that are extracted, focused and accelerated up to 20 kV. It creates fine patterns with a resolution up to several tens of nanometers. The principle of electron beam lithography is based on a shooting of a narrow, concentrated beam of electrons onto a resist coated substrate.

The main components of an electron beam system are:

- electron gun or electron source that provides the electrons;
- electron column that brings in focus the electron beam;
- mechanical stage that moves and positions the sample;
- computer system for controlling the equipment.

5. STRUCTURING OF NANOCRYSTALLINE DIAMOND FILMS

Currently, electron beam lithography is used principally in support of the integrated circuit industry. Its flexibility makes it ideal for making masks that can be used by other technologies including x-ray lithography. It is also used for writing complex patterns directly on the wafers. The procedures involved in electron beam lithography are almost similar with those of photolithography. Both technologies use different resists and chemicals to develop the exposed sections. The most commonly used electron beam resist is polymethylmethacrylate (PMMA). PMMA breaks down into monomers upon exposure to electrons, which is later developed using methyl-isobutyl-ketone (MIBK).

During the exposure of the resist scattering of the electrons in the resist and the substrate may occur. The electron —scattering" (called „proximity effect—) is a result of collisions between the electrons and the resist. By the collisions the electrons are losing part of their energy and thus changing the projected trajectory. The scattering of electrons may be backward (or back scattering, where electrons 'bounce' back), but it is often forward through small angles with respect to the original path. Hence undesirable spots from the resist can be exposed, which is a great problem for fabrication of smaller structures.

The electron beam lithography has many advantages:

- it is an extremely accurate method, allowing very precise control of sub-micron dimensions;
- E-beam patterns can be overlayed to the existing features with very high accuracy;
- it offers a great design freedom as it allows for the creation of any shape.

The main disadvantage of the electron beam lithography is that it is a fairly slow process and takes a long time for creating structures, typically between 2 and 4 hours per square millimeter. Also the EBL apparatus is very expensive.

5.2. Etching

The etching process removes selected areas from substrates or thin films. The two types of etching processes used for fabrication of nanostructures are wet etching and dry etching.

Wet etching is a material removal process that uses liquid chemicals or etchants to remove material from a wafer. The specific patterns are defined by masks on the wafer. The areas that are not protected by the masks are etched away by liquid chemicals. These masks are deposited and patterned on the wafers in a prior fabrication step using lithography [89].

Wet etching process involves multiple chemical reactions that consume the original reactants and produce new reactants. The wet etch process can be described by three basic steps:

- Diffusion of the liquid etchant to the structure that is to be removed;
- Reaction between the liquid etchant and the material to be etched away. A reduction-oxidation (redox) reaction usually occurs. This reaction entails the oxidation of the material then dissolving the oxidized material;
- Diffusion of the products of the reaction from the reacted surface.

All wet etching processes have the same basic limiting factor: isotropy. Whether etching oxide or metal, the amount of lateral etching nearly always approximates the vertical etch depth. Along with the basic technology limiting quality of isotropy, wet etching also has issues like wafer contamination, problems with the resist adhesion and appearance of chemical hazard [90].

The dry etching generally uses plasma to remove material from the substrate. Plasma also referred to as –fourth state of matter". Heating a gas may ionize its molecules or atoms (reducing or increasing the number of electrons in them), thus turning it into a plasma, which contains charged particles: positive ions and negative electrons or ions [91]. Plasma-based etching requires Radio Frequency (RF) power to activate the chemical reactions for removal of surface material. Ion-electron pairs are continuously created and destroyed by ionization and recombination, respectively. A lot of energy (thermal, electrical, or ultra violet and visible light) is

needed to remove the electrons from the atoms to form plasma and without sufficient energy, the plasma recombines into neutral gas. The plasma can be accelerated and maneuvered by electrical and magnetic fields.

The plasma offers three major features that are attractive for different technologies:

1. The temperatures of some plasma components and their energy densities can significantly exceed those in conventional chemical technologies,
2. The plasmas are able to produce very high concentrations of energetic and chemically active species (e.g., electrons, ions, atoms and radicals, excited states, and different wavelength photons),
3. The plasma systems can essentially be far from the thermodynamic equilibrium, providing extremely high concentrations of chemically active species and keeping the bulk temperature as low as room temperature.

These plasma features permit significant intensification of traditional chemical processes, essential increases of their efficiency and often successful stimulation of chemical reactions impossible in conventional chemistry.

The dry etching can be realized by:

1) Physical dry etching (sputtering) - physical removal of the material, usually by momentum transfer;
2) Chemical dry etching - through chemical reactions that consume the material, using chemically reactive gases or plasma;
3) Reactive Ion Etching - a combination of both physical removal and chemical reaction.

The physical dry etching requires high kinetic energy (ion, electron, or photon) beams to etch off the substrate atoms. When the high energy particles knock out the atoms from the substrate surface, the material evaporates leaving the substrate. There is no chemical reaction taking place and therefore only the material that is unmasked will be removed. The high energies of the ions involved in sputtering can significantly damage the substrate material, produce a rough and uneven surface, and yield low etch rates and selectivity and high anisotropy (Fig 21a).

The chemical dry etching (also called vapor phase etching) does not use liquid chemicals or etchants. This process involves chemical reactions with etchant gases to attack the substrate surface. It consists of the following six steps: 1) generation of

reactive species in the plasma; 2) diffusion of these species to the surface of the material being etched; 3) adsorption of these species on the surface; 4) occurrence of chemical reactions between the species and the material being etched, forming volatile byproducts; 5) desorption of the byproducts from the surface; and 6) diffusion of the desorbed byproducts into the bulk of the gas phase. The chemical dry etching process is usually isotropic (removal rate is nearly equal in the vertical and lateral directions on the substrate material) and exhibits high selectivity in contrast to the physical dry etching (Fig 21b). The selectivity refers to the ability of the reactive species to etch away only the material intended for removal, while leaving all other materials intact. In particular, the species used must not attack the mask material over the material being etched as well as the material beneath it. To achieve balance between selectivity and isotropy the both techniques (physical and chemical) should be combined in the same dry etching process. An example of dry etching that employs both physical and chemical processes is reactive ion etching (Fig. 21c).

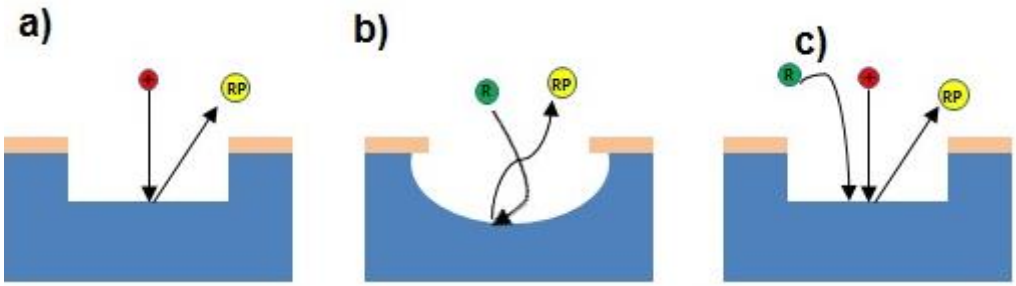

Fig. 21: Scheme of the etch mechanism of : a) physical dry etching, b) chemical dry etching and c) Reactive Ion etching

The reactive ion etching (RIE) is a method of dry etching and is defined as plasma etching under conditions where the etched surface is subjected to energetic (i.e. greater than about 50 eV) positive ion bombardment. The main purpose of RIE is to create an anisotropic etch where the etching will be unidirectional. When plasma is formed by the applied RF potentials, the gas molecules are broken down into a number of fragments and radicals. A significant number of these molecular fragments may become ionized in the plasma and may be accelerated to the various electrode surfaces within the discharge chamber. In many cases, the ion bombardment is very useful in maintaining the directionality, or anisotropy, of the etching process. There are two parts of reactive ion etching: chemical and physical [92]. The bombardment

with energetic ions dislodges atoms from the material (just like purely physical sputtering), in effect achieving material removal by sputtering. In addition to sputter-removal, the bombarding ions used in RIE give part of their energy to the other surface atoms, making them more reactive, so that they will chemically react with the chemical component of the etching mixture. Other type of RIE system is the inductively coupled plasma (ICP) RIE. In this type of system, the plasma is induced by an inductive coil wrapped around a quartz chamber (Fig. 22). The RF coils located in front of the RF transducer induces an alternating magnetic field, and this helps to produce high-density plasma due to confinement of electrons and ions. Very high plasma densities (up to 10^{15} cm^{-3}) can be achieved, though etch profiles tend to be more isotropic in these cases.

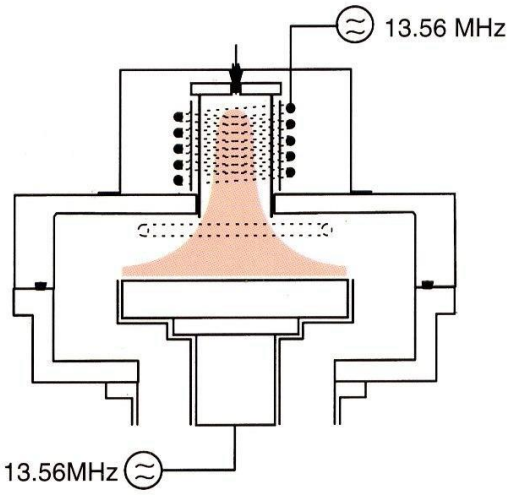

Fig. 22: Scheme of ICP-RIE reactor chamber

A RF source or DC bias can be applied onto the sample stage to extract and accelerate the reactive species from the plasma to achieve anisotropy and deep etching. An ICP etching system requires the use of two RF power sources usually at 13.56 MHz, the ICP that creates and enhances the amount of reactive gases in the chamber and the one that forms the plasma potential at the surface of the substrate. Hence, the control over the coil (ICP) and plate (substrate biasing) powers determine the etch rate and degree of anisotropy.

5.3. Fabrication of diamond nanostructures

Due to its inertness against acids and solvents at normal temperature the CVD diamond is inappropriate candidate for wet chemical etching. Diamond can react with iron and other liquid metals at temperatures above 600 °C [93]. The physical sputtering is also interfered through its high mechanical hardness. The reactive ion etching (RIE) can be much more suitable for fabrication of diamond nanostrucutres. RIE can provide anisotropic etching and better dimensional control of the etched patterns with minimal amount of reactant species [94].

The first report of reactive ion etching of diamond dates back to 1989 by Sandhu et al., where a low etch rate of 350 Å/min was measured for natural single crystal diamond using 0.4 keV oxygen ions (200 W, 80 sccm, 65 mTorr) in a parallel plate RIE system [95]. Bello et al. used hydrogen and hydrogen/argon or hydrogen/oxygen mixtures as reactive gas to etch CVD diamond films in both microwave and hot filament direct current plasmas, without a mask. The etch rates, etched surfaces and the reactive ions were investigated to understand the etching mechanisms, the etch rates achieved were in the range of 100 to 950 nm/h [96]. Otterbach and Hilleringmann studied a modified sample arrangement inside of a commercially available reactive ion etching (RIE) reactor which resulted in distinctly increased etching rates up to 330 nm/min, implying an increase of approximately one order of magnitude in comparison with the standard etching techniques [97].

In general there are two groups of RIE techniques established for diamond etching and they are divided according to the employed chemistry: hydrogen-based [98] and oxygen-based [99,100]. The first one has the huge disadvantage, that high substrate temperatures (> 700 °C) are required, while the second method can be performed at room temperature.

As far as all experiments in this work were carried out in ICP-RIE reactor using oxygen plasma, we shall devote some attention to its etch mechanism. Etching of diamond with a pure oxygen plasma is attributed to the formation of excited O* and O_2* radicals by energetic electrons accelerated by the RF field of the RIE system [101]. Upon interaction of the radicals with the carbon atoms of the diamond surface etching proceeds by the formation of volatile products, such as CO and CO_2. Mass

spectroscopic studies during the RIE of diamond films showed the presence of proportionally more CO_2^+ in comparison with CO^+ species [102]. This phenomenon has been attributed to the formation of CO_2 by the products of the etching process rather than due to etching of the diamond surface. The etching/oxidation mechanism of amorphous carbon and hydrogen terminated diamond films proceeds by hydrogen abstraction and oxygen addition [103]:

$$\text{H-terminated C} + \text{O} \rightarrow \text{C}^{\cdot} + \text{OH (g)}$$

$$\text{C}^{\cdot} + \text{O} \rightarrow \text{CO(s)}, \text{CO(g)}, \text{CO}_2\text{(g)}$$

During the reactive ion etching process chemical etching cannot be treated in isolation, a contribution via physical sputtering is vital for the removal of carbon atoms from the diamond surface, despite the low concentration of ions in the plasma. The addition of argon and fluorine-containing precursors in the oxygen plasma has shown a significant increase of the etch rate of diamond films and crystals [103]. Fluorine containing gases when added to an oxygen plasma increase the formation of atomic oxygen and therefore the increase of diamond etch rate. The same observations have also been verified for ion beam etching, where enhancement of the etch rate is achieved using oxygen as a carrier gas [104].

Using optimized RIE conditions a significant progress in fabrication of diamond nanodevices has been achieved. To take advantage of its optical defects for use in the quantum information technology, it is appropriate to incorporate the color centers in optical structures like photonic crystals, nanopillars or microrings. Riedrich-Möller et al. [105] reported a method for the fabrication of one- and two-dimensional photonic crystal microcavities (Fig. 23a) with quality factors of up to 700 in single crystal diamond. The cavity modes were tuned into resonance with the zero phonon line of an ensemble of silicon-vacancy color centres, and an intensity enhancement factor of 2.8 was measured. Hausmann et al. [106] present at a simulation study of the coupling between a nitrogen-vacancy (NV) color center and optical modes of a nanowire, and have determined that more than 80% of emitted photons can be coupled to the nanowire mode for a range of nanowire diameters between 180 nm and 230 nm. In further papers the same authors also showed practical results [107] demonstrating two different techniques to implant single color centers in diamond nanostructures (Fig. 23b). Faraon et al. [108] demonstrated coupling of the zero-

phonon line of individual nitrogen-vacancy centers and the modes of microring resonators (Fig. 23c) fabricated in single-crystal diamond, which lead to ten-fold enhancement of the ZPL intensity.

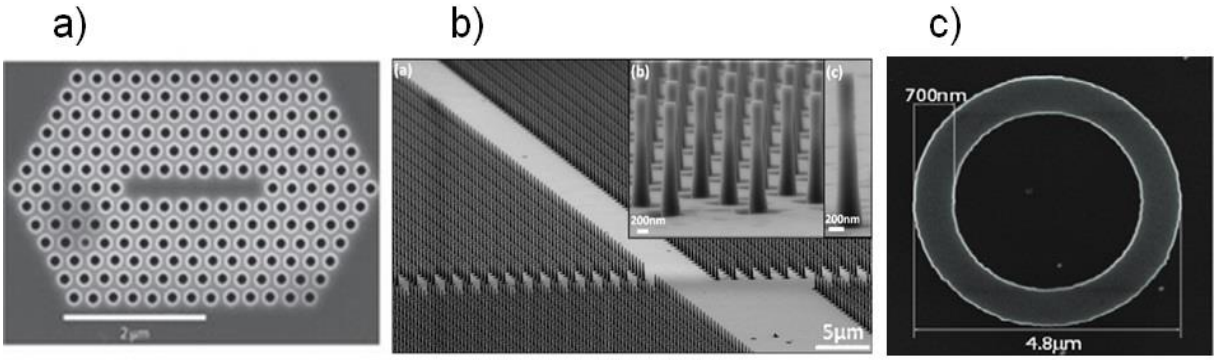

Fig. 23: SEM images of diamond nanostructures: a) photonic crystal [104], b) nanopillars [106] and c) microring [108]

6. DEPOSITION OF DIAMOND FILMS AND SINGLE CRYSTALLITES

In this (first experimental) chapter the entire process of diamond growth, starting with the different types of pre-treatment (for obtaining different nucleation densities) will be introduced. Then vastly description of the two types of CVD set ups (for deposition of either NCD or UNCD) will be given and also the way for production of single diamond crystallites (randomly or site-controlled grown) will be presented.

6.1. Pre-treatment of silicon wafer

As mentioned in Chapter 4 for diamond growth on a foreign substrate (e.g. silicon) a pre-treatment is needed. This is due to the low adhesion probability of diamond building species on the silicon substrate. Combined with the extreme difference of the surface energy between diamond and silicon (5.5 to 1.5 $J.m^{-1}$), these two facts explain the low nucleation density of diamond on single crystalline silicon substrates [109].

There are several pre-treatment techniques (as already comprehensive explained), but in this work the pre-treatment method, using a diamond suspension (of different types) in ultra-sonic bath was established.

The substrates, used in this work are silicon wafers. As explained in previous chapter silicon forms a carbide layer before the actual nucleation starts. In this way a diffusion barrier is built, which induces rising number of adatoms. The incubation time is ascribed to the formation of this interface layer. The species from the gas phase diffuse on the surface and can attach to distinguished places, form aggregates or desorb. When such an agglomeration reaches a critical size, it is stable enough, i.e. it can not be destroyed by other processes, which interfere the nucleation. The critical

size depends on the substrate material, the gas composition and the temperature [110]. No more nuclei besides those already created nucleation places are formed on the substrate. When all nucleation places are occupied with nuclei, then the deposition is going to the next phase. The island growth by diamond is consequence of strong interaction between the layer atoms and very weak interaction between these atoms and the substrate (which can lead to adhesion problems) [111]. However, the biggest obstacle for diamond growth is the extreme low nucleation density on almost every non-diamond substrate (between 10^4 and 10^6 cm^{-2}). Therefore the substrates are pretreated for the enhancement of the nucleation density, in this way the island growth already in height starts by lower thickness. For diamond growth a nucleation density above 10^8 cm^{-2} is needed, as explained in the previous chapter, the most commonly used pretreatment techniques (mechanical scratching, seeding with diamond powders, bias enhanced nucleation) can achieve densities above 10^{10} cm^{-2}.

In this work the seeding with diamond particles in a suspension is used for the pretreatment. It is a very simple mechanical method, which is suitable for pretreatment of substrates, but also for pre-patterned samples, used for site-controlled deposition. Firstly, the Si substrate was etched for 35 s in ammonium fluoride buffered etching solution in order to remove the native silicon dioxide on the silicon substrate. The following treatment is performed in an ultra-sonic (US) bath using two different diamond powders and a commercial diamond slurry. As dispersion media n-pentane was used in case of diamond powders and methanol in case of diamond slurry. The two diamond powders are applied- nanodiamond powder D0.25) (with average grain size of 0.25 μm) and ultra-disperse diamond powder UDDP (with average particle diameter between 3 and 5 nm). For the deposition of closed columnar films, where nucleation density of at least 10^{10} cm^{-2} is required, both powders were used. The established amounts are as followed: 50 mg D0.25μm powder and 80 mg UDDP are dispersed in 80 ml n-pentane. A glass container with the suspension was put in an ultra-sonic bath for one hour, and it had to be additionally shaken every five minutes to avoid clumping of the powders on the substrate. Also the temperature of the bath should not overcome 35 °C to prevent intensive pentane evaporation. The substrate is cleaned afterwards ultrasonically

with acetone and iso-propanol (for 90 s in each) and dried with nitrogen. The above described pre-treatment is called –standard" in the following parts.

In the cases where single crystallites deposition was needed, respectively a lower nucleation density, the diamond suspension contained only D0.25 μm powder. The US pre-treatment was only 5 minutes. In case of site-controlled growth after US cleaning the sample was additionally etched in ammonium fluoride etch solution to remove from the surface the undesirable diamond particles, which were embedded not on the pre-patterned places (holes in the silicon substrate).

To estimate the nucleation density an atomic force microscope (AFM) images (Fig.24) were taken from pre-treated substrates with the standard method. The calculated values were higher than 10^9 cm^{-1} which confirms the literature data mentioned above.

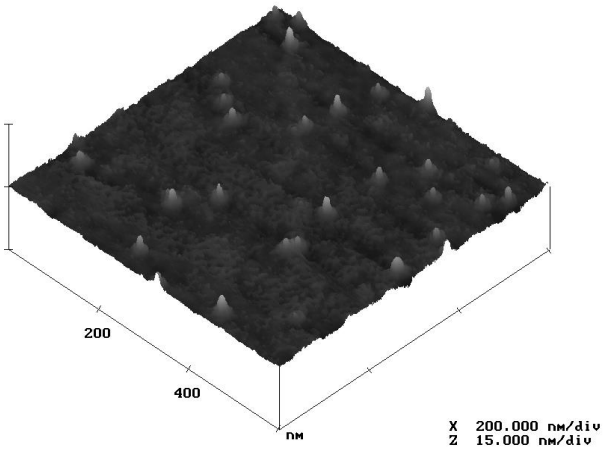

Fig. 24: AFM image of pretreated silicon wafer

Diamond slurry was used for achieving nucleation density above 10^{11} cm^{-2}. 20 ml from the diamond slurry was diluted in 60 ml methanol and the duration of the US pretreatment was 30 minutes (there was no need of shaking, because of the homogeneity of the suspension). Afterwards the sample like in the other cases was ultrasonically cleaned with acetone and iso-propanol and dried with nitrogen.

6.2. Nanocrystalline diamond films by HFCVD

6.2.1. HFCVD set-up

The deposition of nanocrystalline diamond films was carried out in a self-assembled Hot Filament Chemical Vapor Deposition (HFCVD) set up. The reactor is made of stainless steel, with a height of 141 mm and a diameter of 264 mm; the estimated volume is about 7.7 l. There are four flanges on the reactor walls. A glass window is put on one of them, which allows sight in the reaction chamber (for better process control). On the second one a mechanical pressure analyzer (for measuring of the working pressure) is attached. The power supplies for the filaments and the heating plate are attached to the reactor bottom (Fig. 25). The connections for the pump system, the gas lines and the thermocouple are also placed on the bottom of the reactor chamber. All three parts of the chamber, midsection, top and bottom parts, are sealed by Viton-O-rings, double-walled and connected to cooling water system. The reactor chamber can be evacuated to a basic pressure down to 10^{-3} mbar via pump type D8B from Fa. Leybold with pumping speed of 8 $m^3.h^{-1}$. It is connected to the reactor via a master valve for aspirating of rest gasses and creation of fine vacuum, the working pressure of 25 mbar is adjusted via parallel connected needle valve.

The filaments (diameter 0.3 mm and length about 12 cm) are stretched between two parallel cooper blocks above the sample holder. The tungsten wire, from which the filaments are cut, is delivered by Fa. Heraeus. Self-made feather coils are used to secure the straight position of the filaments. They provide a tension on the filaments, which is needed because of their elongation during the carburization. A fixed holding would lead to a filament bending, since the filaments are extremely thermally strained by the reached filament temperature above 2000 °C. The current required for such temperature is about 70 A. The filament temperate was measured with a pyrometer, type ISQ/LO from Fa. Impac Electrronic.

For the additional cooling of the reactor a ventilator is attached on the reactor bottom to cool the power supply lines during the deposition. The substrate holder is not cooled, but heated via a heating plate. It is made of boron nitride (diameter 77 mm, thickness 2.2 mm) with graphite as a heat guide with heat power up to 45 $W.cm^{-2}$ (Fa, Boralectric (model HT/0213)) [112]. The heating plate is operated via a three-

phase-voltage transformer. The plate is placed on top of five ceramic cylinders and is not fixed to prevent short circuit with the reactor walls and also to avoid mechanical strain. On the top of the heating plate is the sample holder made of molybden (diameter 80 mm, thickness 9.8 mm). On the bottom side of the holder there is a notch, where a NiCr/Ni thermoelement (diameter 0,5 mm, Fa. Thermocoax) is placed.

They are two gas lines introducing gases from the bottom side of the reactor chamber to a distribution ring positioned above the filaments. All gas flows (hydrogen and methane) are regulated via mass flow controllers (Fa. MKS, type 247). An additional gas flow line (nitrogen) was incorporated for cooling of the deposition chamber after the end of the process.

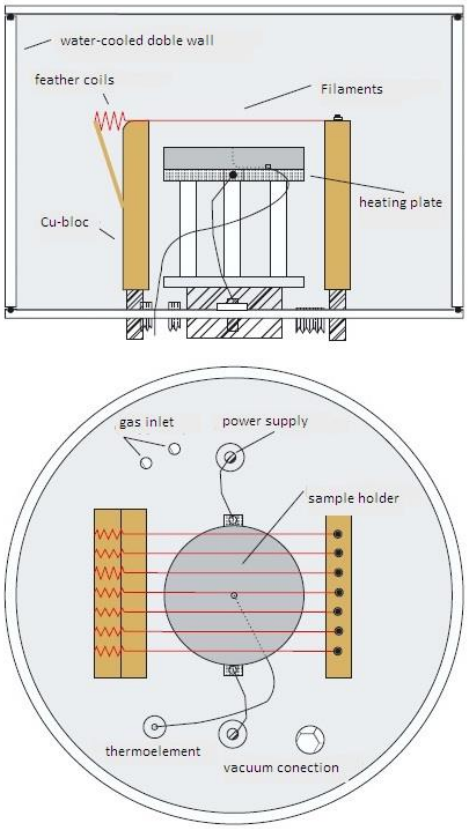

Fig. 25: Scheme of the Hot Filament CVD set up

Before the deposition process the filaments must be carburized. After this step the silicon substrate is placed into the reactor chamber. The carburization of the tungsten filaments is associated with their elongation and increased brittleness. The filaments are strained (by a feather) during the carburization to keep the appropriate position

above the substrate. During the process of carburization of the tungsten filaments carbon diffuses into the filaments till they consist exclusively of W_2C and WC [113] resulting in an increased resistivity. The carburization is carried out at the same parameters as the deposition process, the only difference is the absence of substrate heating. The other parameters are as follows – 25 mbar chamber pressure and gas flows of 500 sccm H_2 and 5 sccm CH_4 (which equates ~ 1% methane in the gas phase). The process starts with switching on of the hydrogen flow and justification of the chamber pressure via a by-pass valve. Then the power supply for the filaments must be turned on, and stepwise increased to 60 A (it results in current of 8.5 A per filament). A stabilization of the filaments in hydrogen environment is needed. This step takes approximately one hour and in-between the current is increased stepwise up to 10 A per filament. After one hour methane is added for at least three more hours, when a constant resistance is reached (Fig. 26).

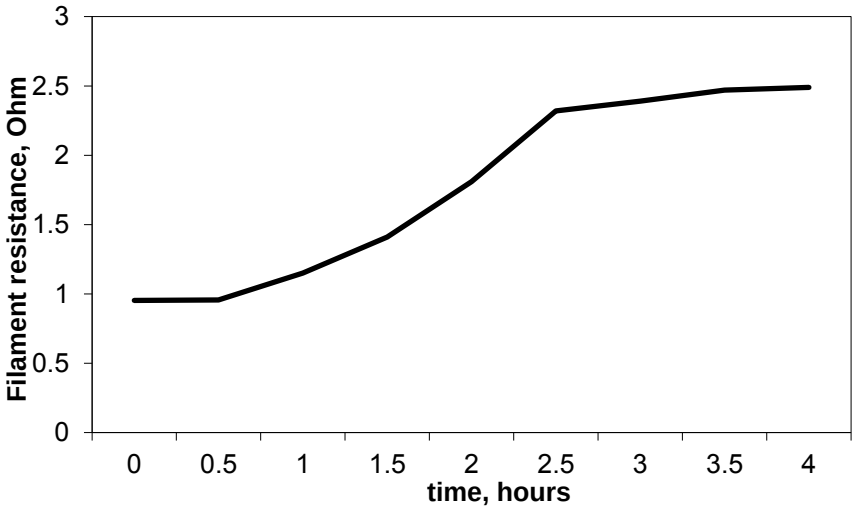

Fig. 26: Filament resistance dependence from carburization time

6.2.2. Deposition and characterization of NCD films grown by different temperatures

In Fig. 27, the temperatures measured as a function of the total filament current for the two cases , namely with substrate heating (applied voltage U_H = 120 V)and without heating (U_H = 0 V), are plotted. The following observations can be made:

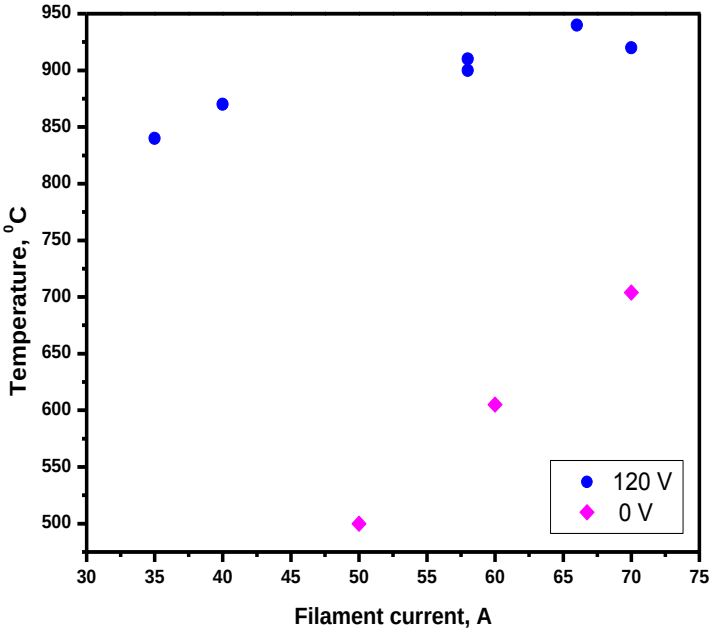

Fig. 27: Substrate temperature T_s as a function of the total filament current I_F

- In the case of U_H = 120 V the temperature increases only slightly with I_F. The temperature is mainly determined by the heating element with only slight contributions from the filaments.
- In the case of U_H = 0 V, there is a linear increase of T_S with I_F. This is a consequence of the fact that filament current is the only source of heating.

According to the working plan after assembling the HFCVD set up the first objective was to obtain closed NCD films. Based on previously experience of the group and literature search the following conditions have been chosen: a working pressure of 25 mbar, a gas mixture with 1% methane in hydrogen with flow rates of 5 sccm CH_4 and 500 sccm H_2; a current of 40 A applied to the tungsten filaments (because of several broken filaments during loading of the sample), and a substrate heating adjusted to 120 V, achieving a substrate temperature of 840 °C. The duration of the diamond growth was three hours (which was also accepted as standard deposition duration for later experiments). The obtained first sample DHF 1 was thoroughly investigated by scanning electron microscopy (SEM) and atomic force microscopy (AFM) to confirm their morphology and topology. For investigation of the composition and the chemical

bonding structure samples were sent to partners in order to perform X-ray photoelectron spectroscopy (XPS) and Raman spectroscopy measurements.

The nanocrystalline diamond layers obtained after the above mentioned pretreatment and deposition conditions were closed and columnar (Fig. 28). The film thickness was about 930 nm and the calculated growth rate 5.3 $nm.min^{-1}$. We have observed pyramidal (111) structures of well-defined crystals with columnar growth starting from distinct nucleation sites on the silicon surface, as shown by the SEM cross-section images. The nucleation density (> $10^{10}cm^{-2}$) achieved during the pretreatment step ensures the formation of diamond nanocrystallites, which in the course of the deposition grow until they coalesce to form a closed film (without voids at the interface), afterwards growing only in height.

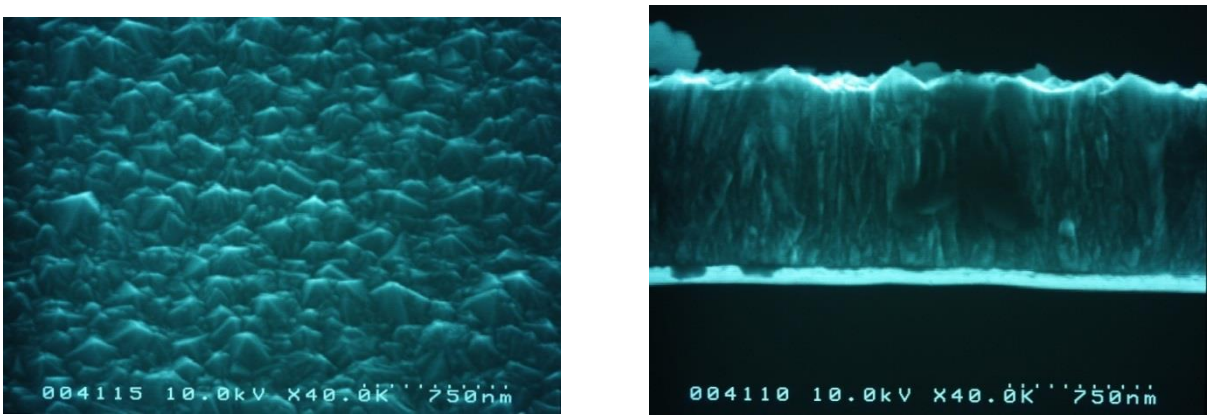

Fig. 28: SEM images of DHF 1 (840 °C): a) top view, b) cross-section

The next step was to increase the temperature in order to investigate whether there is a significant influence on the morphology and growth rate. The variation of the substrate temperature was achieved in two ways: In the first experiments, the substrate was heated with a voltage U_H = 120 V applied to the heating element. An additional heating of the substrate took also place by the filaments. In these experiments, the number of the filaments was not constant as not always all filaments were intact at the time of the experiment. As a rule of thumb, 10 A were applied to each filament. These different filament currents led to slight differences of T_S for a constant U_H. In the second set of experiments of this series, U_H was set to zero.

After a couple of short time depositions (which will be presented in the next section, devoted to deposition of single diamond crystallites), the next experiment DHF 4 was performed with the same conditions as DHF1, only I_F was increased by 10 A (totally

50 A), which resulted in ca. 90 °C higher substrate temperature (930 °C). From Fig. 29 it can be seen that the film is closed, dense, columnar and has almost the same texture as DHF1, dominated by four-walled pyramidal facets, which have kept their size. Besides the similar morphology the sample has almost the same thickness, respectively growth rate.

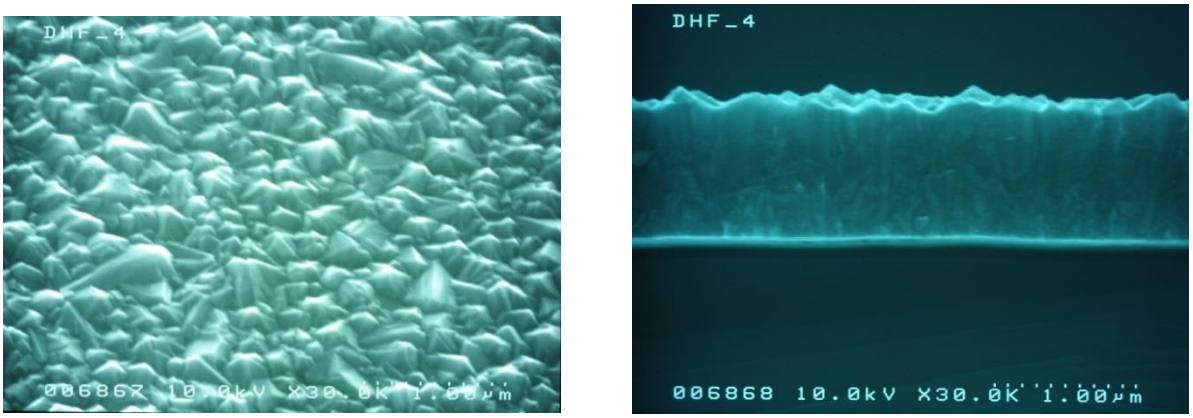

Fig. 29: SEM images of DHF 4: a) top view, b) cross-section

The next significant experiment was DHF 8 (Fig. 30) with a substrate temperature of 870 °C which is in temperature range between DHF 1 and DHF 4.

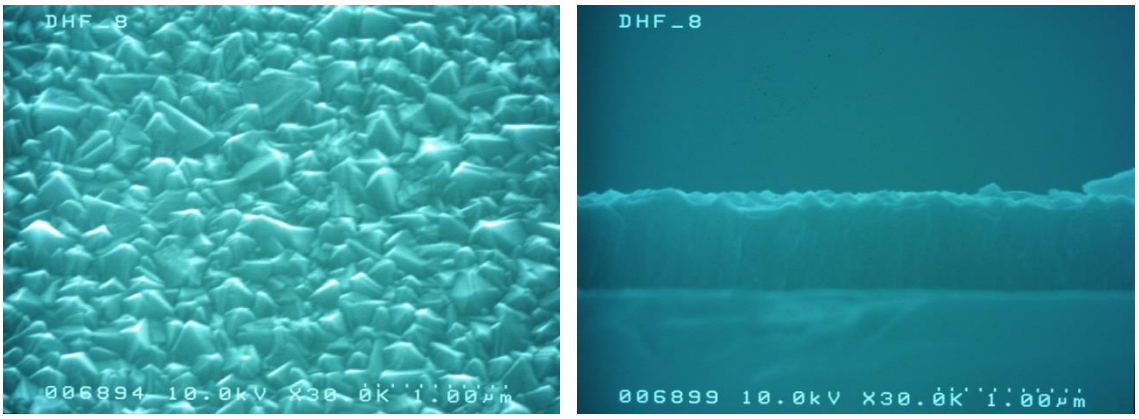

Fig. 30: SEM images of DHF 8: a) top view, b) cross-section

There were no differences in the texture and the structure compared with DHF 1 and DHF 4. After the first series of experiments it could be concluded that all NCD samples obtained at temperatures in the range 840-930 °C after the standard pretreatment are very similar concerning texture and structure.

Further experiments were carried out to investigate the influence of the nucleation density on the growth, respectively the morphology of the films. As mentioned above

there were several pretreatment recipes and we have compared our standard pre-treatment procedure (UDDP+D0.25 suspension in one hour US bath - DHF 8) to a pre-treatment with a diamond slurry (30 min in US bath – DHF 12).

The SEM images reveal the change of the nucleation density. The crystallites of the sample after standard pretreatment are larger and have typical facets. By the other sample an increased nucleation density is observed, leading to decreasing of the crystallites size, nevertheless the crystal orientation is kept (determined by the growth parameters).

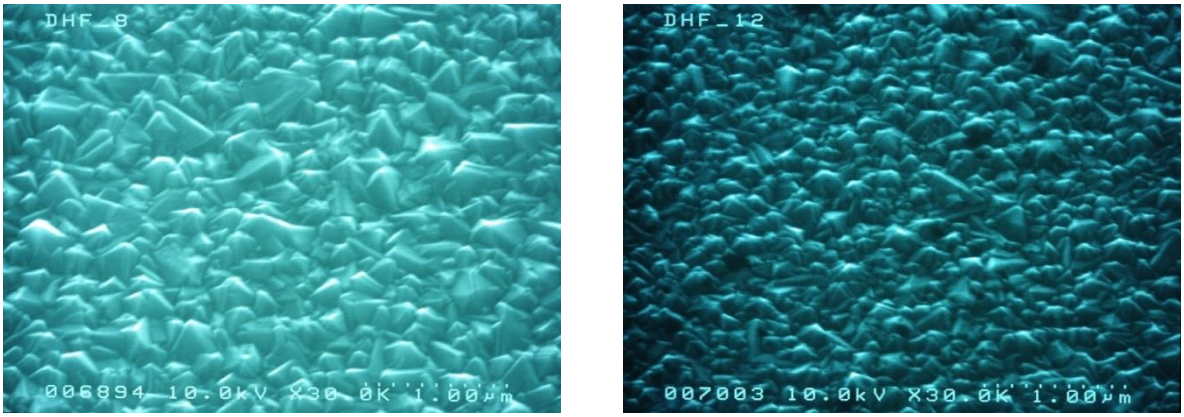

Fig. 31: Comparison of morphology between DHF 8 and DHF 12

Raman spectroscopy with different wavelengths was used in order to investigate the bonding environment. The samples were sent to a partner at the Hungarian Academy of Science, Budapest, where the measurements were carried out with a Renishaw 1000 Raman spectrometer attached to a microscope. A 785 nm laser diode and a 488 nm line of an Ar ion laser served as excitation sources. Firstly spectra from samples DHF 4, DHF 8 and DHF 12 were taken with 488 nm excitation wavelength, which showed the characteristic diamond peak at 1332 cm^{-1} (Fig. 32). In addition to the diamond line, some additional peaks related to non-diamond carbon phase can be seen:

- the well-known graphite-related G and D bands at 1570–1600 cm^{-1} and about 1350 cm^{-1}, respectively, originating from sp^2 -bonded material in the grain boundaries;
- peaks at 1150-1180 cm^{-1} and ca. 1460 cm^{-1} stemming from trans-polyacetylene-like structures, which are observed in the amorphous grain boundary material of nanocrystalline diamond [114];

- the G-peak for DHF 12 appears at higher wavenumbers than for DHF 4 and DHF 8, which may be a consequence of the different pretreatment/nucleation density. Since the Raman sensitivity for sp^2-carbon by 488 nm excitation is roughly 50 times that for diamond [115] it can be concluded that although containing some sp^2-bonded material, all samples under investigation consist predominantly of diamond.

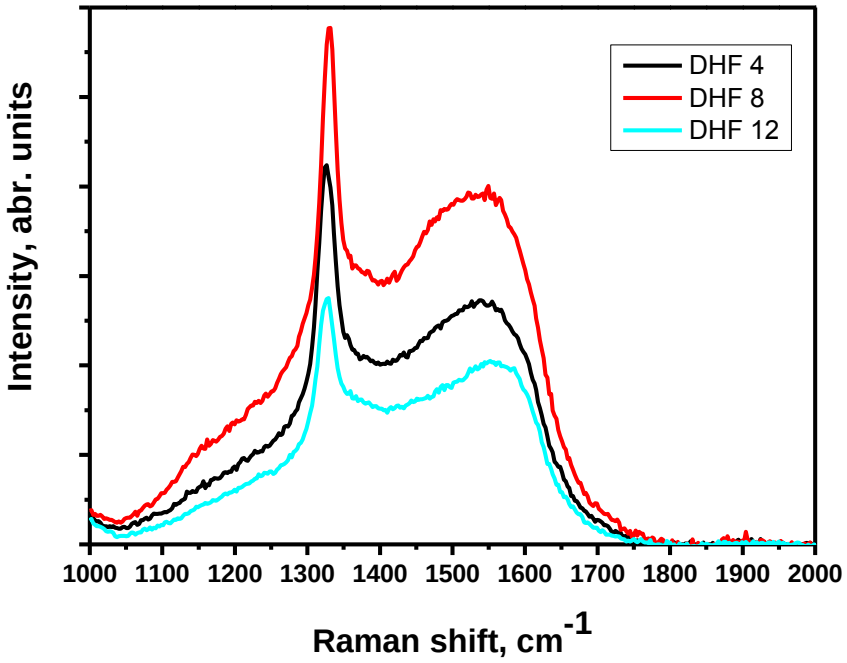

Fig. 32: Raman spectra of DHF 4, DHF 8 and DHF 12, obtained with 488 nm excitation

The spectra taken with 785 nm excitation are shown in Fig. 33. They are dominated by two peaks:

- The diamond line which is still positioned at about 1332 cm^{-1}. This is in agreement with the literature;
- On the left side of the diamond line the graphite-related D band can be found. It has increased in intensity with respect to the diamond line and shifted to considerably lower wavenumbers at about 1280 cm^{-1};
- On the other hand, the G band is reduced considerably in its intensity. This is most pronounced for DHF12. Interestingly, for this sample also the visible spectrum in Fig. 32 showed an anomaly, either a shift of the peak or a missing component at lower wavenumbers.

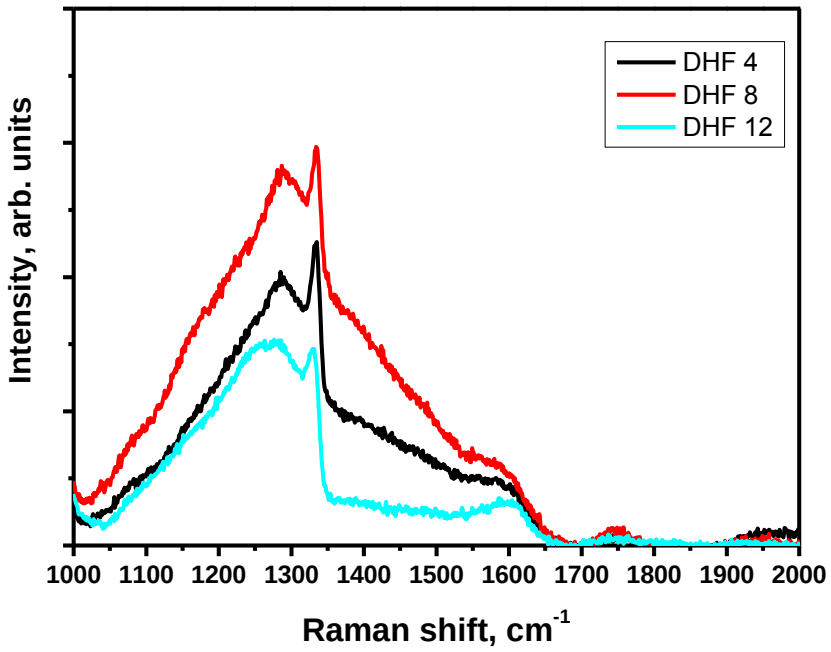

Fig. 33: Raman spectra of DHF 4,8 and 12, obtained with 785 nm excitation

A number of samples have been sent to partners at the Institute for Health and Consumer Protection, Ispra, Italy for XRD analysis. The measurement were performed with Philips XRD equipment, with 0.15418 nm Cu Kα wavelength, a grazing angle of υ = 0.5 ° and a step width of 0.2 ° (Fig. 34).

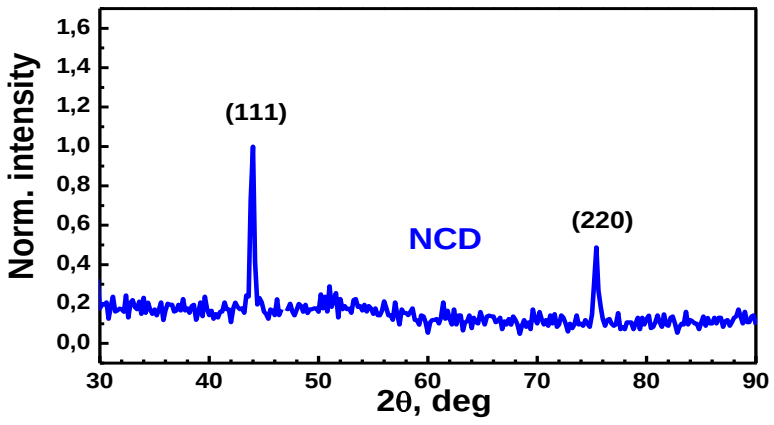

Fig. 34: XRD pattern of DHF 1

The typical XRD pattern shows the (111) and (220) reflections of diamond at 2θ = 44.0 ° and 2θ= 75.4 °, respectively. The Full Width at Half Maximum (FWHM) is on the order of 0.3°. If one applies the Debye-Scherrer formula one gets for the average grain size d:

$$\mathrm{d} = \frac{360\,^\circ}{2\pi}\frac{k\lambda}{FWHM cos\theta} = \frac{360\,^\circ}{2\pi}\frac{0.89*0.15418}{0.3\,^\circ \cos(22\,^\circ)} = 28\ \mathrm{nm},$$

where k is a dimensionless shape factor, λ the X-ray wavelength, θ the Bragg angle.

This means that the average crystallite size must be larger than 28 nm. It must be considered that the crystallite size depends on two major factors: on the one hand on the nucleation density and on other hand on the deposition time. The first factor is responsible for the crystallite width and the second for the height, i.e. the film thickness. In our case the thickness of DHF 1 is about 930 nm. This means that the estimated size is assigned to the width. The estimated size of diamond crystallites from the SEM top view images (Fig. 28-31) is larger than the calculated one. As explained in Chapter 4, the grain sizes of NCD increase with the thickness according to the van der Drift model, i.e. the tops of the largest crystallites appear on the surface.

The activation energy for the growth of NCD films was determined for series of experiments performed at different substrate temperatures (as summarized in Table 5).

Table 5. Growth rates of NCD films deposited at different temperatures

Sample	Temperature, K	Deposition time, min	Thickness, nm	Growth rate, nm.min^{-1}
DHF 1	1115	180	930	5.3
DHF 2	1148	30	160	5.2
DHF 5	1195	180	920	5.1
DHF 9	973	180	350	1.9
DHF 10	878	180	190	1.05
DHF 11	776	180	80	0.44

The activation energy is defined as the minimum energy that must be put to a system in order to proceed a reaction. The activation energy can be thought of as the height of the potential barrier separating two minima of potential energy (of the reactants and of the products of the reaction). The Arrhenius equation expresses the growth rate V_g as a function of the activation energy E_a and the temperature T:

$$V_g = V_0 \exp\left(-\frac{E_a}{k_B T}\right)$$

where V_0 is the maximal growth rate, k_B the Boltzmann constant (8.61×10^{-5}eV), T the temperature (in K).

On the other hand the growth rate can be determined (like in Table 5) as the average film thickness d per time interval t.

$$V_g = \frac{d}{t}$$

According to the Arrhenius presentation for the calculation of the activation energy, the correlation between the Naperian logarithm of V_g and the reciprocal value of the substrate temperature in Kelvin must be represented. For this purpose the Arrhenius equation must be logarithimized:

$$\ln V_g = \ln V_0 - \frac{E_a}{k_B}\frac{1000}{T}$$

From the Arrhenius presentation of the growth rate in Fig. 35, two different groups of samples can be distinguished:

- Samples DHF1, DHF2 and DHF 4 (squares in Fig. 35) where the growth rate decreases very slightly with temperature;
- Samples DHF9 – DHF11 (dots) with a strong increase of the growth rate with T_S which follows fairly good an Arrhenius behavior.

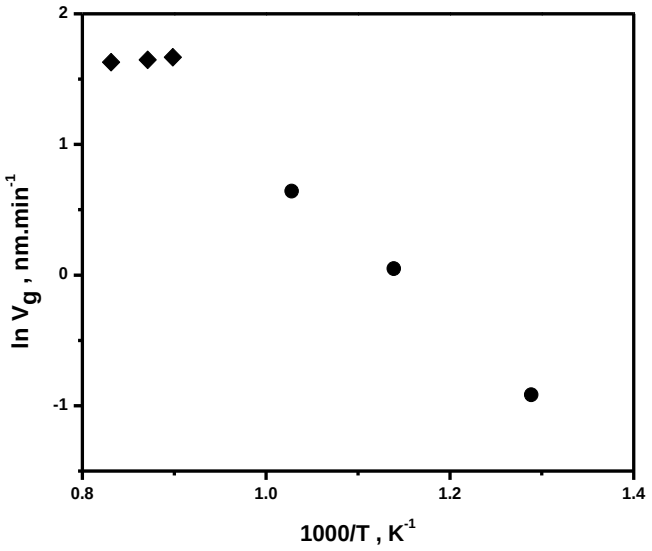

Fig. 35: Arrhenius presentation of the growth rate of NCD films prepared by HFCVD

The growth rates of the first group are as expected in generally higher than those of the second one , ascribing to the much higher substrate temperatures. The estimated value of the activation energy is 0.45 eV, which corresponds to the literature data [116,117]. A previous work has determined the activation energy for UNCD to be lower about 0.25 eV, which also fits to the literature [116,117].

6.3. Random and site-controlled deposition of single diamond crystallites

The next step in the investigation on nanocrystalline diamonds was the deposition of single nanocrystallites. There were two different strategies: the first was random deposition of crystallites (using diverse pretreatment ways) and the second one was deposition on pre-patterned silicon wafer (here the pretreatment procedure was also modified), the so called site-controlled deposition. Changing the pretreatment procedure aiming to lower the nucleation density, this is the first factor for the crystallite size (no spatial constrains by growth). The second one, as mentioned above, is the deposition time, so the deposition time was shortened from three hours to thirty minutes. With an average growth rate up to 5.3 nm.min^{-1} , the maximal growth rate determined from previous experiments,there was no chance the crystallites to coalescence in a closed film. The main goal was achieving single diamond

nanocrystallites with an average size of 70 to 80 nm, which would be appropriate for incorporation of a single NV center [118]. The first step was to change the diamond fraction in the suspension, where only diamond powder with an average grain size of 0.25 µm was applied. The other pretreatment parameters were kept the same as for the NCD films.

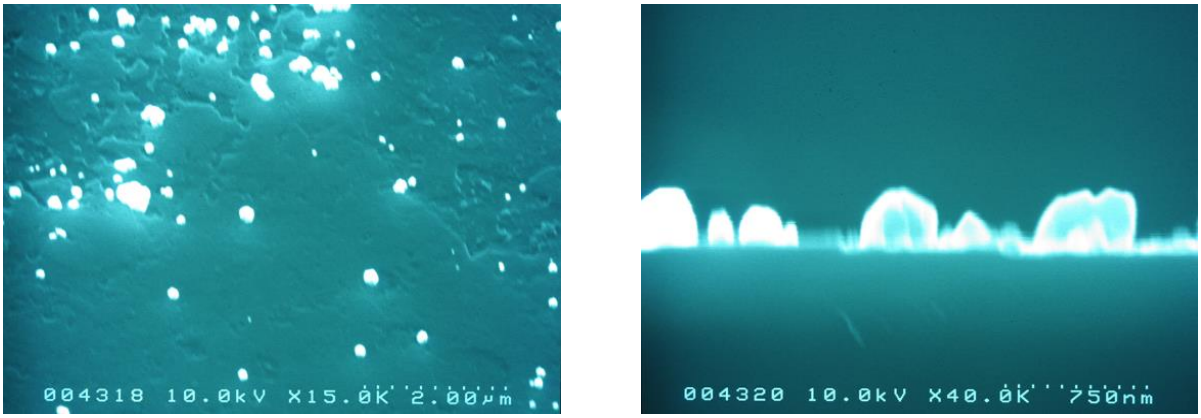

Fig. 36: SEM images of single diamond nanocrystallites DHF 3: a) top view, b) cross-section

The deposition time was 15 min with conditions thesame as for the above explained NCD film DHF 4 (T= 870 ^{o}C). There are several notable differences: The achieved nucleation density was considerably lower; this result was — based on all our previous experiments — to be expected. Moreover, the distribution of the diamond nanocrystals on the substrate is strongly non-uniform. There are several more important informations which can be derived from the images in Fig. 36:

- Most of the crystallites which can be seen are by no means single crystals. Some of them seem to be due to the coalescence of adjacent nuclei, others are probably the results of crystal defects (stacking faults);
- The maximum height of the crystallites shown in Fig. 36 is 330 nm. This is roughly one third of the thickness of DHF4 grown under the same conditions but with a much higher nucleation density. On the other hand, the deposition time was only 15 min. Thus the deposition rate is about 22 nm.min^{-1}, which is much higher than the rates of the corresponding samples of about 5 nm.min^{-1}. A possible reason for this is the large free space on the surface between the growing crystallites. Thus growth species from a large area can diffuse over the surface and finally join one of the few existing nuclei (e.g. crystallites);

- The crystallites possess neither the same shape nor the same height (the latter may be due to different incubation times).

From these results it can be concluded that starting diamond growth from a rather low density of randomly created nucleation sites is not a technique suited for the fabrication of ordered arrays of diamond nanopilars, which will be one of the further tasks of this work – the nucleation as well as crystallite shape are not uniform.

For site-controlled growth of diamond nanocrystallites pre-patterned wafers (as shown in Fig. 37) have been used. Silicon (100) substrates were patterned by electron beam lithography (EBL) with sub-100 nm diameter holes with various periods between 200 nm and 1 µm. The silicon surface was coated with positive tone electron beam resist PMMA; then the holes were defined on the resist by single pixel dot exposure. After the resist development the holes were etched to a depth of 30-40 nm in the silicon substrate using an optimized dry inductively coupled plasma (ICP) etching process involving SF_6 and CHF_3. After the lithography step the resist was removed by soaking the sample in acetone for two minutes; thereafter the sample was thoroughly cleaned with standard laboratory solvents as well as in oxygen plasma asher to remove any organic contaminants left after the process.

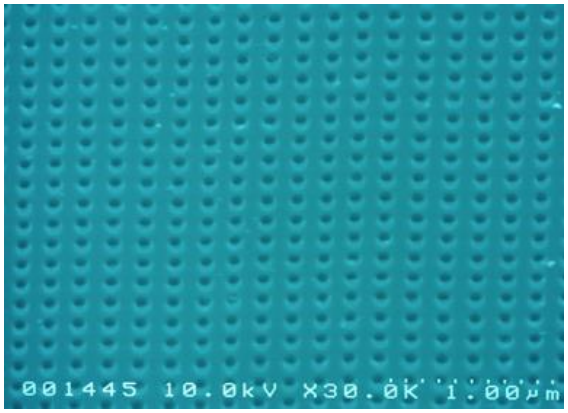

Fig. 37: SEM image of pre-patterned silicon wafer

The pretreatment was modified in order to create nucleation sites only in the pre-patterned holes, allowing growth of ordered arrays of diamond crystallites. The pretreatment time was reduced to only five minutes, followed by 30 sec etching in ammonium fluoride buffered etching solution to remove nuclei, positioned not in the holes. The deposition time remains 15 minutes like for DHF 3. The SEM images (Fig. 38) reveal some interesting facts:

- The pattern of the holes is clearly distinguishable in all pictures;
- Many of the holes are decorated with diamond crystallites;
- On the other hand, not all holes have served as nucleation sites;
- Despite the efforts to create nucleation sites only in the holes, diamond nucleation has also taken place in between the holes;
- The crystallites grown over the holes are by no means perfect. In many cases, more than one crystallite has grown, in other cases there are strong hints at twinning.

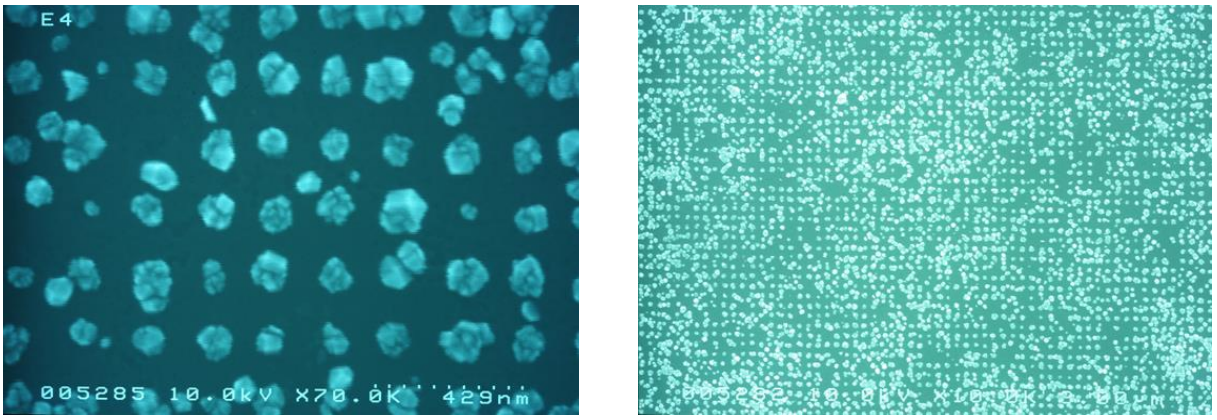

Fig. 38: SEM images of site controlled grown diamond nanocrystallites (DHF 6)

6.4. Ultrananocrystalline diamond films by MWCVD

Ultrananocrystalline diamond films were deposited in ASTEX MWCVD set up, which includes a stainless steel reactor with water-cooled walls (Fig. 39).

The reactor is connected to turbo molecular and rotary pumps which provide a base pressure of about 10^{-3} mbar. The substrates were placed on a movable graphite holder inside the chamber which was inductively heated by a copper coil within the holder. The working gases (CH_4 and N_2) were introduced in the upper part of the chamber (above the substrate holder), their flows were regulated by mass-flow controllers. The signal from the MW plasma generator (*Astex Inc.*, 800 W, 2.45 GHz) was introduced by an antenna with a variable length into the chamber through a quartz window at the top of the reactor.

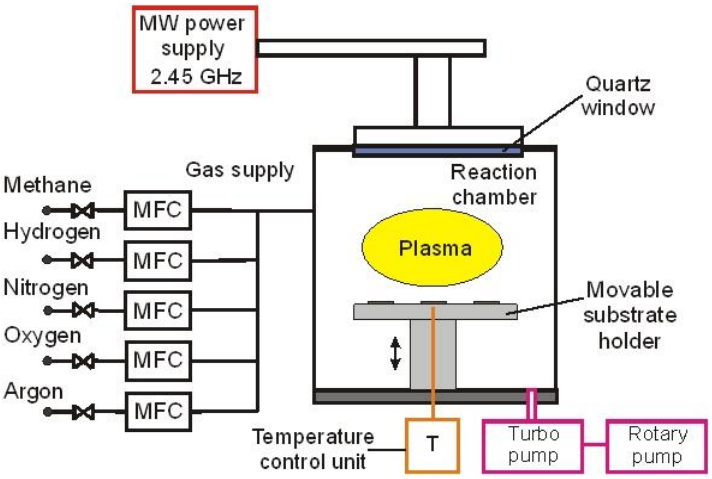

Fig. 39: Scheme of MWCVD set up

The process parameters were as follows: gas mixture 17 % methane and 83 % nitrogen (total gas flow of 300 sccm), working pressure of 23 mbar, substrate temperature 575 °C and deposition time of 360 min.

The SEM image (Fig. 40) reveals the typical UNCD structure (so called „cauliflower— structure).

Fig. 40: Top view SEM image of ultrananocrystalline diamond film

All UNCD samples were deposited at the same conditions and the film thickness is assumed to be around 1 μm based on previous investigations. After determining its morphology the reference sample was studied in order to confirm its crystallinity and bonding environment. Both XRD and Raman results were compared to those of NCD film (Fig.41).

In both XRD patterns, two peaks are clearly recognizable at 2θ = 44.0° and 2θ = 75.4°, which can be identified with the (111) and (220) reflections of diamond (according to JCPDS card 6-675). From the figure it can be seen that the peak

positions are the same for both films; there are, however, differences with respect to the intensity ratio of the two peaks. Most striking are the differences of the widths of the peaks for both types of films. The peaks of the UNCD film are much broader than those of the NCD film which is a consequence of the much smaller crystallite size. From the width of the XRD reflections the average crystallite size of the UNCD films can be calculated by the Debye-Scherrer formula. With a Full Width at Half Maximum (FWHM) estimated to be around 2.7°, the calculated mean crystallite size is 4 nm.

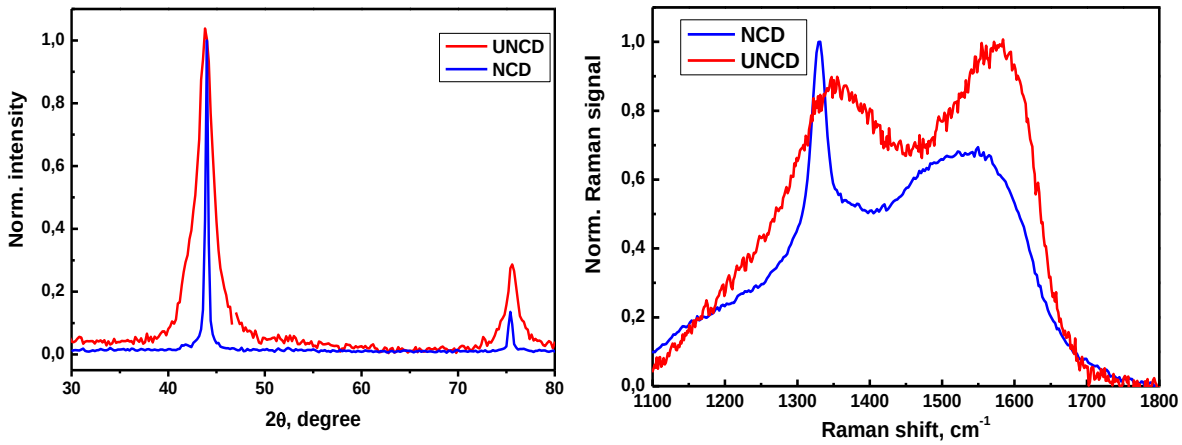

Fig. 41: Comparison of XRD and Raman spectra of UNCD and NCD

From the normalized Raman spectra (excitation wavelength of 488 nm) presented in Fig. 41, the following differences between the two types of films are evident: The diamond line at 1332 cm^{-1} is only visible for the NCD film. In the spectrum of this film also a rather broad G-band (around 1500 cm^{-1}) and the also graphite related D band at about 1350 cm^{-1} are observed. Taking into account that the Raman cross section for sp^2 bonded carbon is about 50 times higher than that of sp^3 bonded carbon, and also the nanocrystalline character of the film which implies a certain amount of sp^2 - grain boundary material, the spectrum of the NCD film can be explained. The diamond line is not present in the Raman spectrum of the UNCD film in Fig. 41. This is a consequence of the very small grain size (confirmed by the XRD measurements). This spectrum can be deconvoluted into four bands two of which (the G and D bands) are related to the carbon matrix, the other two to the grain boundary material between matrix and crystallites [119].

7. TEMPERATURE DEPENDENCE OF DIAMOND GROWTH AND PROPERTIES

In this chapter the temperature dependence of the growth and properties of NCD and UNCD films will be presented. The obtained films were thoroughly characterized concerning their morphology and structure by scanning electron microscopy (SEM) and concerning their crystalline properties by X-ray diffraction (XRD). The composition was analyzed by X-ray photoelectron spectroscopy (XPS), whereas XPS and Raman spectroscopy were applied to get information on the bonding structure.

7.1. Dependence of the NCD films on the temperature

After establishing the standard conditions for growth of nanocrystalline diamond films, a series of experiments with lowering the substrate temperature during the deposition have been carried out. The purpose of this investigation was to obtain information about at which lowest temperature high quality nanocrystalline diamonds still can be produced. Reducing the substrate temperature can simplify the integration of diamond films in devices with temperature sensitive materials, like e.g. III/V semiconductors.

For all experiments from this series the same standard pretreatment procedure (two types of diamond powders in pentane solution for one hour in ultra-sonic bath) was used. All deposition parameters were also kept constant, except the substrate temperature. The first temperature chosen was about 700 °C, because it is known from the literature, that this is the lowest temperature [120] for obtaining high quality diamond films. The SEM image (Fig. 42a) reveals the facettes typical for nanocrystaliine structures. However, there seem to be small regions between the facetted crystals without any structure (amorphous regions). The same impression is

confirmed from the cross-sectional image (Fig 42b). Such regions are clearly not present in the corresponding images of sample DHF8 (grown at a temperature of 870 °C). It can be also noticed, that the crystallite size is decreased, compared to the above-mentioned sample and some crystallites tend to agglomerate, building „monster crystallites".

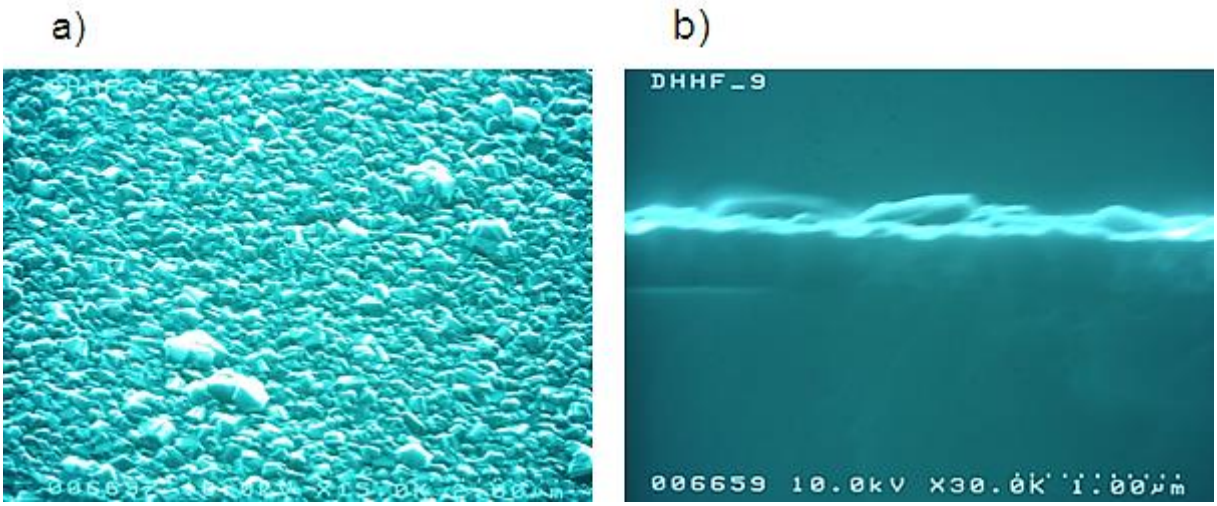

Fig. 42: SEM images of DHF 9 (700 °C): a) top view, b) cross-section

The changes become even more pronounced if the temperature is lowered to 607 °C. The crystallite size has decreased even more and there are agglomerates of different sizes. The facets are not well defined, there is no more clear texture present (Fig. 43a). Most important, however, is the observation that the film appears no longer homogeneous on the micrometer scale, like it can be seen from the SEM image with lower magnification (Fig. 43b).

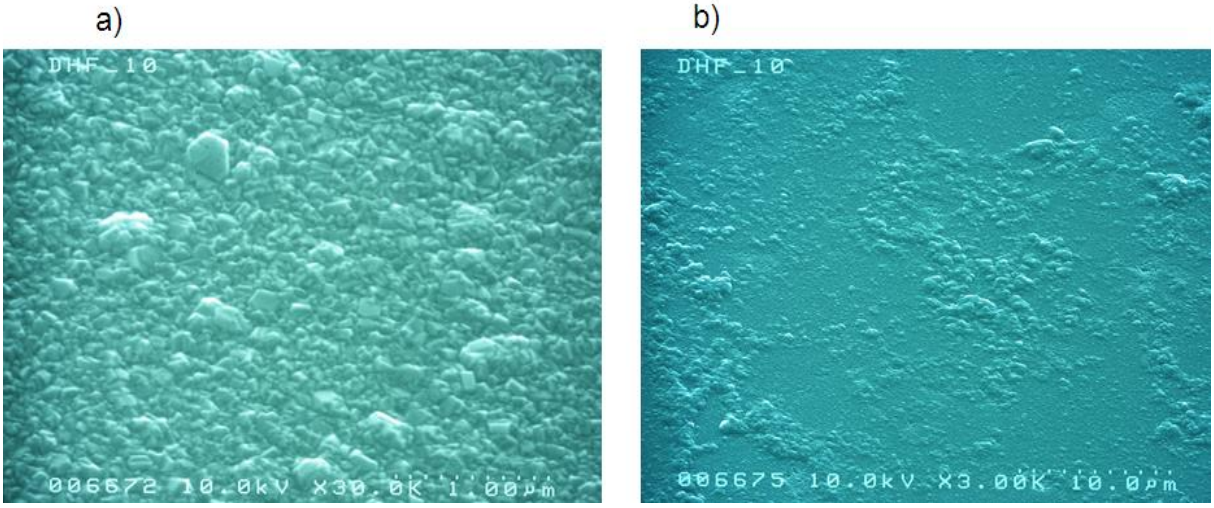

Fig. 43: SEM images of DHF 10 (607 °C): a) higher resolution, b) lower resolution

Sample DHF11 was deposited at 500 °C only. From both SEM pictures (Fig. 44 a and b) it can be seen, that this film is not closed which is not surprising taking into account the very low growth rate and the small thickness of this film of 80 nm only. A clear texture can not be determined, on the other hand the crystallites do not possess the typical rounded features of the UNCD samples. It can be assumed, that the film obtain at such low temperature (leading to UNCD formation), but otherwise at conditions for NCD growth (gas phase composition), is somewhat in between. It is clearly not ultrananocrystalline, but it is also clearly not high quality single crystallites but rather medium quality NCD features.

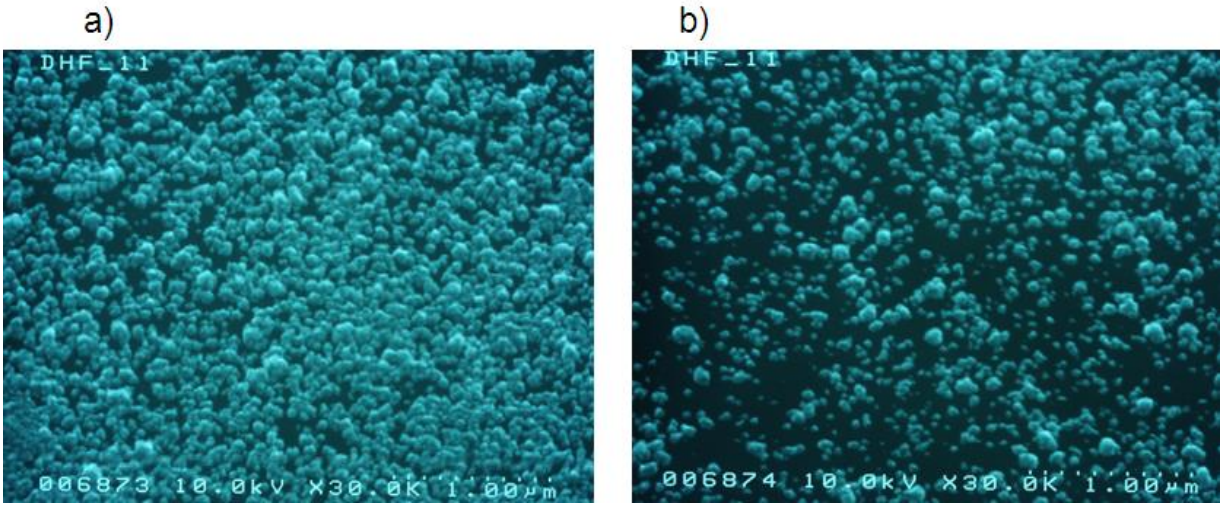

Fig. 44: SEM images of DHF 11 (500 °C): a) top-view, b) cross-section

The crystalline properties of all samples have been investigated by grazing incidence XRD with υ =1°. Figure 45 shows the development of the (111) and (220) peaks, which are clearly discernable at 2θ = 44.0 ° and 75.4 °, respectively, as a function of the substrate temperature. There are several observations to be made in this diagram which deserve discussion: first of all, the positions of the reflections are constant and in agreement with JCPDS card 6–675 of diamond. This means that stress plays no role for the whole set of samples.

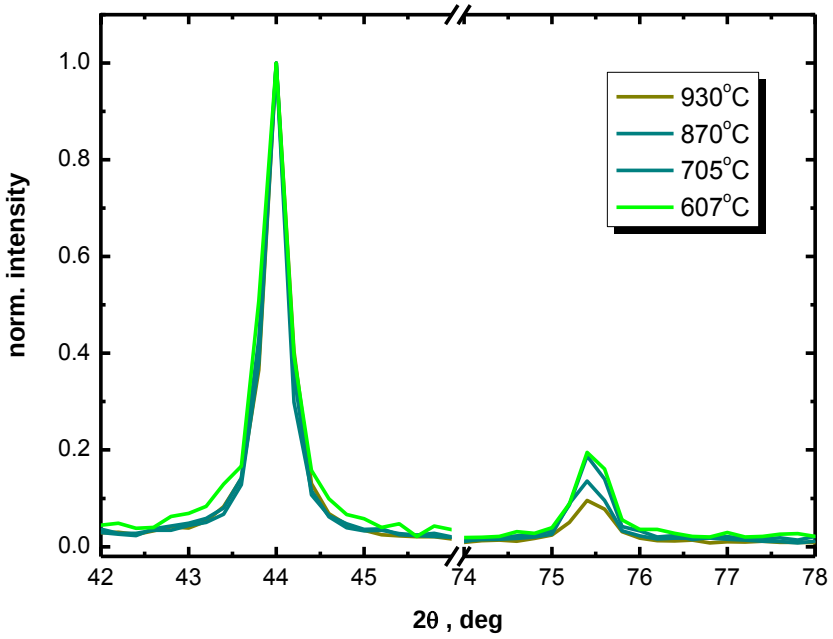

Fig. 45: X-ray diffraction patterns of NCD films as function of the temperature

Second, the ratio of the diamond (220) and (111) reflections as a function of the substrate temperature for the NCD films is worthy for discussion. According to the JCPDS card 6-675 for randomly oriented diamond powders this ratio is 0.25 (indicated by the dashed horizontal line in Fig. 46). For the NCD films, two observations can be made:

- In all cases I_{220}/I_{111} is below the line,
- There is a significant decrease of I_{220}/I_{111} with temperature.

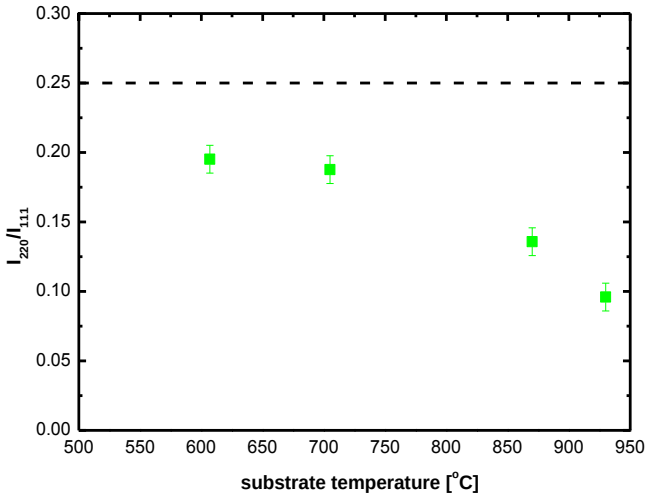

Fig. 46: The intensity ratio I_{220}/I_{111} determined from the XRD patterns of the NCD films as a function of the substrate temperature

Taking both observations together this means that the NCD films possess a texture, and that the degree of the texture increases with the temperature. As the relative intensity of the (111) peak increases, the films are showing pyramidal crystallites, i.e. (111) facets, which is in agreement with the observations from the SEM images of the high temperature samples shown above. This observation confirms once again the van der Drift model [121]: The fastest growing crystallites will survive. It has been previously shown that the ratio of the growth velocities v_{220}/v_{111} critically depends on parameters such as the substrate temperature and the methane concentration and even on impurities in the gas phase [122,123].

To investigate the bonding structure of the obtained films they were analyzed with Raman spectroscopy. All samples were investigated with wavelengths of 488 nm (2.54 eV) and 785 nm (1.56 eV) (Figs. 47 and 48).

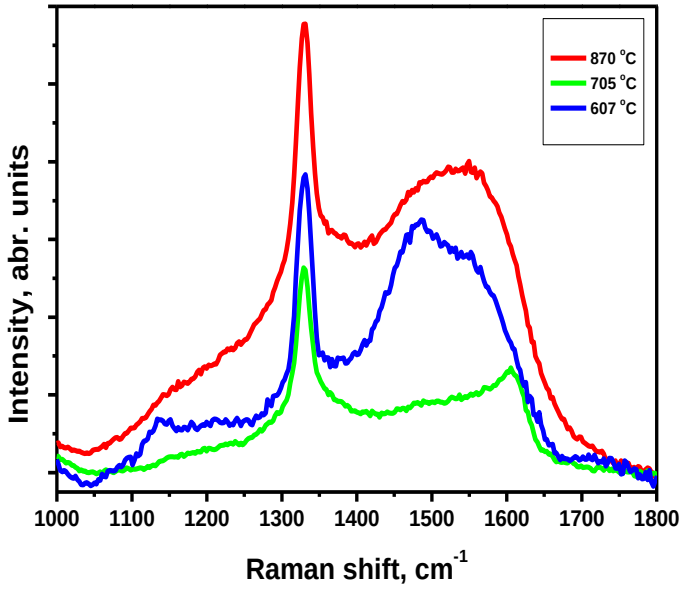

Fig. 47: Raman spectra obtained at 488 nm as a function of the temperature

The Raman spectra obtained at 488 nm show the following features:

- The fundamental diamond line at 1332 cm^{-1} ;
- The graphite-related G (at 1350^{-1} cm) and D (at 1570^{-1} cm) bands;
- Peaks related to trans-polyacetilene (TPA) at about 1160 and 1480 cm^{-1}. These peaks are, however, clearly present only for the low temperature film.

First of all it has to be stated that the ratio of sp^3 to sp^2 bonded material does not change drastically in the temperature range investigated. Besides the diamond line, all features present in the spectra of this figure stem from sp^2 material. Although the position and the shape of these features vary considerably, the intensity ratio of all sp^2 and sp^3 related peaks, respectively, is not affected very much. However, there are drastic changes in the nature of sp^2-bonded materials in these films from 870 to 607 °C. In the first case, the spectrum closely resembles that of all standard diamond films. Besides the diamond line, the G peak and the D peak are present. At 607 °C, in contrast almost all sp^2 material seems to be present as TPA-like grain boundary material typical for NCD films. The intermediate spectrum obtained from the 705 °C sample shows a kind of transitional character. The TPA peaks are already present although very faint, there is also a very strong shift of the G band which is accompanied by a sharpening, which show that the typical graphite-like spectrum is no longer present.

The conclusions drawn from this diagram are corroborated by the 785 nm spectra of these films which are presented in Fig. 48.

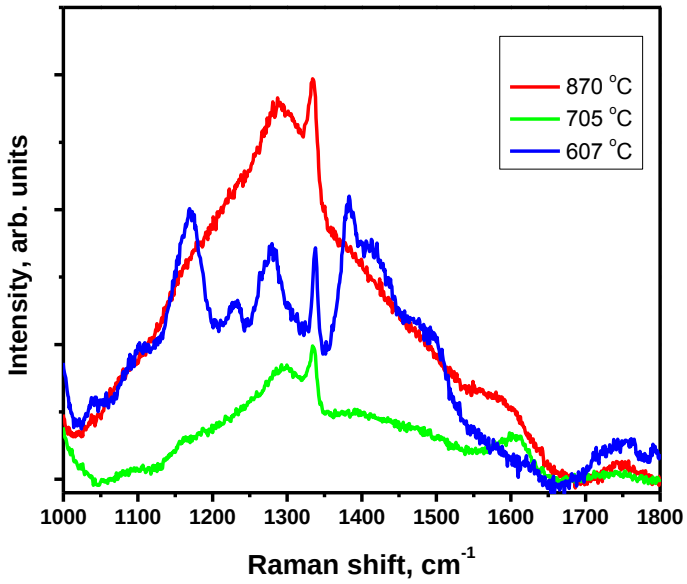

Fig. 48: Raman spectra obtained at 785 nm as a function of the temperature

Again, a drastic change of the nature of the spectra can be observed if the temperature is lowered from 870 via 705 to 607 °C. The diamond line is still present in these spectra but not as dominant as in Fig. 47 which is a consequence of the

lower excitation energy leading to an even lower Raman cross-section for sp^3 carbon. For the remaining peaks which all stem from sp^2 carbon, the same observations as from Fig. 47 can be made: There are gradual changes if the temperature is lowered to 705 °C but substantial changes if it is further lowered to 607 °C. The two spectra obtained at higher T_S have a clear resemblance to the spectra of standard diamond films while the spectrum of the 607 °C film is completely different. It seems to consist of ‚peaks‘‘ rather than of ‚bands.‘‘ This can be explained as follows: the grain boundary material does no longer consist of more or less homogeneous sp^2 material of slightly different bond lengths and angles but rather of smaller structures of different sizes and shapes (rings or chains) giving rise to these distinct peaks. It is tempting to assign the peaks at least in part to the TPA-like material becoming apparent in the 488 nm spectra in Fig. 47.

From the SEM images presented in Fig. 43 it is evident that sample DHF10 is rather inhomogeneous. In order to get more insight in the nature of this inhomogeneity, some additional Raman measurements (using 785 nm excitation wavelength) with a small spot size (1 µm) were performed on different positions of DHF10 (Fig. 49). From the SEM image of this film in Fig. 43 it can be concluded that a 1 µm spot includes several tens or even hundreds of nanocrystals. From the XRD measurements discussed above an average crystallite size of some tens of nm can be inferred, in agreement with the SEM image. Thus if the films were homogeneous on a larger scale with inhomogeneities only in the nanometer range (diamond nanocrystals, different grain boundary materials) all Raman spectra should be more or less identical. As this is not the case one has to conclude that the film is inhomogeneous on a larger scale. This is in agreement with the SEM image shown in Fig. 43b. Furthermore the inhomogeneity of this film can at least in part be attributed to differences in the shape and the size of sp^2 clusters forming the grain boundary material.

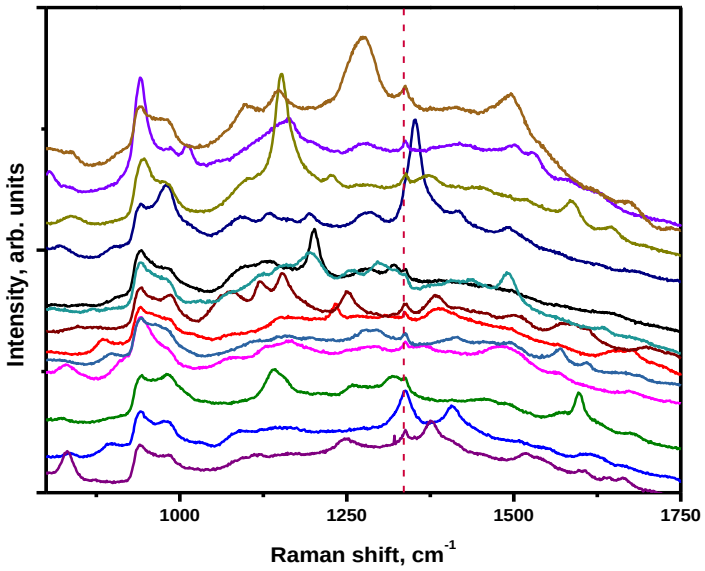

Fig. 49: Raman spectra taken on different positions of DHF 10 (607 °C)

The surface composition of the NCD films deposited at difference temperatures has been investigated by XPS. The results of these measurements are summarized in Table 6. The main information from this table is that with one exception the surfaces of all films are very clean. This is a consequence of the fact that all NCD samples are hydrogen terminated and that hydrogen terminated diamond films are chemically extremely inert [124, 125]. From the table it can be seen that all samples possess a slight oxygen contamination of 1–2 at.%, except for the sample, deposited at the lowest temperature DHF 11. Here the surface concentration of silicon and oxygen are about 10 at.% each. This observation can easily be explained by the fact that this film is not closed (see the SEM image of the sample in Fig. 44). No nitrogen was found in any of the samples under investigation within the detection limit.

Table 6. Composition of the NCD films investigated by XPS.

	C, %	O, %	Si, %
DHF 8 (870 °C)	98.6	1.3	-
DHF 9 (705 °C)	97.7	1.9	-
DHF 10 (607 °C)	99.1	0.2	-
DHF 11 (503 °C)	79.9	9.7	9.9

XPS C 1s core level spectra have been taken from almost all NCD films. A normalized presentation of the core spectra as a function of the temperature is presented in Fig. 50. There are no significant differences between them. Two types of materials are contributing to these peaks: the diamond nanocrystals and the grain boundary material between them, consisting of either C–C or C–H bonds. The light fluctuations on the high binding energy side of the peaks can be attributed to some carbon-oxygen bonds, which can be confirmed by the composition presented in Table 6. There are no differences on the low energy side of the peaks. Possible deviations on the low energy side of the C 1s peaks would mean an increase of the sp^2 content of the films, but no broadening is observed. This means that within the whole set of samples the sp^2/sp^3 ratio is almost constant and it is not affected from the temperature decrease. If one looks at the SEM images of all samples and takes the drastic changes into account which the morphology of the NCD films undergoes in the temperature range investigated, this result is at a first sight rather surprising. But it means that the changes occurring are to be found mainly in the amorphous part of the film.

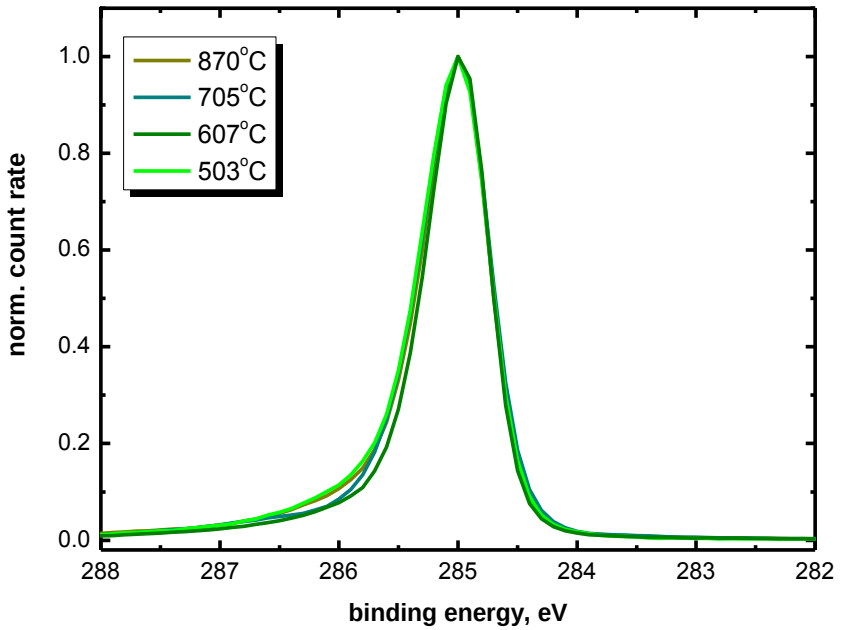

Fig. 50: XPS C1s core spectra of the NCD films as a function of the substrate temperature

.

7.2. Dependence of the UNCD films on the temperature

The ultrananocrystalline diamond films were deposited by microwave plasma-assisted chemical vapor deposition set up as explained in the previous chapter. Also

these samples were pretreated before deposition using a suspension of two diamond powders in an ultra-sonic bath (as explained above). The standard conditions for deposition of UNCD films were used (gas phase composition, pressure, MW power, etc.), only the process temperature was varied.

First, like in NCD case, the morphology was investigated. Fig. 51 (a-d) shows the change of the morphology of the films with decrease of the temperature.

From the SEM pictures of the UNCD films, almost no differences in the morphology of the films can be distinguished for the temperature range from 770 down to 450 °C. As a consequence also the surface roughnesses as determined by AFM measurements are very similar - they range from 9 to 13 nm. The surfaces consist of rounded features of some hundred nm diameter formed by substructures of much smaller diameter, which however, seem to be not homogeneous but to consist of even finer structures. All in all these pictures have at least some similarities to fractals. This is a consequence of the very high rate of secondary nucleation in the case of UNCD growth [126].

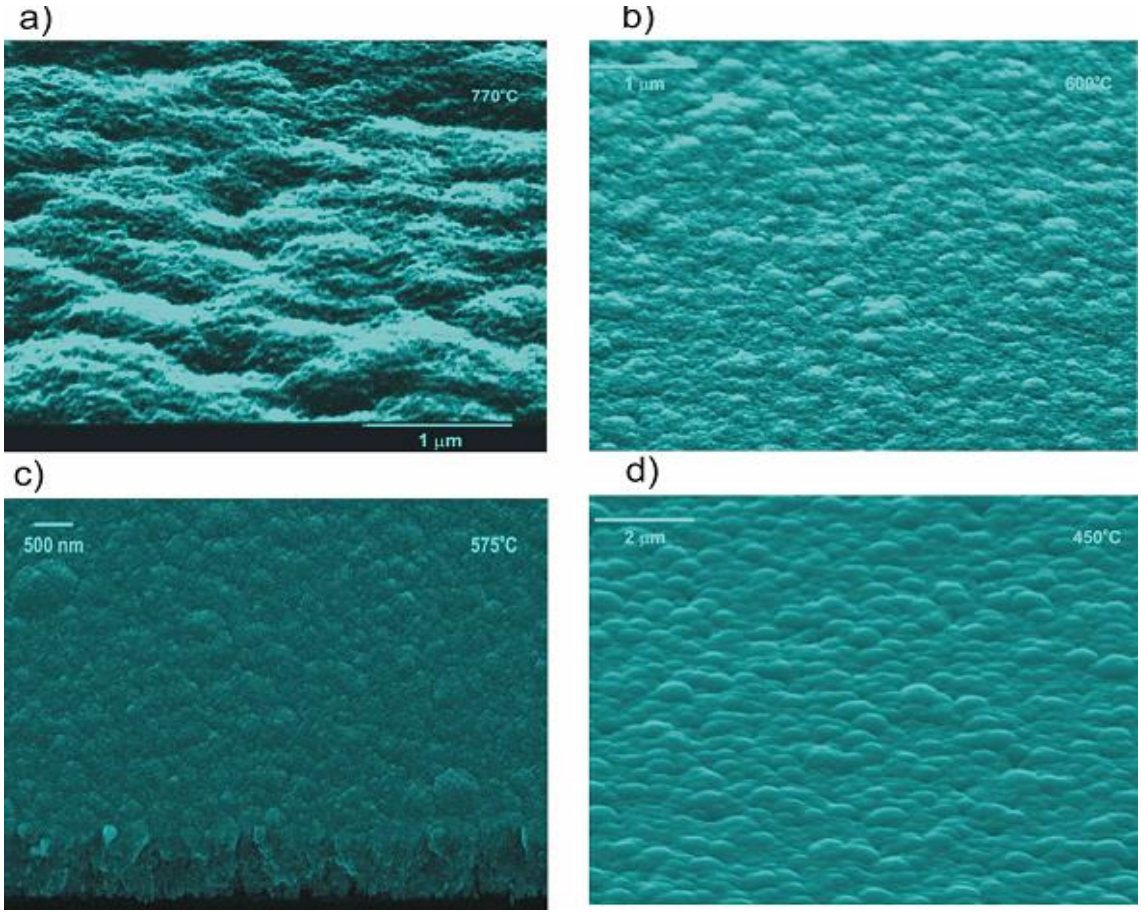

Fig. 51: SEM images of UNCD films deposited at: a) 770 °C, b) 600 °C, c) 575 °C, d) 450 °C

The barely morphology change of the UNCD films compared to the drastic changes of the morphology of the NCD films emphasizes one more time the complitely different nature of these two types of diamond films and their growth mechanisms.

The crystalline properties of the UNCD films were investigated by grazing angle XRD with u = 0.5 °. Two peaks, associated with the (111) and (220) reflections of diamond are clearly discernable at 2θ = 44.0 °and 2θ = 75.4 ° (Fig 52).

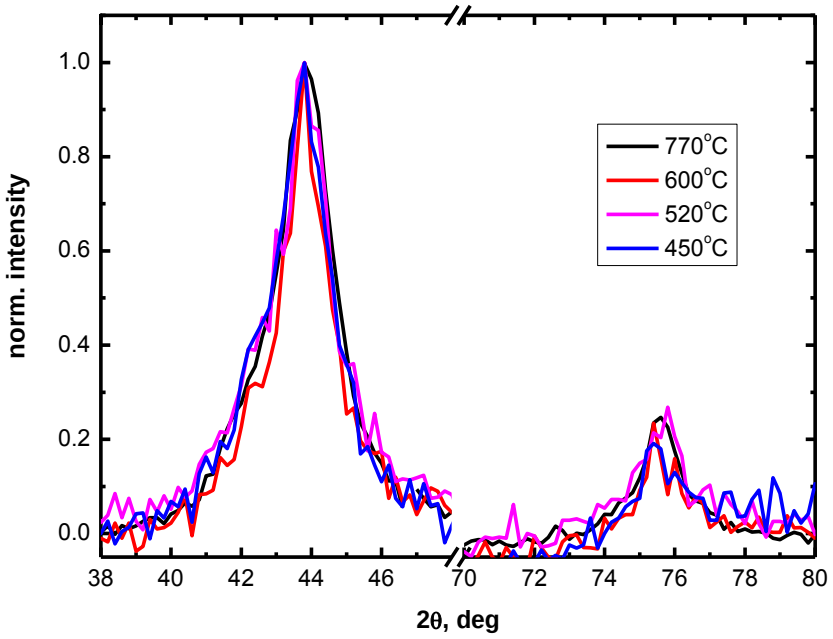

Fig. 52: XRD patterns of UNCD films as function of the temperature

The widths of the peaks are approximately constant, but compared to the NCD the peaks are much broader, ascribed to the smaller crystalline size in UNCD. Another big difference between the two types of films is that the intensity ratio I_{220}/I_{111} stays constant with temperature decrease in contrast to the NCD films (Fig. 53).

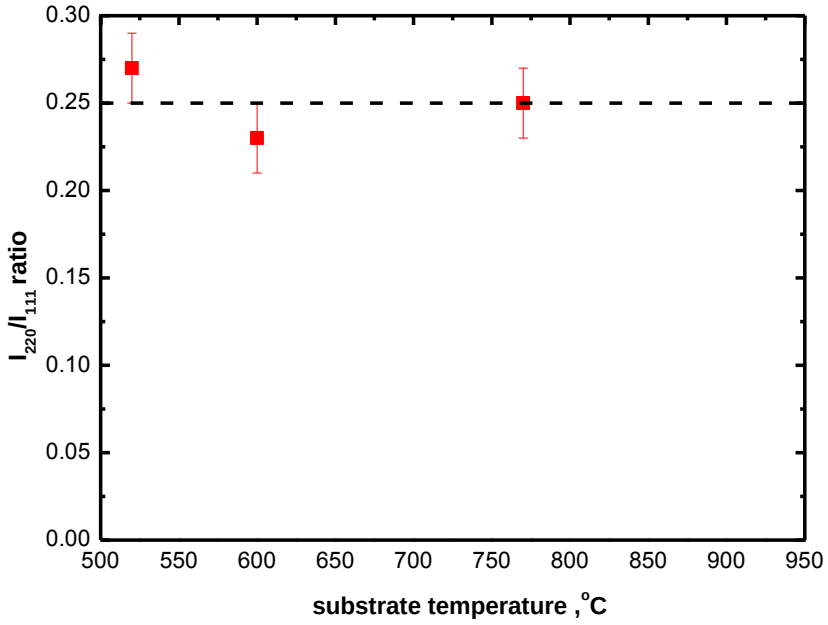

Fig. 53: The intensity ratio I_{220}/I_{111} determined from the XRD patterns of the UNCD films as a function of the substrate temperature

Raman measurements of all UNCD films have been performed with the excitation wavelength of 514 nm (Fig 54).

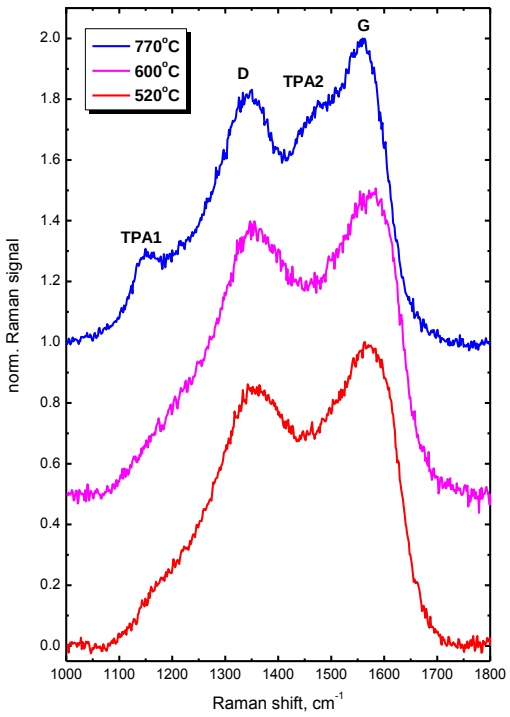

Fig. 54: Raman spectra of UNCD films as function of the temperature

The first striking remark is the absence of the fundamental diamond line at 1332 cm^{-1}. The spectra are dominated by a broad band between 1100 and 1700 cm^{-1} which can be deconvoluted into four contributions:

- The graphite-related G band at 1560–1590 $^{-}$ cm^{-1};
- The graphite-related D band at ca. 1350 cm^{-1};
- The peak labeled TPA 1 at 1140–1190 cm^{-1};
- The peak labeled TPA 2 at ca. 1480 cm^{-1}.

There are only minor differences between the spectra as a function of the temperature. The two TPA-related peaks are most clearly visible for the 770 °C film. Thus from the spectra presented, it can be concluded that in the temperature range investigated the structure of the UNCD films hardly changes in contrast to the NCD films.

The surface composition of the UNCD films of this study has been investigated by XPS. The results of these measurements are summarized in Table 7.

Table 7. Composition of the UNCD films investigated by XPS

	C, %	O, %	N, %
D 98 (770 °C)	95.6	3.6	0.8
D 99 (600 °C)	97.6	2.2	0.8

The main information from this table is that the surfaces of both samples are clean, containing small amounts of oxygen and traces of nitrogen. This, like in the case of NCD film, is a consequence of the hydrogen termination rendering the surface chemically extremely inert [127, 128].

XPS C1s core level spectra have been taken from two UNCD samples of this investigation prepared at different substrate temperatures (Fig. 55). Compared to the C 1s spectra of the NCD samples (Fig. 50) these spectra are much broader. This is due to the fact, that in the case of NCD films, two types of materials are contributing to this peak: the diamond nanocrystals and the grain boundary material between them. In the case of UNCD films there is a third component: the amorphous carbon

matrix. Thus there are three different materials contributing to the C 1s peak of UNCD films, which possess a wide variety of bond angles and bond lengths and may explain the rather large width of this peak.

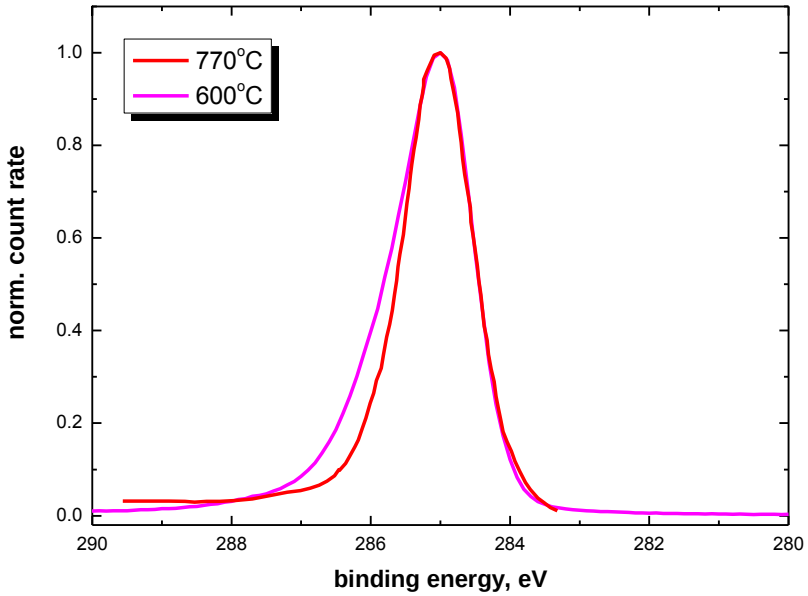

Fig. 55: XPS C 1s core spectra of the UNCD films as a function of the temperature

Concerning only the two UNCD samples, hardly any development with temperature is discernable. There are light fluctuations on the high binding energy side of the peaks and these tails can be attributed to C–N, C–O, and C ═O bonds. Possible deviations on the low energy side of the C 1s peaks are more interesting as a broadening to this side would mean an increase of the sp^2 content of the films, but no broadening is observed. This means that within each set of samples(either NCD or UNCD) the sp^2/sp^3 ratio is almost constant. In the case of the UNCD films it is about 10–15%. For the NCD films it has to be much lower as judged from the overall width of the C 1s peak (Fig. 50). But in both cases it can be inferred (from Figs. 50 and 55) that the sp^2/sp^3 ratio is independent of the substrate temperature.

8. INVESTIGATIONS ON ETCHING MECHANISMS OF NCD AND UNCD LAYERS

In this chapter the optimization of the etching parameters will be presented. All process parameters (ICP power, RF power, oxygen flow, pressure and temperature) were varied and optimized with respect to the quality of the diamond pillars. Primarily silicon dioxide was chosen as a hard mask material, the results were compared afterwards withthose applying gold mask. The etch mechanisms of NCD and UNCD films was compared via simultaneous etching of the both samples without masks.

8.1. Optimizing of the process parameters

After the deposition and thorough characterization, the NCD were used for fabrication of nanopillars. The etching process was optimized with respect to the etching rate, the quality of the nanopillars (verticality of the walls, smoothness, and desired size) and the surface between the pillars by variation of the major process parameters: RF power, ICP power, O_2 flow, working pressure and temperature. For the initial experiments silicon dioxide was chosen as a hard mask and the fabrication process included the following steps (as-shown in Fig. 56): a) deposition of a 250 nm SiO_2 layer as a hard mask, b) deposition of the resist; c) electron beam lithography definition of the nanopillars in the resist; d) reactive ion etching (RIE) of the SiO_2 mask, e) ICP-RIE of the diamond nanopillars with oxygen.

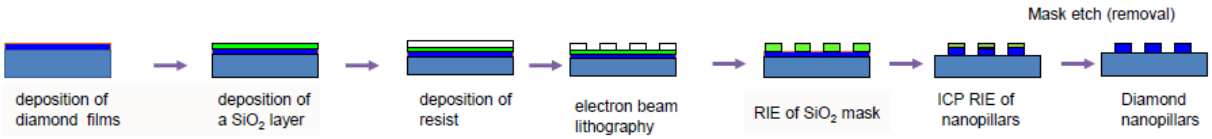

Fig. 56: Scheme of the etching recipe using SiO_2 mask

The structuring of the SiO_2 mask after EBL was performed by RIE in Oxford ICP set up, using the following parameters: RF power of 230 W, ICP power of 0 W, 3 sccm

CHF_3 flow, 5 sccm Ar, 30 °C substrate temperature and working pressure of 26.3 x 10^{-3} mbar.

Based on previous experience, for the start recipe for NCD etching the following parameters were used: RF power of 100 W, ICP power of 1000 W, 10 sccm O_2 flow, 30 °C substrate temperature and working pressure of 13.33×10^{-3} mbar. The SEM images of samples etched using the start recipe show that the desired structure can be achieved but improvement of the topography and especially the removal of the —diamond grass" between the pillars are required (Fig. 57).

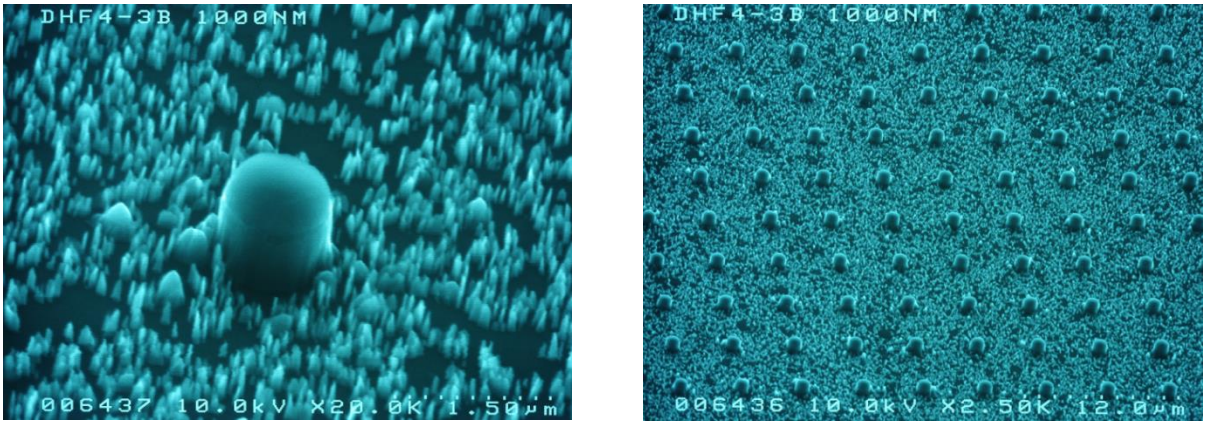

Fig. 57: A single pillar and array of diamond pillars etched with the start recipe

Therefore every parameter of the start recipe was optimized, starting with the RF power, keeping the rest of the parameters constant.

- ***RF power***

The RF power applied to the substrate holder to generate a bias voltage was varied between 50 and 300 W. The two SEM images in Fig. 58 present a field of many structures and a single structure fabricated with the lowest RF power. Both pictures show that all pillars are presented and of similar shape, but on the right picture (with lower magnification) there are many diamond remnants (—diamond grass") observed.

Another feature is that the pillars are taper, which can be easily seen from both pictures although the SiO_2 mask is not yet removed.

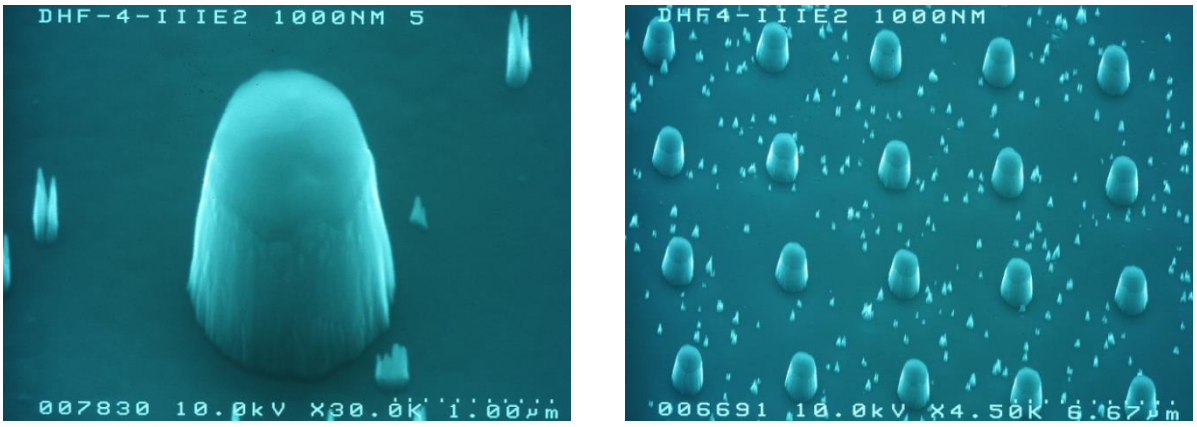

Fig. 58: A single pillar and array of diamond pillars etched with RF power of 50 W without varying the other parameters from the start recipe

The RF power was increased to 100 W and the SEM pictures (Fig. 59) show that the amount of remnants at the bottom between the structures has decreased, but the pillars still have taper shape.

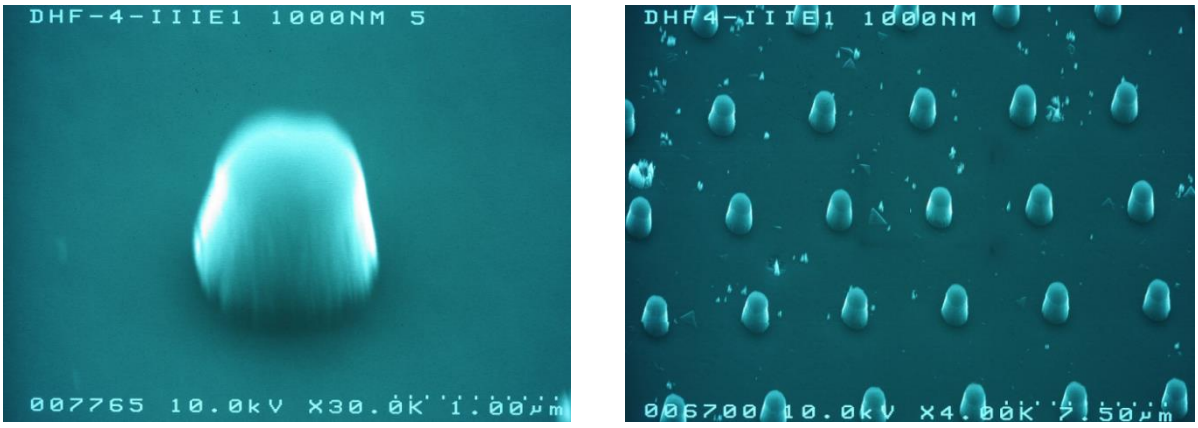

Fig. 59: A single pillar and array of diamond pillars etched with RF power of 100 W without varying the other parameters from the start recipe

Increasing the RF power to 200 W (Fig. 60) leads to further reduction of the ~~-d~~iamond grass" between the pillars. Another important remark from the SEM pictures is that the pillars are not any more tapered and have a columnar shape.

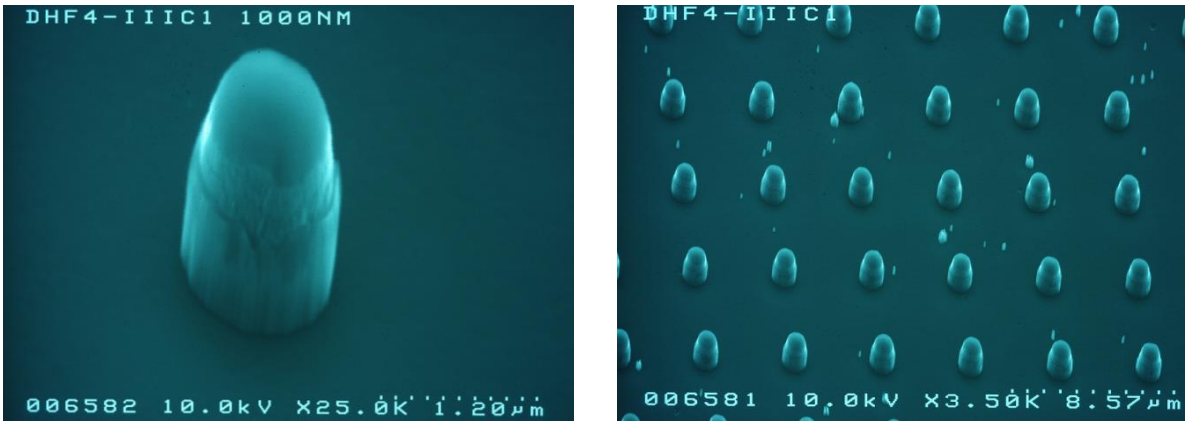

Fig. 60: A single pillar and array of diamond pillars etched with RF power of 200 W without varying the other parameters from the start recipe

Further increase of the RF power to 300 W (Fig. 61) did not lead to improvement of the sample, even there were more diamond remnants and the pillars were tapered, compared to the previous sample (with RF power of 200 W).

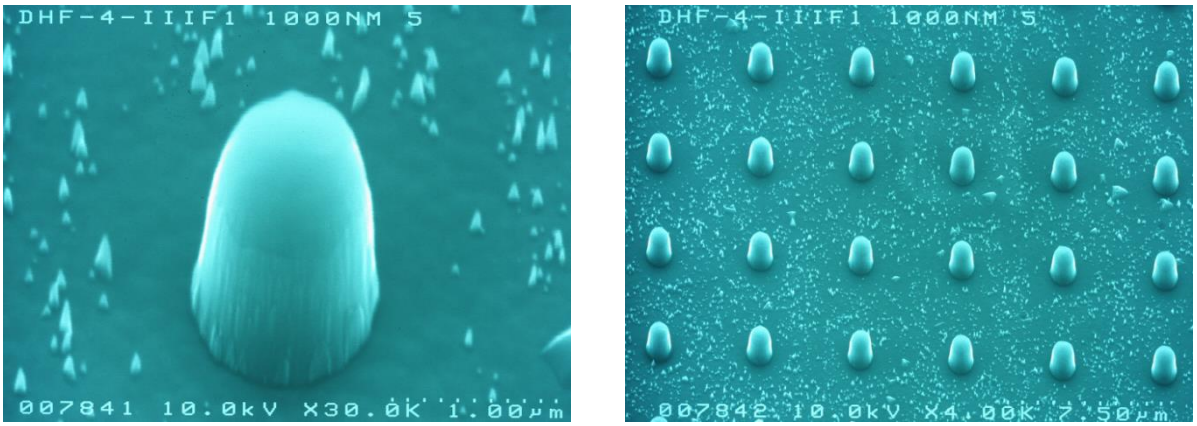

Fig. 61: A single pillar and array of diamond pillars etched with RF power of 300 W without varying the other parameters from the start recipe

As a conclusion it can be stated that, the increase of the RF power from 50 to 300 W resulted in a significant improvement of the shape of the pillar walls and the surface between the pillars. The best results were achieved applying 200 W RF power with smooth and vertical pillar walls and clean surface between the pillars (Fig. 60). This value was chosen for the further experiments.

- ***ICP power***

The SEM images of the samples etched varying the ICP power between 500 and 2000 W are presented in Fig. 62.

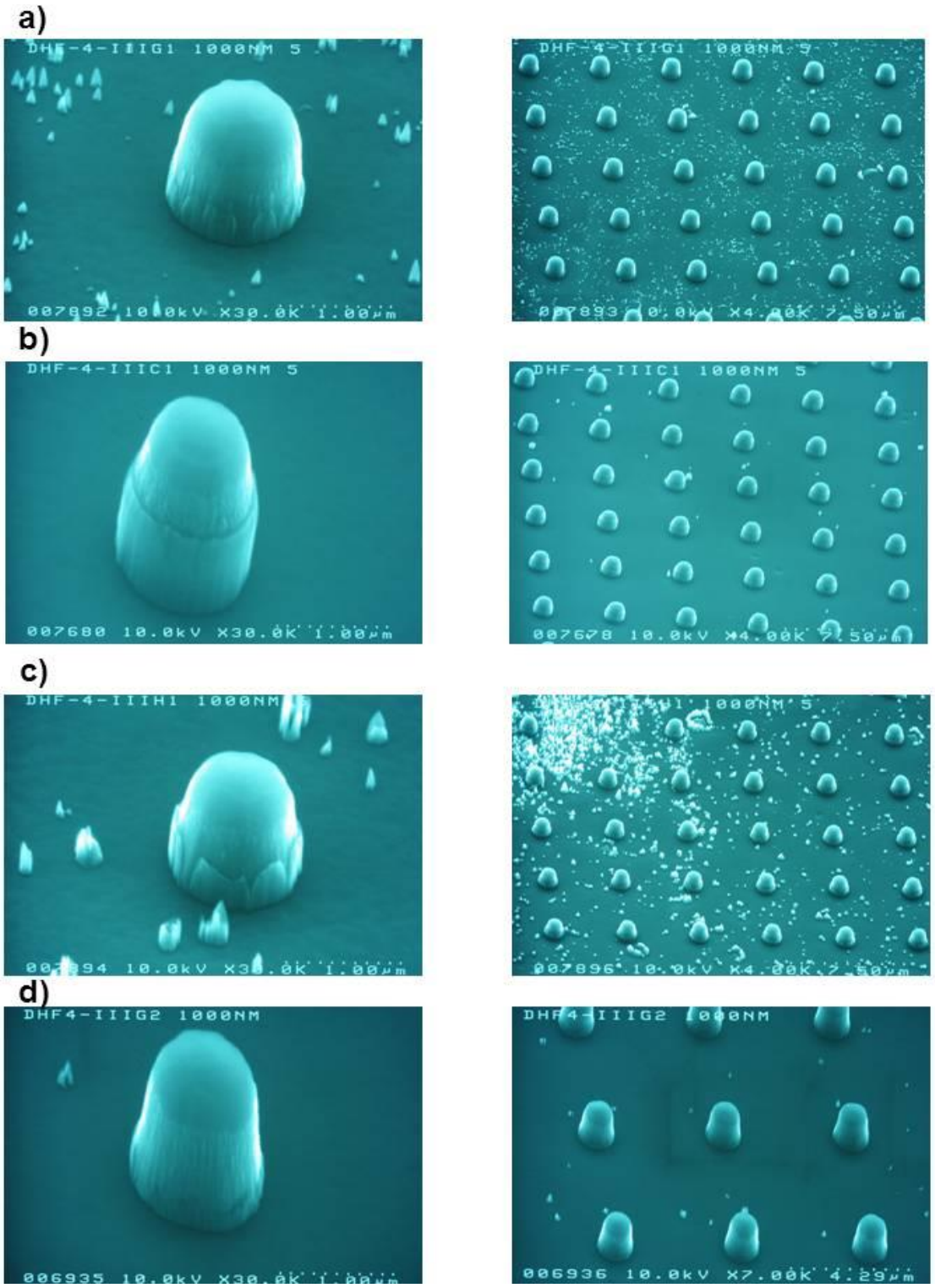

Fig. 62: A single pillar and array of diamond pillars etched with ICP power of: a) 500 W, b) 1000 W, c) 1500 W and d) 2000 W

From the SEM images it can be seen, that with increasing the ICP power more vertical walls were obtained. It has been also found that the lower powers result in —grass" appearance (Fig. 62 a); furthermore the top of the pillar was undercut. The

sample etched with ICP power of 1500 W (Fig. 62 c) shows a large amount of remnants and also pillars with taper shape. The best topography and surface exhibited the sample obtained with ICP power of 1000 W (Fig. 62 b) and the sample with the maximum applied ICP power of 2000 W (Fig. 62 d). Since the high ICP power leads to higher ion density, respectively faster material removal, retaining the high anisotropy, an additional experiment with ICP power of 3000 W was performed. Although the higher energy did not cause any negative effects concerning the form and size of the pillars (or mask degradation), the process was instable and for further experiments ICP power of 1000 and 2000 W was used.

- ***Oxygen flow***

The next etching parameter to be varied was the oxygen flow. There only higher values than in the start recipe (10 sccm), namely 20 sccm, 30 sccm and 40 sccm were used (Fig 63). The higher flow rates lead to strong —grass" formation and appearance of an over-etching. Thus from this series of experiments it can be concluded that the increasing of the oxygen flow from the start recipe is not just inefficient, but also leads to worse results in respect to the pillar quality and the surface smoothness. For this reason an oxygen flow of 10 sccm was applied for further experiments.

a)

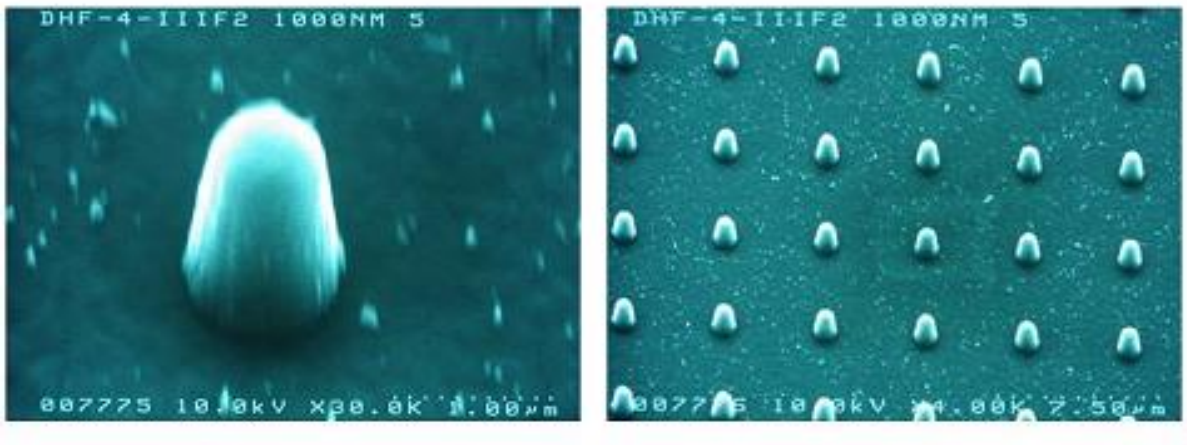

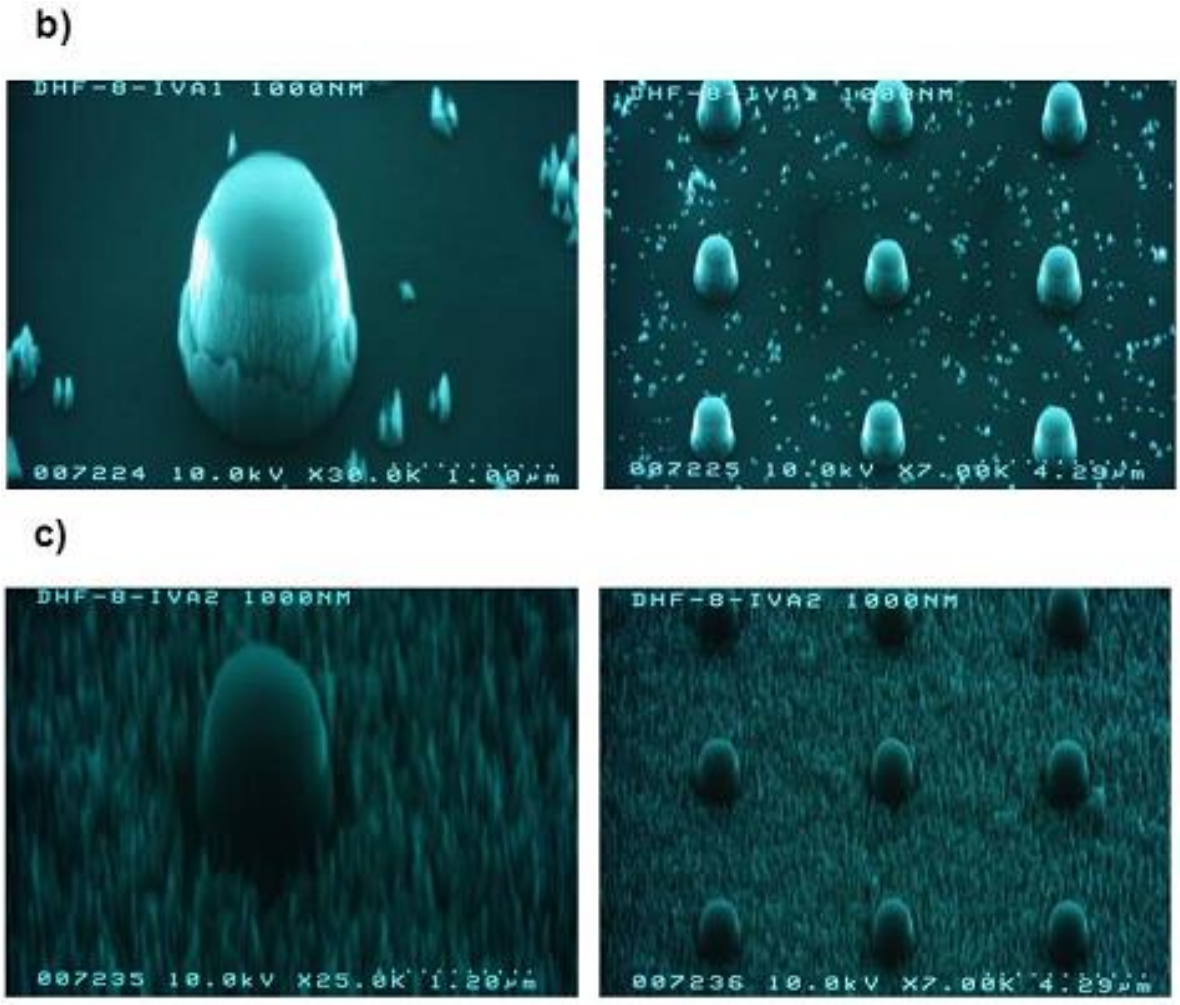

Fig. 63: A single pillar and array of diamond pillars etched with O_2 flow of: a) 20 sccm, b) 30 sccm and c) 40 sccm

- **Working pressure**

The working pressure was varied between 6.66×10^{-3} mbar (5 mTorr) and 19.99×10^{-3} mbar (15 mTorr). Since the pressure determines the decrease of the mean ion energy (the higher the pressure the more hits between ions on their way to the substrate) the 6.66×10^{-3} mbar etching should be with the highest ion energy and the etching at 19.99×10^{-3} mbar with the lowest. This is confirmed from Fig. 64, where the more diamond remnants are present, the higher pressure is used. After the variation of the working pressure, the best results concerning not only the shape of the pillars, but also the appearance of grass between them, were shown using the value of 13.33×10^{-3} mbar (from the start recipe) and this was kept for the further experiments.

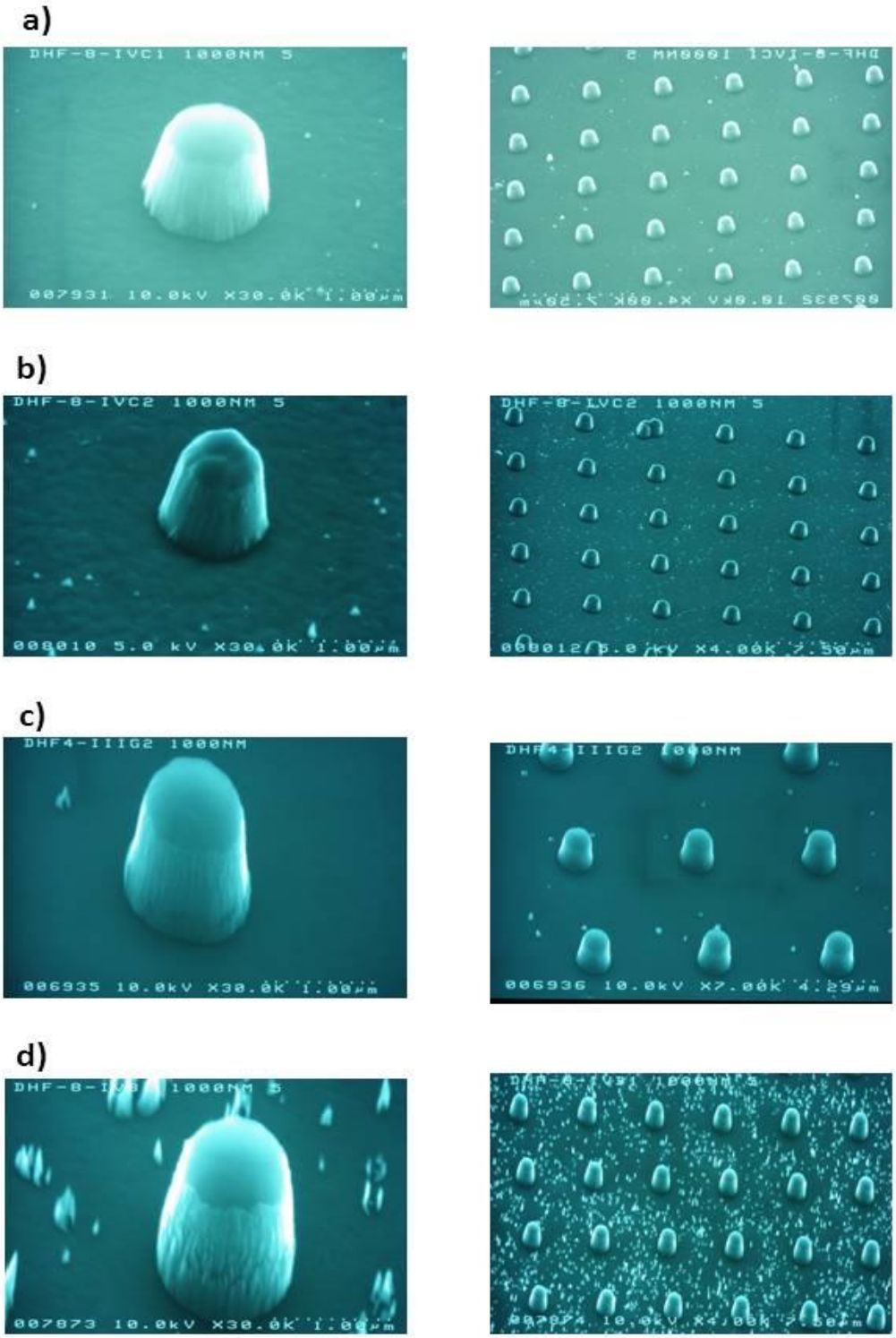

Fig. 64: A single pillar and array of diamond pillars etched at a pressure of: a) 6,66x10^{-3} mbar, b) 9.33x10^{-3} mbar, c) 13.33 x 10^{-3} mbar and d) 19,99 x 10^{-3} mbar

- **Temperature**

The next step was the variation of the substrate temperature, a lower temperature (0 °C) and a higher one (100 °C), compared to the start temperature (30 °C) were chosen.

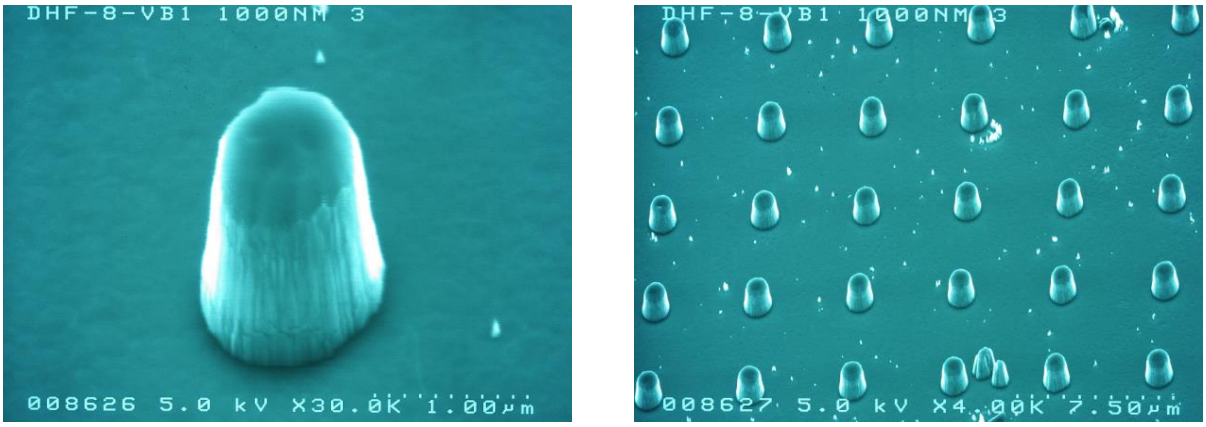

Fig. 65: A single pillar and array of diamond pillars etched at temperature of 0 °C

Lowering of the substrate temperature to 0 °C (Fig. 65) did not show any improvement. Rather the pillar wall has taper shape and the surface between the pillars is not completely free from diamond remnants. The temperature from the start recipe 30 °C (Fig. 66) shows much better results with respect to verticality and smoothness of the pillars and cleanness of the silicon surface.

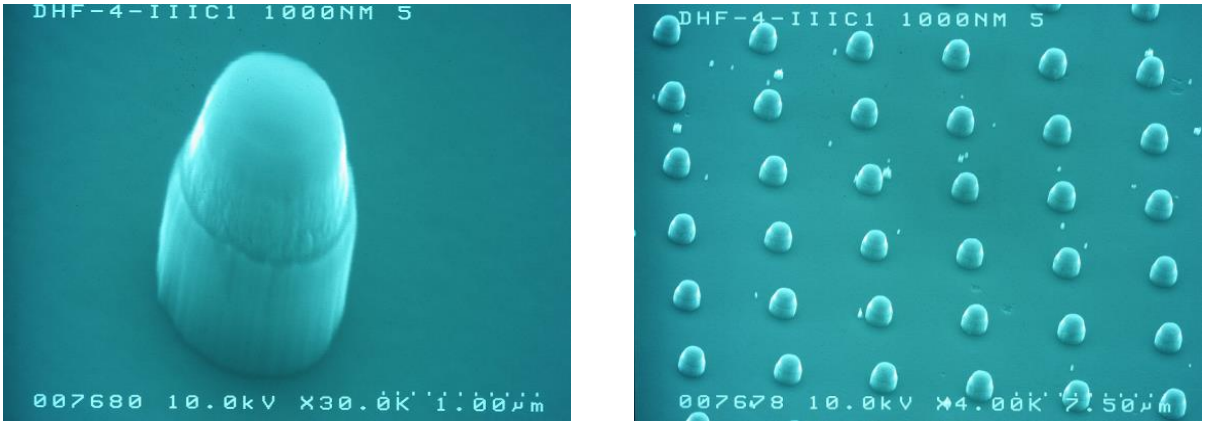

Fig. 66: A single pillar and array of diamond pillars etched at temperature of 30 °C

Increasing the temperature to 100 °C (Fig. 67) leads to appearance of diamond grass on the silicon substrate and also worse pillar quality. Additional drawback of the temperature variation was the instability of the plasma, which led to lowering of the

ICP power in the following experiments from 2000 W to 1000 W. Because the substrate temperature did not cause significant improvements of the pillar quality, the temperature from the start recipe was kept for the further experiments.

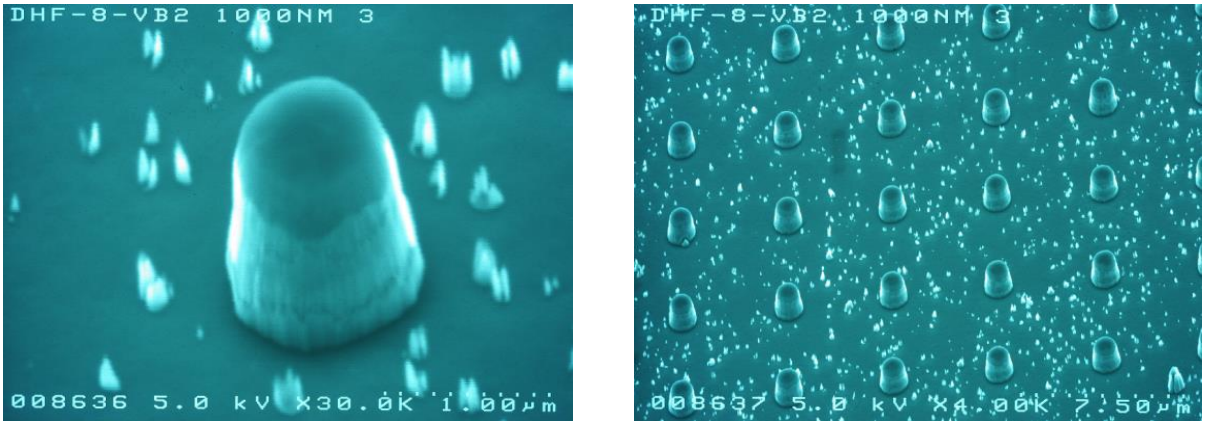

Fig. 67: A single pillar and array of diamond pillars etched at temperature of 100 °C

According to literature [129, 130], the addition of argon to the gas phase should enhance the reactive ion etching of diamond. After addition of Ar to the plasma gas mixture almost vertical walls with desired diameter were obtained, but with increasing the Ar flow rate, significant —grass" formation was observed (Fig. 68). This was the reason not to use argon in the optimized etching recipe.

After considering all above mentioned parameters and their influence on the quality of the diamond pillars an optimized recipe was established. The optimized etching parameters which were used for fabrication of diamond nanopillaars are summarized in Table 8.

Table 8. Etch process parameter after optimization

RF power [W]	**ICP** power [W]	Temperature [C°]	**O_2 flow** [sccm]	**Pressure** [mTorr]
200	**1000**	**30**	**10**	**5**

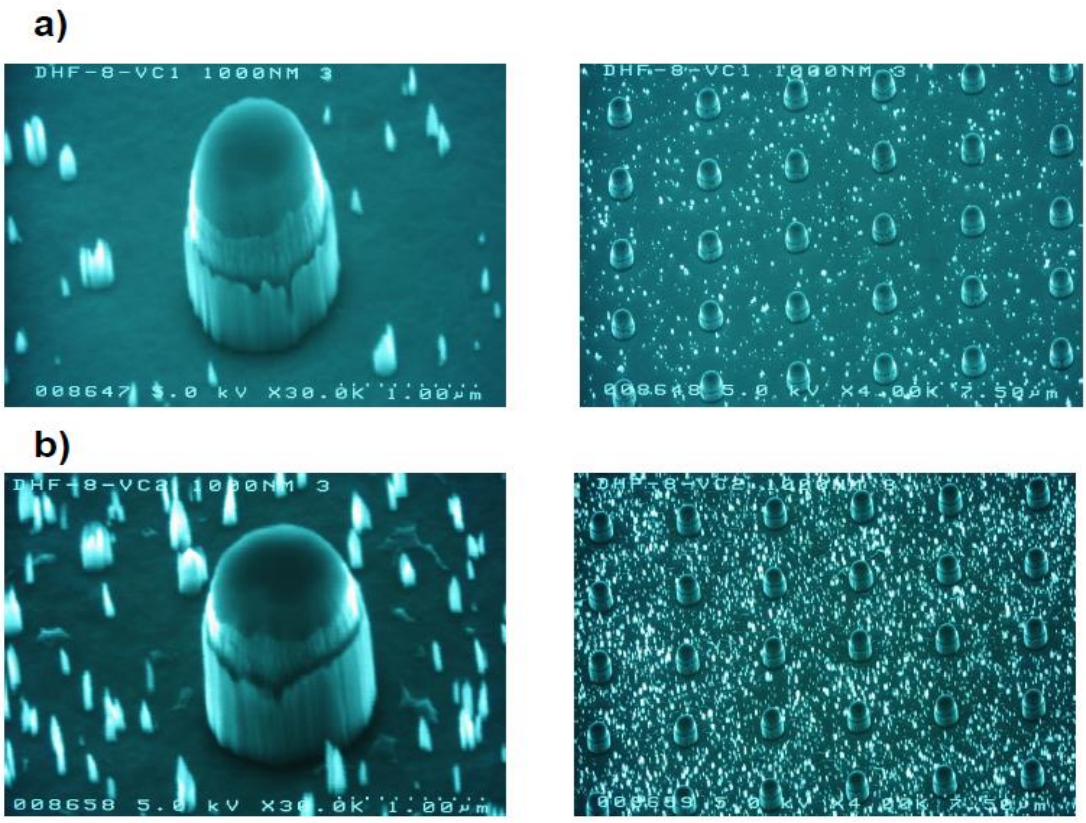

Fig. 68: A single pillar and array of diamond pillars etched with additional argon flow of: a) 2 sccm, b) 4 sccm

- **Etch rates**

The diamond etch rate depends basically on the RF power and the ICP power. The RF power, applied to the substrate holder, determines the energy of the ions reaching the sample surface and the ICP power determines the plasma density. Higher powers lead to higher ion density, respectively bombardment with high-energy ions and accordingly to faster material removal. From Fig. 69 a) and b) it can be seen the fairly linear dependence of the etch rate on the RF and ICP powers. Higher powers lead also to quicker mask degradation, therefore a balance between both parameters must be established.

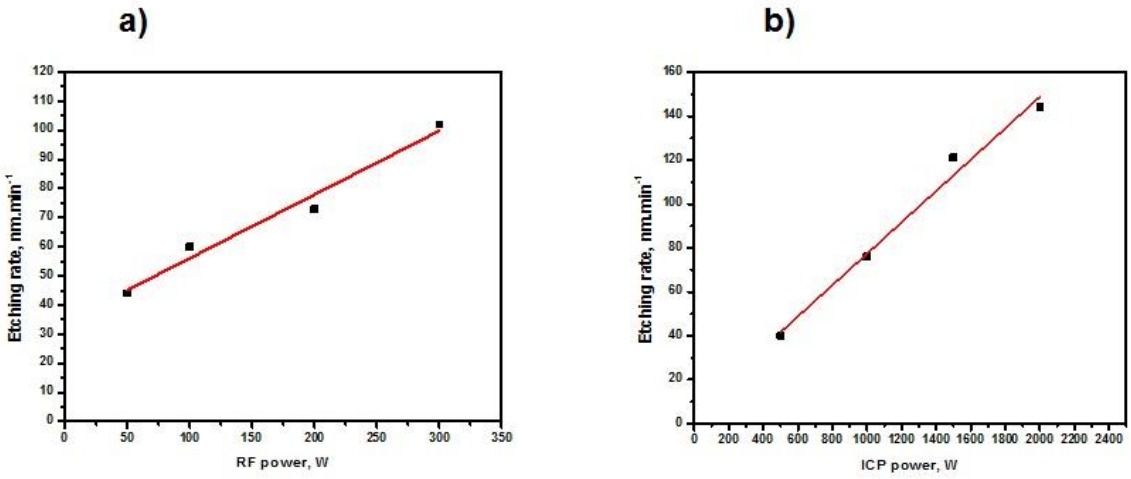

Fig. 69: NCD etch rate as a function of: a) RF power, b) ICP power

Although the etch rate must depend on the gas flow (higher gas flow rate in the chamber should lead to increase of the etch rate), it is not the case, as it is shown in Fig. 70 a). There is a slight increase of the etch rate visible from the figure, but one can state that within the range of errors, it is independent of the oxygen flow rate in the experimented range. Probably the oxygen flow has another influence on the etch process, such as providing better shape of the pillars or smoothness of the surface.

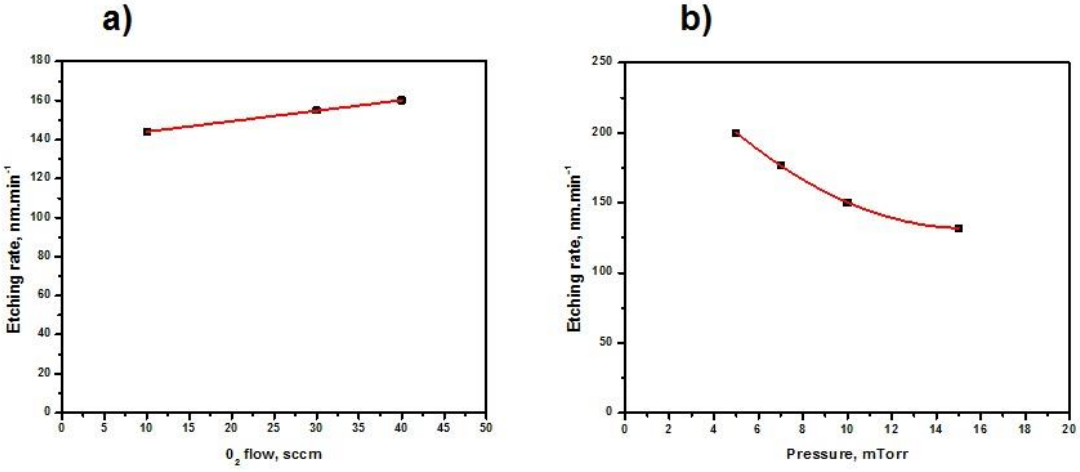

Fig. 70: NCD etch rate as a function of : a) oxygen flow, b) pressure

It can be seen from Fig. 70 b) that the etching rate decreases with the increase of the working pressure. With increasing the pressure raises the probability that the ions will

undergo collisions (for example charge exchange processes) in the plasma sheath which will reduce the mean ion energy, leading to lower etch rates.

8.2. Comparison of etch mechanisms of NCD and UNCD films

After optimization of the process parameters, the etch mechanisms of NCD and UNCD films have been investigated. These applied parameters allow stable etch process, obtaining of good shaped structures and an etch rate of about 100 nm.min^{-1}.

- ***Etch mechanism of NCD***

The first experiments were carried out with nanocrystalline diamond film (about 500 nm thick). A number of pieces were loaded into the ICP-RIE reactor; after a defined time (first 30 s, later the intervals were reduced to 10 s), the process was stopped and one piece removed; thereafter, next etching step was carried out with the remaining pieces.

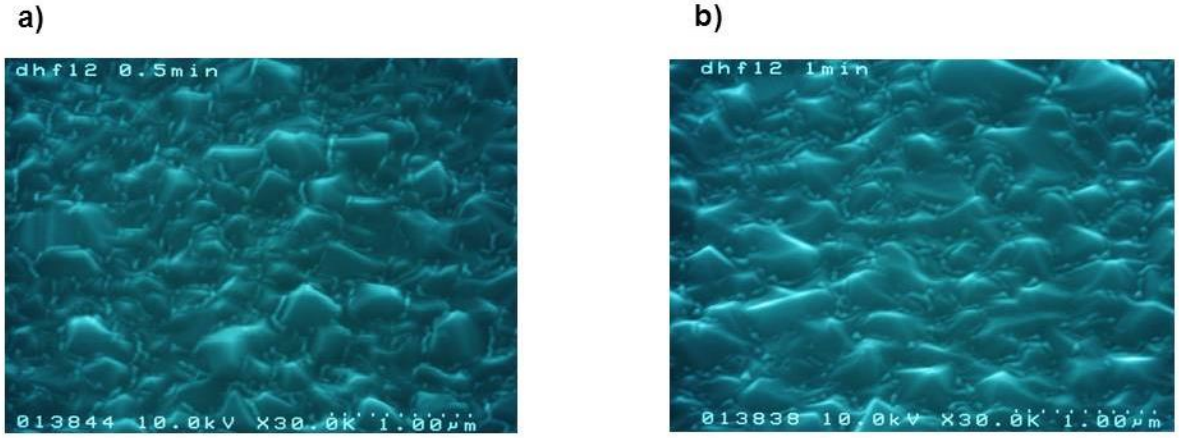

Fig. 71: SEM images of NCD film after: a) 30 s etching, b) 1 min etching

Fig. 71a) shows a top-view SEM image after 30 s etching. The first thing that attracts the attention is the slight rounding of the sharp edges of the facetted crystallites. One can also notice the presence of small needle-like structures, preferably situated at the

grain boundaries between the crystallites, which are not seen on the surface of the deposited nanocrystalline diamond film.

After 1 min etching (Fig. 71b) the facets of the diamond nanocrystallites are still clearly discernable, just as the rounding of the edges of the crystallites and the needle-like structures. These features appear preferably in the deep valleys between the various crystallites.

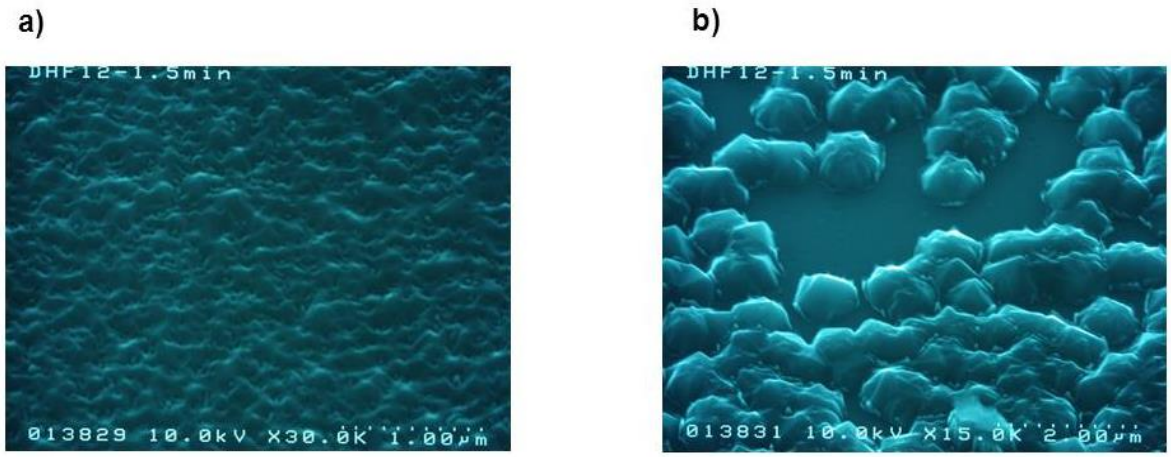

Fig. 72: SEM images of NCD film after 1 min and 30 s etching

First after 90 s etching (Fig. 72) there are some major differences recognizable. The crystallites seem to be more rounded (Fig. 72a), they start to lose their facettes and there is appearance of small holes in the film. Another significant difference is the absence of the small structure in the grain boundaries. In Fig. 72b) an image originating from a region where the film was not closed (at the rim of the sample) is present. The following interesting conclusions can be made: The crystallites are well facetted but irregularly shaped. This hints at a relatively high number of defects such as stacking faults but this regards the growth and not the etching process. The crystallite size is on the order of 800 – 1000 nm, measured from the picture scale. The thickness of the NCD sample was 480 nm. Thus the crystallite size is about twice the film thickness which means that at this very position the nucleation density was for some reasons lower than for the rest of the substrate. Very probably this corresponds to the fact that the film is not closed at this position. There is quite a number of small structures visible in this image in difference to the other image. Most of them are situated at the bottom of the substrate but close to adjacent crystallites. There are no needles in the large free spaces between the crystallites which is not surprising as in these places no diamond crystallites have nucleated and grown. This

is a clear hint that these needles are the results of the etching process and have nothing to do with re-deposition.

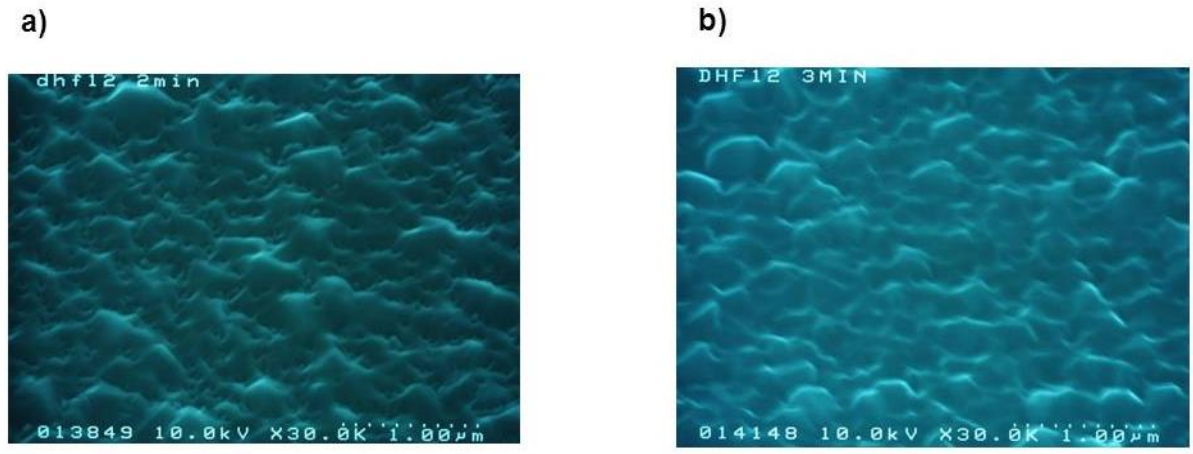

Fig. 73: SEM images of NCD film after: a) 2 min etching, b) 3 min etching

A top-view image after an etching time of 2 min is presented in Fig. 73a). Here the following observations can be made: First, the crystallites have become more and more rounded; the facets are less and less defined. The second one is the appearance of small holes (about 100 nm) all over the film. It is not possible to decide whether these holes already reach the substrate, because cross section images could not be obtained. The number of needle-like structures seems to have been reduced as compared to Fig. 71. The needles have not increased in relative height.

Increasing the etching time to 3 min (Fig. 73 b) leads to completely disappearance of the needles-like structures between the crystallites. The structures seem to lose their facets completely and the holes increased considerably in diameter.

As last for this series of experiments the etching time was increased to 4 min and the results are shown in Fig. 74. The following comments can be made from the SEM images: The initial NCD morphology is hardly discernable. The number of holes has increased considerably. Likewise, their diameters have increased and there are no longer small, needle-like structures between the crystallites.

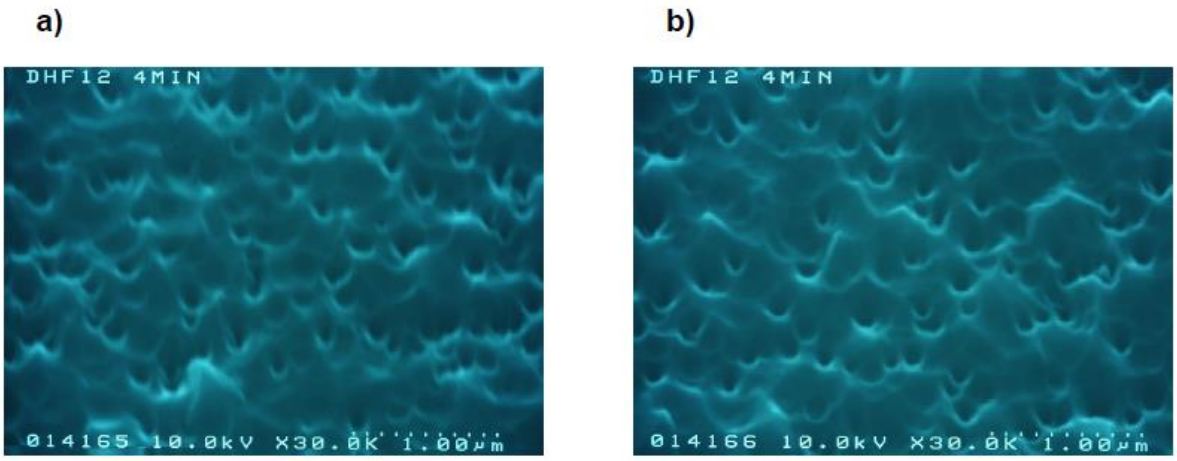

Fig. 74: SEM images of NCD film after 4 min etching

Since increasing the etch time with one more minute (5 min) leads to complete etching of the diamond layer, a new step was taken with 10 s interval. In Fig. 75 the result of 4 min and 10 s etching is shown revealing no big differences to the 4 min process (Fig. 74).

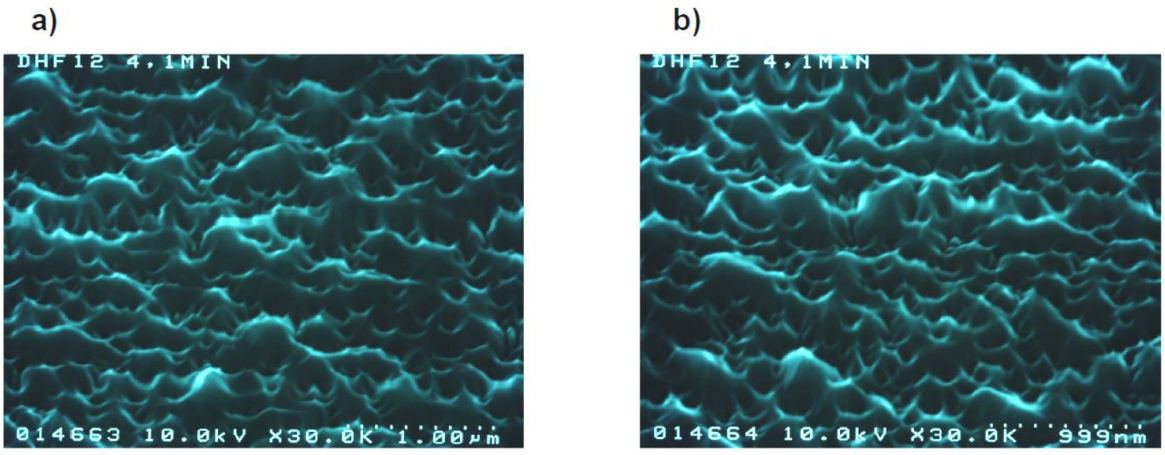

Fig. 75: SEM images of NCD film after 4 min and 10 s etching

Increasing the etching time to 4 min and 20 s (Fig. 76 a), respectively to 4 min and 30 s (Fig. 76 b) lead to significant changes on the surface. There is almost nothing in the images remembering at the diamond nanocrystallites. On the other hand, it is obvious that quite a number of holes exist within the film.

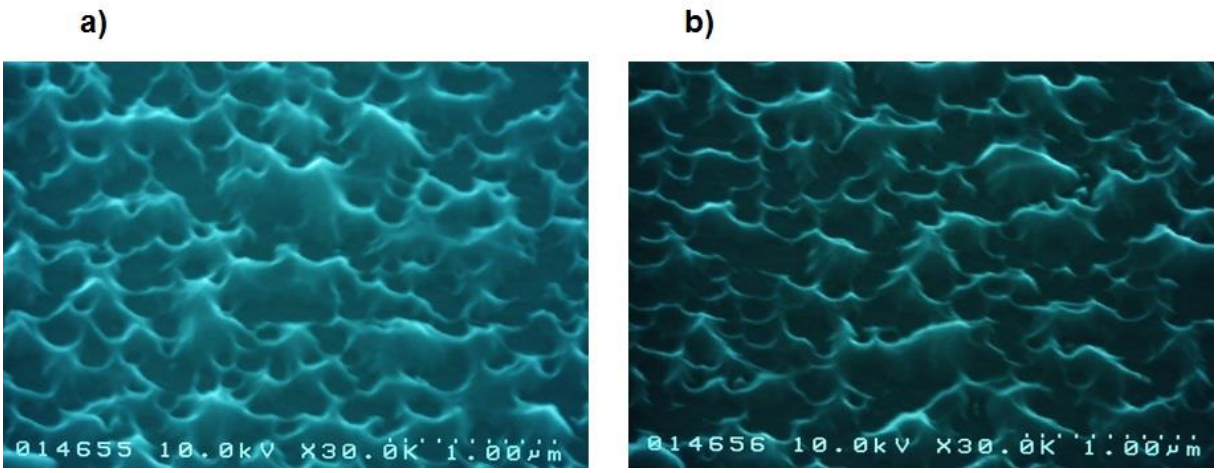

Fig. 76: SEM images of NCD film after: a) 4 min and 20 s etching, b) 4 min and 30 s etching

Finally in Fig. 77 are presented the results after 4min and 40 s etching.

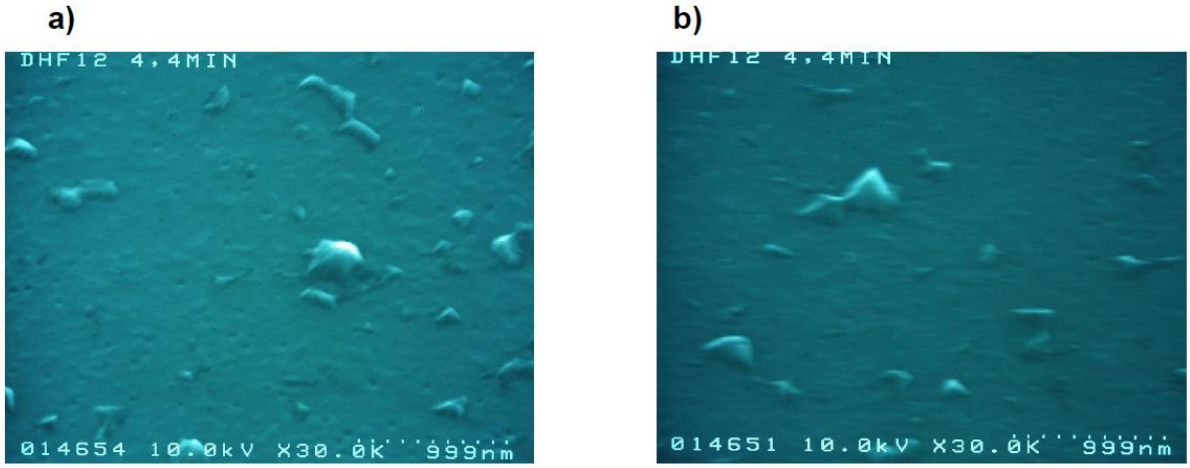

Fig. 77: SEM images of NCD film after 4 min and 40 s etching

The images show that the film is almost completely etched and only a few remnants are present on the bare silicon wafer. It also indicates that the etching rate is higher than the assumed one (~ 100 $nm.s^{-1}$).

From all presented SEM images it can be concluded that the etching mechanism of NCD material is not homogeneous along the whole surface - the etching is slower at some places than in the surrounding parts of the films. The average etching rate is considered to be 100 $nm.s^{-1}$ or more. The nanocrystalline diamond film consists of diamond nanocrystallites separated by a more or less undefined grain boundary material. This means further that these grain boundaries are the week points of the system. A diamond facet should be etched homogeneously but it is unpredictable

what happens at the grain boundaries. A second week place are the point or linear defects within the crystallites, where they are preferentially etched.

- ***Etch mechanism of UNCD***

Using the same etch parameters ultrananocrystalline diamond layer has been etched to compare the etch mechanisms of both type of diamond films. The UNCD layer has the same thickness as the NCD. Based on the obtained SEM images (Fig. 78) drastic differences of the etch mechanism of UNCD compared to that of NCD layer can be determined:

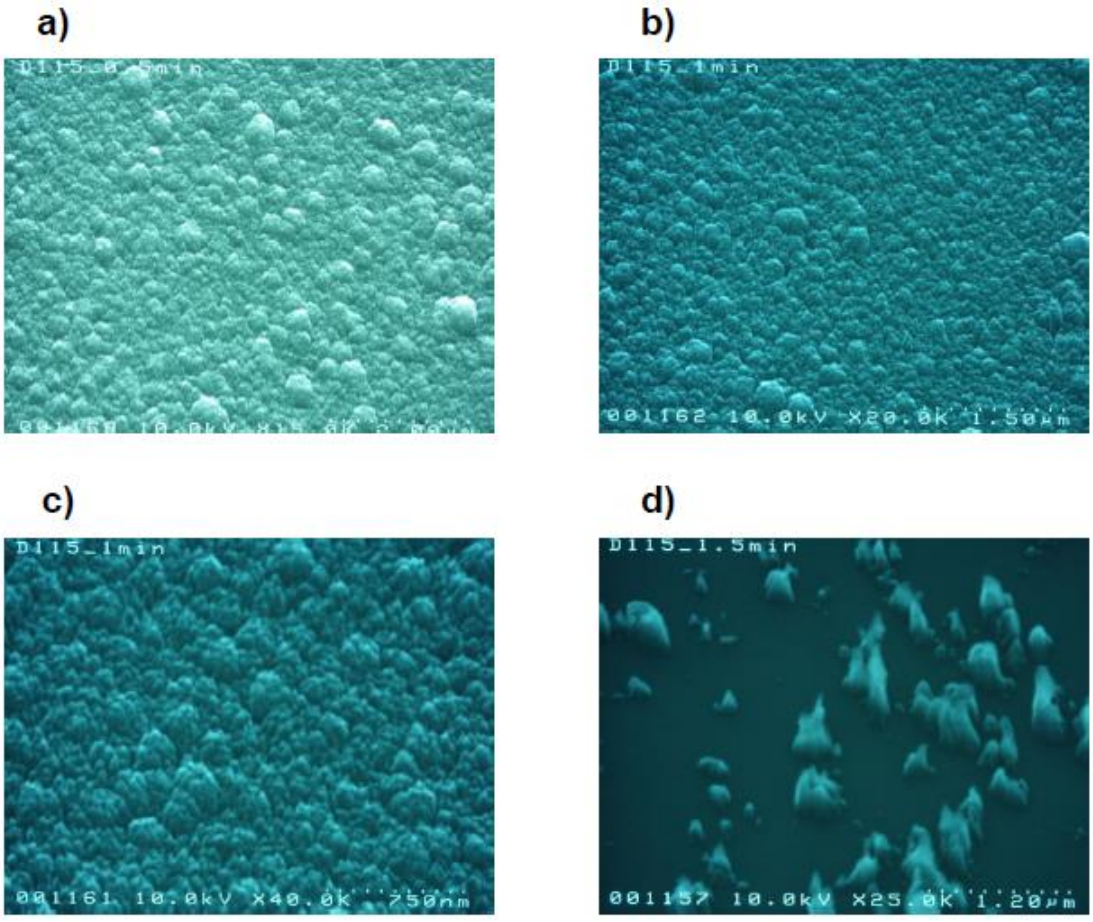

Fig. 78: SEM images of UNCD film after: a) 30 s, b) & c) 1 min, d) 1 min and 30 s etching

On the first picture (Fig. 78a) after 30 s etching there are no changes of the typical topography of the ultrananocrystalline material but increased roughness due most probably to preferential etching of the amorphous carbon matrix. After 1 min etching (Fig. 78b & c) the larger structures (presumably originating from the nucleation sites)

survived and the smaller structures in-between were etched reminding of the NCD etch mechanism. After 1 min and 30 s (Fig. 78d) the diamond layer was almost completely etched, which indicates the much higher etching rate of UNCD compared to NCD (more than double). This must be ascribed to the nature of UNCD, composed of diamond nanocrystallites (smaller than 10 nm), embedded in an amorphous carbon phase, with a ratio of the two fractures close to 1. The etching rate of the amorphous phase containing mainly sp^2-bonded but also some sp^3-bonded carbon atoms is much higher than of the crystalline diamond phase, determing the different etching mechanism of UNCD and the overall higher etching rate.

9. FABRICATION OF NANO- AND ULTRANANOCRYSTALLINE DIAMOND PILLARS

In this chapter the choice of hard mask for the reactive ion etching will be commented. Two different materials were used, namely silicon dioxide and gold, in the cases where gold mask was used, a lift-off technique was applied. Using the recipe obtained after the preliminary investigations (depicted in the previous chapter) diamond nanopillars were etched from NCD and UNCD material.

9.1. Choice of hard mask

All experiments depicted in the previous chapter were performed with silicon dioxide hard mask. The optimized recipe showed good results concerning the surface between the diamond pillars and also for the pillars with larger diameters (1000 and 500 nm) which possessed vertical and smooth walls. For smaller diameters this was not the case, the pillars became sharper as shown in Fig. 79. The tapering observed cannot be caused by an overetching of the mask at the outer rim of the pillars. The SiO_2 mask is strongly rounded by the etching process but still present over the entire pillar diameter. This is in agreement with the observation that the pillars possess their nominal diameter at their tops.

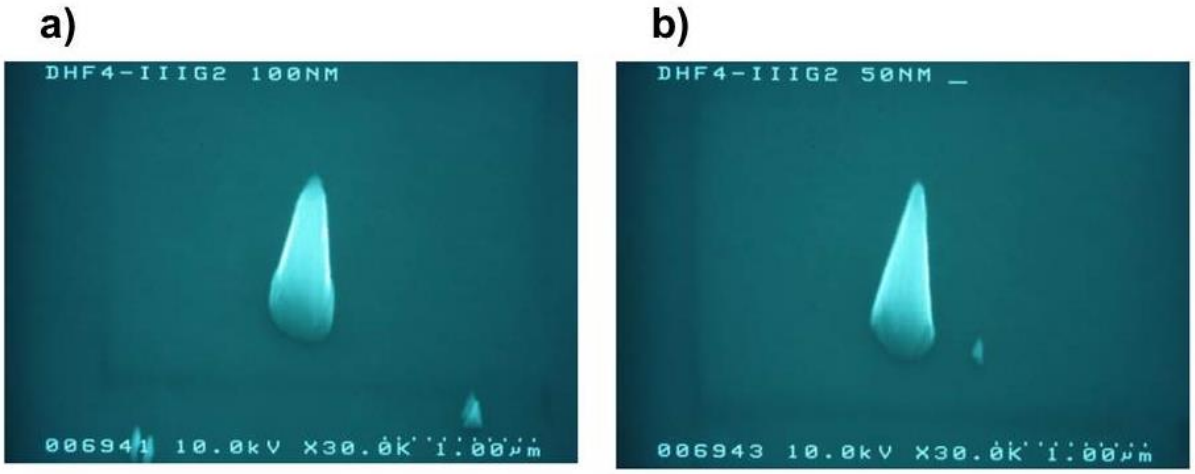

Fig. 79: Diamond pillars with nominal diameter of: a) 100 nm, b) 50 nm

A closer inspection of the SEM image of a single NCD pillar shown in Fig. 80 reveals that there is a kind of rim visible roughly in the middle of the structures. This is not the boundary between the diamond and the mask which can clearly be seen in the upper part of each structure. Rather, this rim occurs in the diamond part of the pillars. This effect is ascribed to the erosion of the silicon dioxide mask during the etching process.

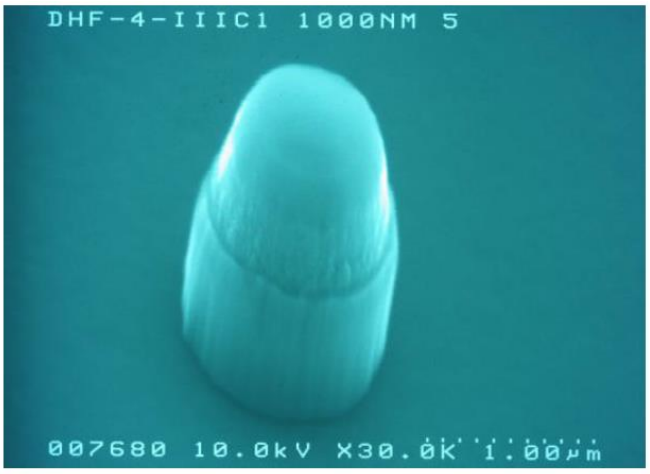

Fig. 80: Diamond pillar with unremoved SiO_2 mask after the etch process

In order to overcome the problem with tapered smaller pillars, the use of another hard mask was considered. According to the literature data, a gold mask is much more stable against sputter effects [106]. Therefore the experiments with SiO_2 mask, showing the best results, were repeated with a gold mask. The schemes of the whole fabrication processes of the diamond pillars using the different masks are shown in Fig. 81.

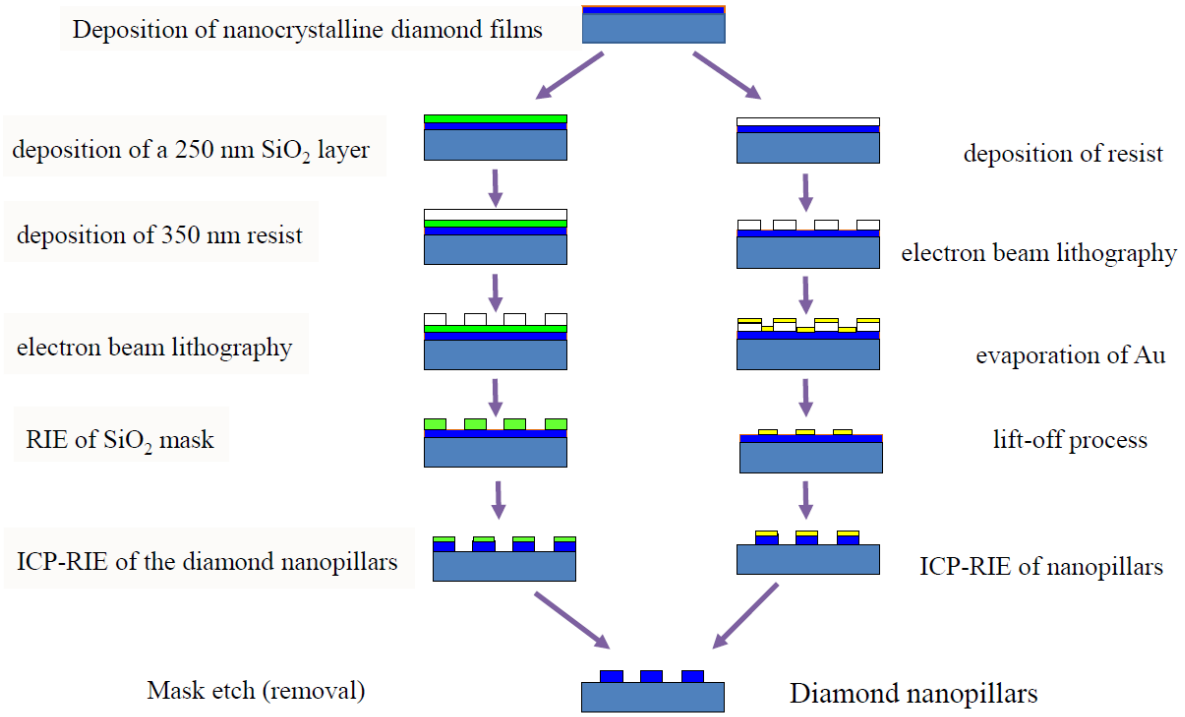

Fig. 81: Schemes of the lithography and etching processes using a SiO_2 mask or a gold mask

In the case of the gold mask the so called lift-off process was used. First a positive resist was deposited on the diamond film, followed by the definition of the pillars using e-beam lithography. After the development, a thin titanium layer (5 nm) was deposited for the better adhesion of the gold mask (200 nm). The lift-off was carried out using 1-methyl-2-pyrrolidone. The optimized recipe described in previous chapter was used for diamond etching. Already the first experiments showed better results compared to the experiment with silicon dioxide mask. The surface between the pillars was free from undesired structures and the pillar walls were smooth and vertical for all diameters (Fig. 82).

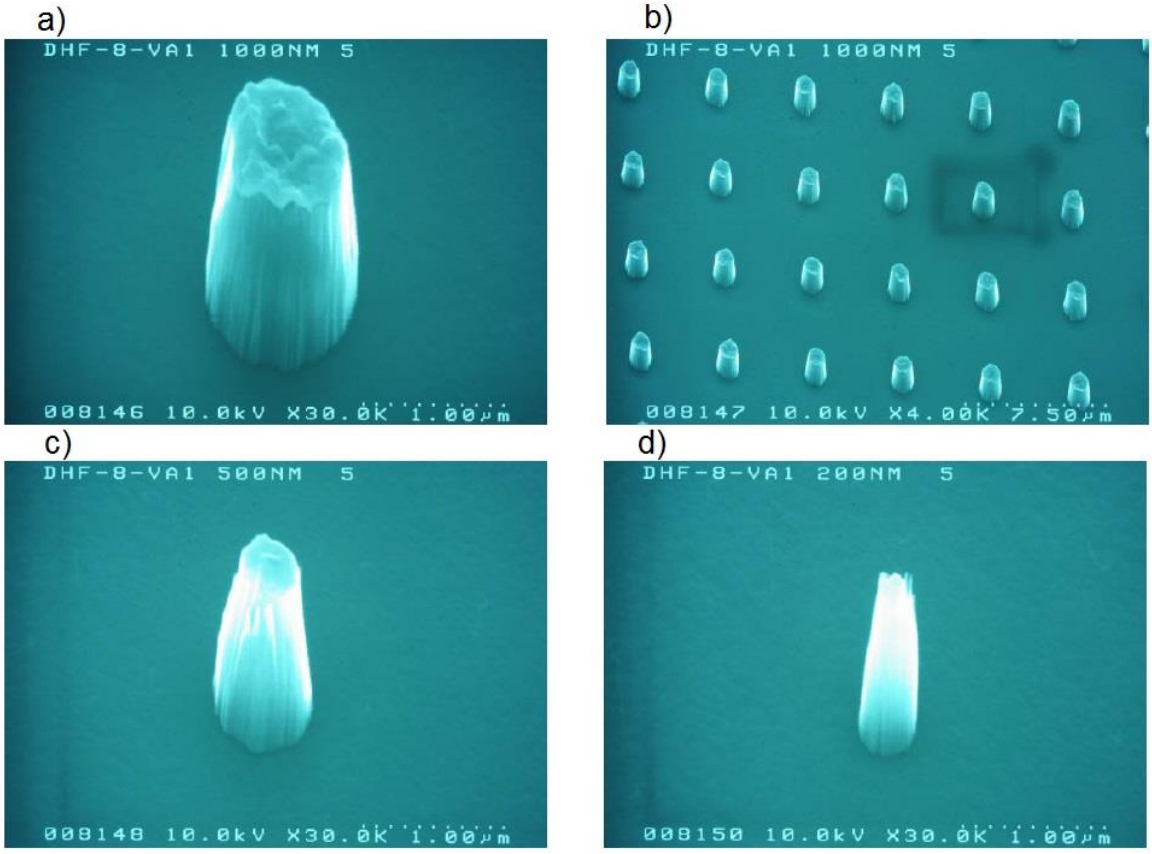

Fig. 82: Diamond pillars etched with Au mask: a), b) d= 1000 nm, c) d= 500 nm, d) d= 200 nm

In a following step the process parameters (ICP power, pressure, gas composition, and temperature) were varied once again to determine their eventual influence by using the different hard mask.

The increase of the working pressure from 5 mTorr to 10 mTorr lead to worse topography: the pillar walls are tapered and the surface in between is not completely clean from remnants (Fig. 83a). After increasing the ICP power from 1000 W to 2000 W the obtained pillars have larger diameter than the nominal one and the walls are rougher compared to the start recipe (Fig. 83b). Although the addition of argon in the process chamber was found to have a good influence on the form of the structures in the case of SiO_2 mask, in the case of gold mask the addition of argon lead to damaging of the silicon substrate and worse quality of the pillars (Fig. 83c).

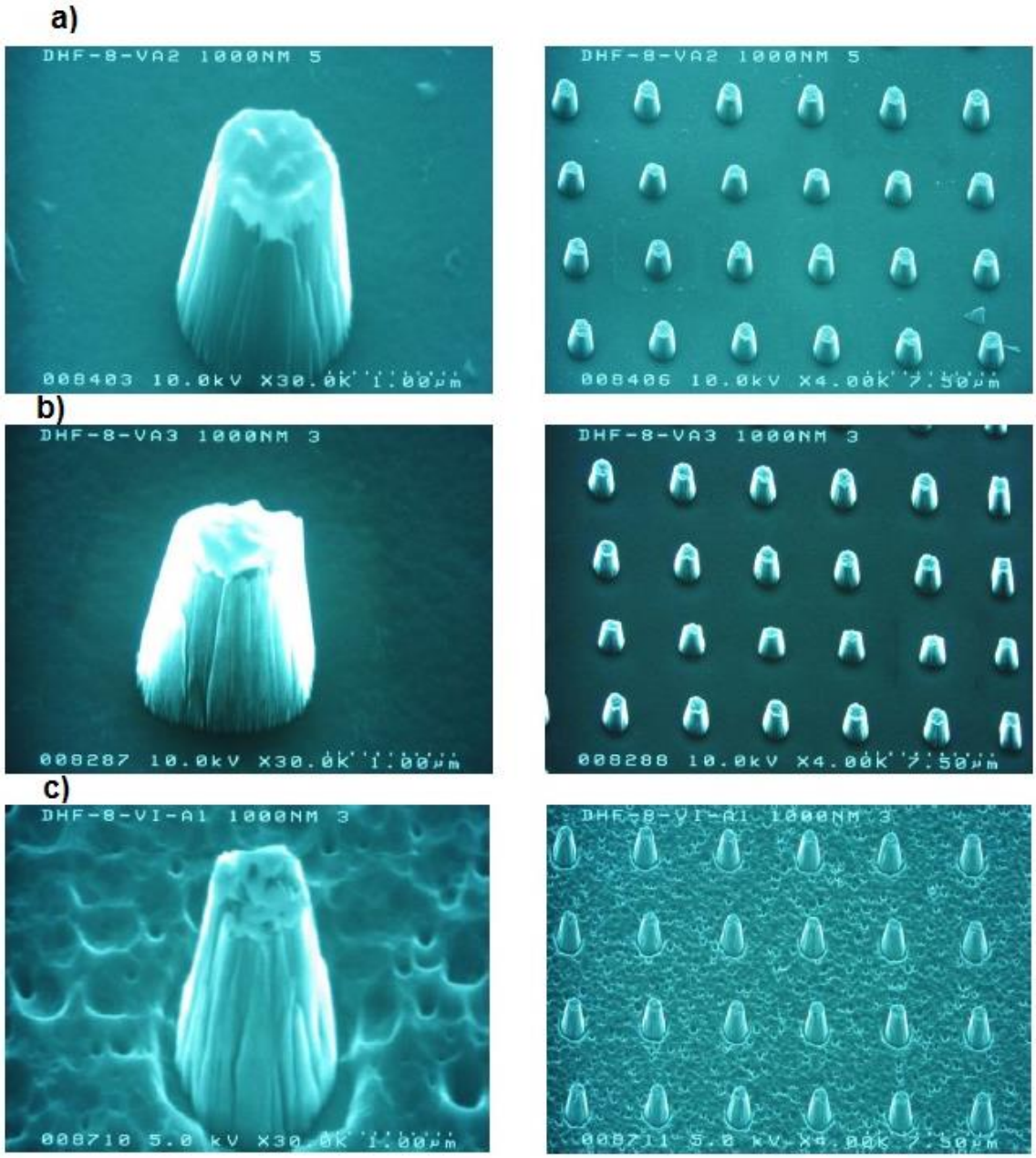

Fig. 83: A single pillar and array of diamond pillars with d= 1000 nm etched with: a) p= 10 mTorr, b) ICP power 2000 W, c) Ar flow 4 sccm

The decreasing of the process temperature to 0 ºC (Fig. 84) did not lead to any significant differences compared to the results at 30 ºC. The improvement of the topography is negligible, while the decreasing of the temperature is a time-consuming process and it is not profitable to make use of it.

Since the optimizing attempts did not lead to any improvement of the results, the start recipe was used for producing pillars from the nano- and ultra nanocrystalline diamond layers.

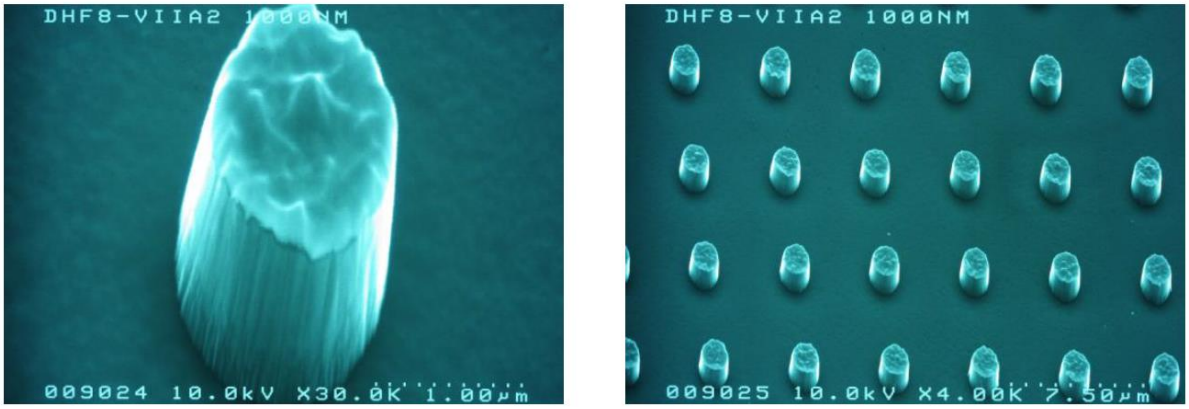

Fig. 84: A single pillar and array of diamond pillars etched at 0 ºC

9.2. Fabrication of pillars from NCD layers

The lithographic pattern used for the fabrication of diamond pillars is presented in Fig. 85. There are arrays with 5 different pillar diameters: 1000 nm, 500 nm, 200 nm, 100 nm and 50 nm. The center-to-center distance between the pillars in the arrays is 5 µm.

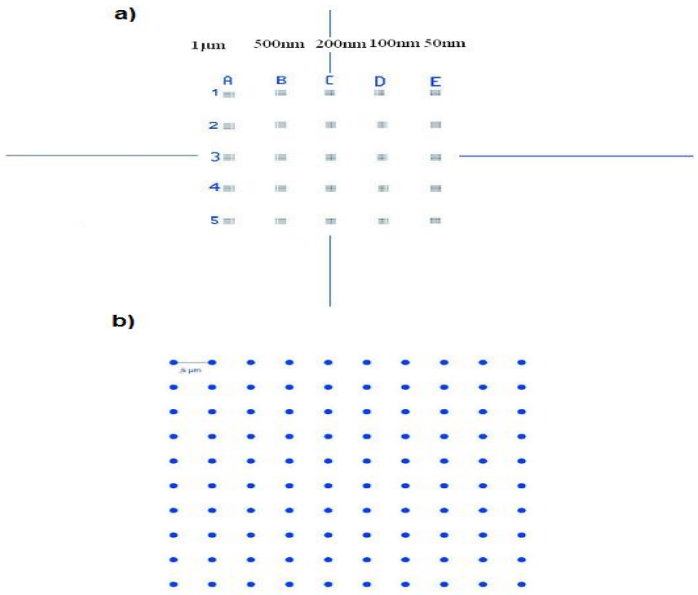

Fig. 85: Lithography design for all samples: a) scheme of the arrays with structures and orientation marks, b) scheme of a single array for one structure unit

9. FABRICATION OF NANO- AND ULTRANANOCRYSTALLINE DIAMOND PILLARS

After all optimizations of the fabrication process (including etch parameters, choice of hard mask and changes in the lithographic process) the final parameter can be summarized in Table 9.

Table 9. Final etch process parameter

RF power [W]	**ICP** power [W]	Temperature [C°]	**O_2 flow** [sccm]	**Pressure** [mTorr]	**Hard mask**
200	**1000**	**30**	**10**	**5**	**Gold**

Examples of the obtained NCD pillars with different diameters between 1000 and 50 nm are presented in Fig. 86.

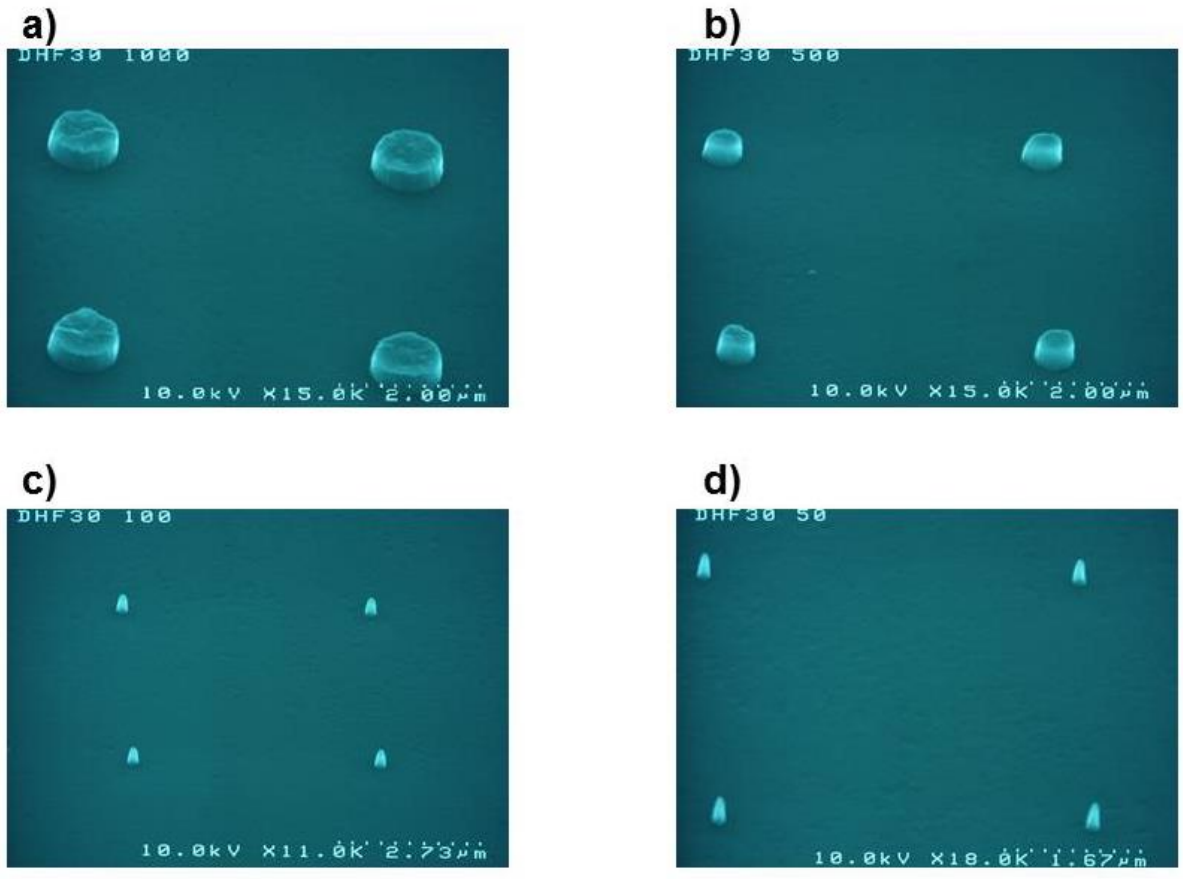

Fig. 86: Pillars etched with the final recipe: a) d = 1000 nm, b) d = 500 nm, c) d = 100 nm, d) d = 50 nm

In order to investigate whether the material within a single pillar still consists of NCD, or whether the processing has led to degradation or even an amorphization of the material within, micro-Raman spectroscopy has been performed with single pillars. To this end a Renishaw 1000 Raman spectrometer with an excitation wavelength of 488 nm and a spot size of 1 µm was employed which corresponds to the largest pillar diameter. Fig. 87 shows normalized spectra of a continuous NCD film and a NCD pillar of 1 µm diameter. From the figure it is evident that both spectra are dominated by the diamond line at 1332 cm^{-1}. As the Raman cross section of sp^3 carbon material is lower by a factor of 50 than that of sp^2 carbon it is clear that diamond is the predominant material within the pillar. There are two minor deviations between the two spectra: The silicon peak is easily explained by a slight mismatch of the pillar and the Raman laser spot. The reasons for the slight increase of the sp^2 peak in the spectrum are currently investigated. But taking into account the different Raman cross sections of sp^3 and sp^2 carbon, this slight increase is of minor importance only.

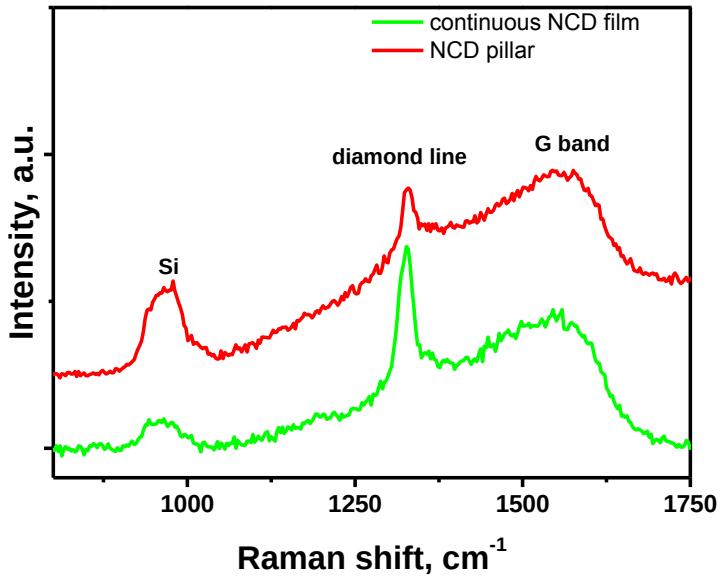

Fig. 87: Normalized Raman spectra of NCD layer and 1 µm NCD pillar

The pillars, obtained with this fabrication process, were used for the optical investigations, described in the next chapter.

9.3. Fabrication of pillars from UNCD layers

The etch mechanism of ultrananocrystalline diamond material and its differences to the etching of nanocrystalline diamond has been discussed in the previous chapter. A layer deposited by standard conditions in the microwave plasma assisted CVD set-up, described in Chapter 6.2., was used for the fabrication of UNCD pillars. The etching process was carried out using the optimized parameters in Table 9.

The SEM images of the pillars with a diameter of 1000 nm (Fig. 88) reveal surface between the diamond pillars, which is clean from any remnants. The pillar walls are smooth and vertical (the pillar diameter on top seems not to differ from that on the bottom of the pillar).

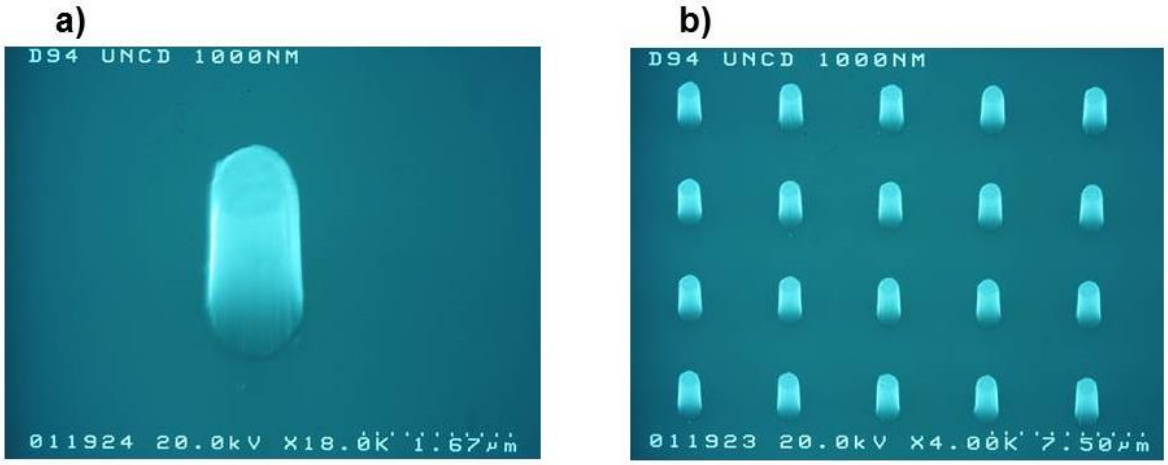

Fig. 88: A single pillar and array of ultrananocrystalline diamond pillars with a diameter of 1000 nm

This is not the case by the pillars with smaller diameters (Figs. 89 and 90). The shapes of the structures become more and more tapered the smaller the nominal structure diameters are. This could not be ascribed to a mask degradation, since the gold mask is still visible (and undamaged) on the top of the structures on the pictures in all series. Since the top diameters correspond to the nominal ones for all series, the tapering of the structures is not due to some kind of overetching but due to the fact that with increasing the etching depth not all material is properly removed. The different etch mechanism of NCD and UNCD material should explain why the recipe, which is showing good results for NCD does not result in the same by the etching of UNCD pillars.

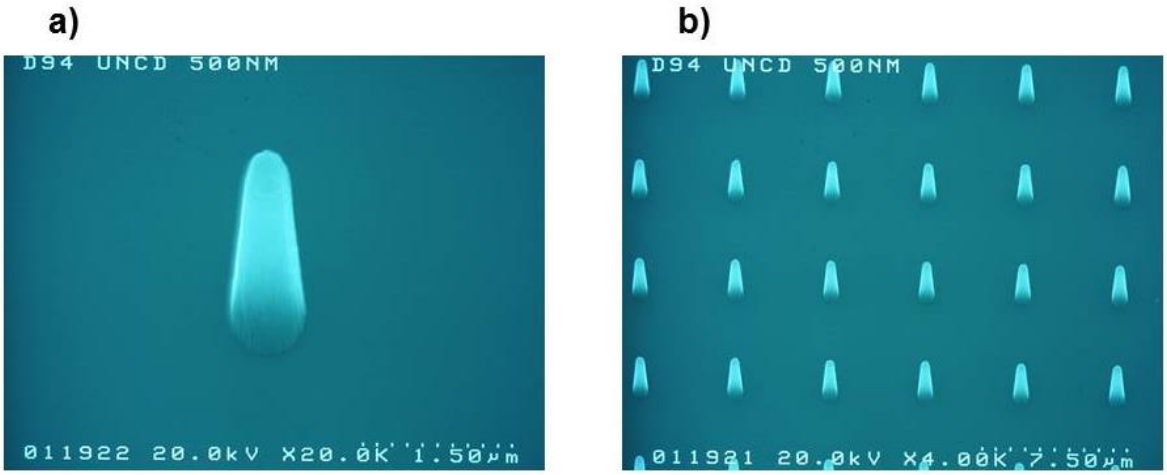

Fig. 89: A single pillar and array of ultrananocrystalline diamond pillars with a diameter of 500nm

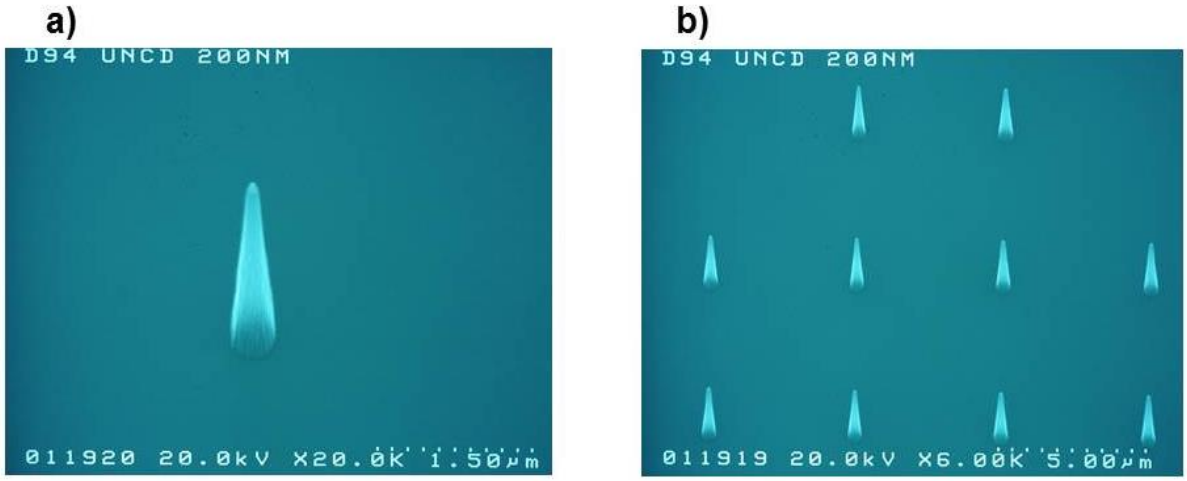

Fig. 90: A single pillar and array of ultrananocrystalline diamond pillars with a diameter of 200nm

10. OPTICAL INVESTIGATION OF DIAMOND NANOSTRUCTURES

In this chapter the optical investigations of the diamond nanostructures - single diamond nanocrystallites and diamond pillars will be presented. Fluorescence mapping of the samples was carried out as well as photoluminescence measurements to proof the presence of nitrogen-vacancy (NV) centers in the structures.

10.1. Investigation of diamond layers and single crystallites

10.1.1. Nitrogen content in the NCD films

Since the deposition method of the diamond films does not include addition of nitrogen gas in the chamber (relying only on the background pressure in the CVD set up) and the samples are not implanted with nitrogen ions afterwards, before the optical investigations of the samples, their nitrogen content has to be confirmed. Time-of-flight secondary ion mass spectroscopy (ToF-SIMS) has been carried out at IFOS, TU Kaiserslautern on a NCD layer, deposited at standard conditions. It was performed with Bi_3 ions on an area of 60 μm x 60 μm in the center of the sputter crater which has been created by Cs^+ ions of 3 keV on an area of 150 μm x 150 μm. The depth profile is presented in Fig. 91.

The results should be compared with the XPS investigations (shown in Chapter 7), which revealed a clean diamond surface with 1.3 % O and no other elements present. Fig. 90 shows the depth profile of five species along the whole diamond layer (about 600 nm): H (mass 1), C (mass 12), O (mass 16), CN (mass 26), and Si (mass 28) . The following observations can be made:

- The concentration of all species is constant along the diamond film and they stay constant also in the silicon substrate;
- ^{1}H, ^{16}O and $^{12}C^{14}N$ (^{12}C as well) were also detected in the Si substrate, (starting at ca. 600 nm) - there seems to be a slight increase of their

concentrations shortly before the interface. It is the so-called knock-on effect. The heavy Cs ions used for sputtering knock parts of the lighter elements deeper into the film rather than to sputter them. As the matrix changes from NCD to Si, this knock-on behavior changes. As a consequence a new sputter equilibrium has to be established for the elements O, N and H driven into the top layer of the Si substrate where knock-on is not as easy. As a consequence there is a peak of these elements at the interface;

- The peak of the concentrations of the species shortly before the interface can be explained also with the fact that the crystallite size of NCD films is increasing with thickness i.e. towards the surface. Thus near the interface with Si there is more grain boundary material which would explain the slight increase of the H content at the interface;
- The intensity measured for ^{16}O in the diamond layer is only a little bit higher than the one measured in the Si substrate. This indicates that O is contained only as traces in the diamond, which corresponds to the XPS measurements.

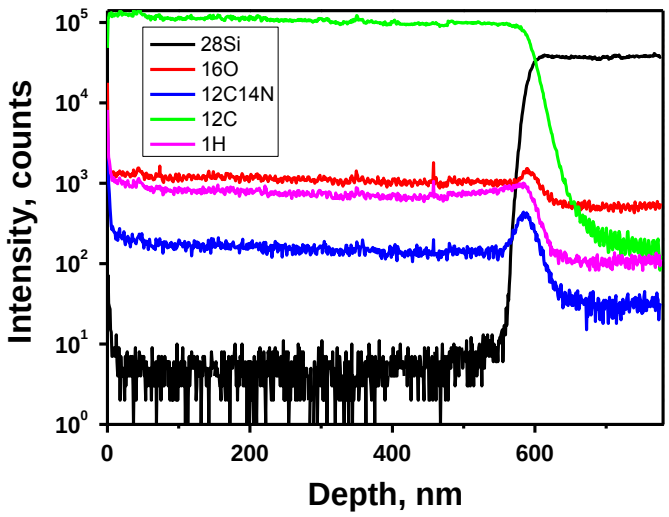

Fig. 91: ToF-SIMS depth profile of nanocrystalline diamond film

To study in more details the species concentrations at the diamond surface the depth profile for the first 100 nm of the diamond layer is shown in Fig. 92, the following comments can be made:

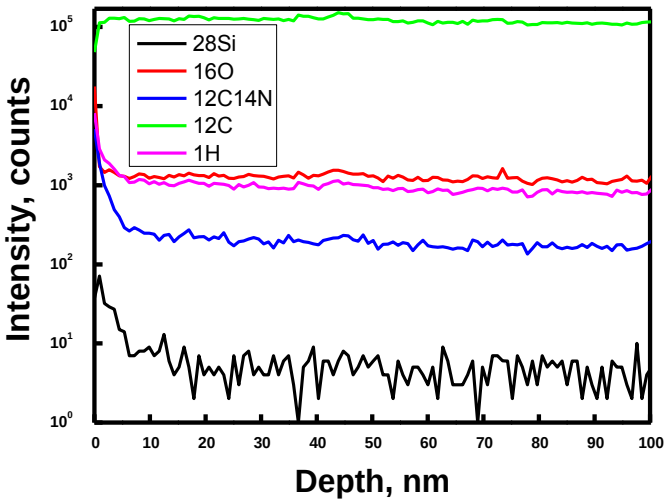

Fig. 92: ToF-SIMS depth profile of the first 100 nm of the nanocrystalline diamond film

- There is enhanced hydrogen concentration at the diamond surface, which can be ascribed to the hydrogen termination of the diamond surface during the deposition;
- The other species whose concentration is rapidly decreasing is $^{12}C^{14}N$, what should proof that nitrogen incorporates preferably near the diamond surface.

After detailed examination of the ToF-SIMS spectra it can be concluded, that the diamond film is clean from impurities and there is a low concentration of nitrogen near the diamond surface. As next optical investigations were performed to study the possible formation of NV centers in NCD.

10.1.2. Fluorescence mapping of single diamond crystallites

Samples with diamond nanocrystallites were investigated with a confocal microscope (50x air objective, 0.95 NA). The excitation of the NV centers was achieved with a 532 nm CW diode pumped solid-state laser (Coherent, Compass) using 600 μW excitation power. The fluorescence was collected through the same objective and filtered from the excitation light using a long-pass interference filter. The second-order autocorrelation function $g^{(2)}(t)$ was measured using two avalanche photodiodes in a Hanbury–Brown – Twiss configuration.

The confocal images of single diamond nanocrystallites showed bright spots randomly distributed on the surface (Fig. 93). The intensity is about $2.5x10^6$ counts per second (cps), which in one order higher compared to literature data [37].

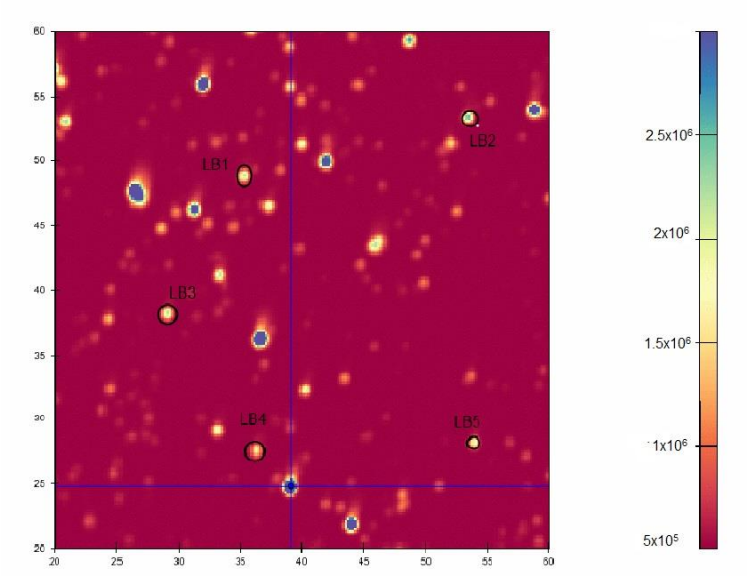

Fig. 93: Fluorescence mapping of single diamond nanocrystallites

10.1.3. Photoluminescence measurements of single diamond crystallites

First photoluminescence (PL) measurements were performed at the Hungarian Academy of Science. As-grown samples from diamond layer and single diamond crystallites were sent for photoluminescence (PL) measurements recorded on a Raman system using 488 nm excitation with a Jobin Yvon Fluorolog FL-3-221 PL fluorimeter. The excitation spot diameter was ca. 0.5 cm. For comparison a diamond reference sample (suspension of fluorescent diamond nanocrystallites with an average size of about 17 nm, 10-15% of them possessing NV centers, which was spin coated on Si wafer) was used. Not normalized and normalized PL spectra of the three samples are shown in Fig. 94.

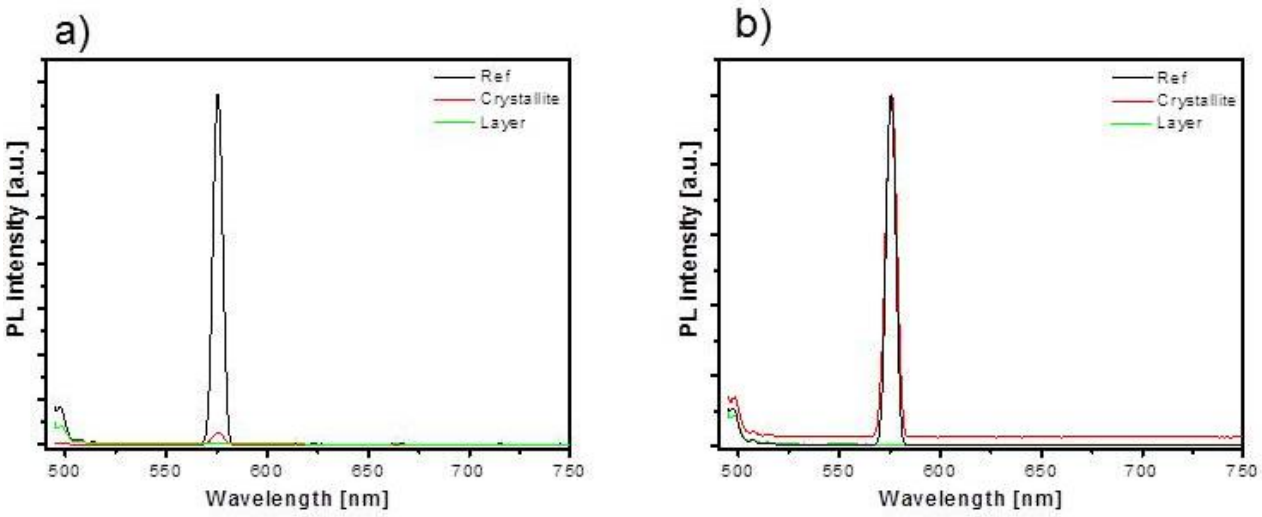

Fig. 94: PL spectra form a reference sample, single crystallites and diamond layer: a) not normalized, b) normalized

The spectra of the reference sample and the sample with diamond crystallites reveal peak at 575 nm which corresponds to the neutral nitrogen vacancy (NV^0) center. No signal was detected from the NCD film, which corresponds to literature data [106]. From the not normalized spectra (Fig. 94a) it can be seen that the intensity from the reference sample is much higher compared to the single crystallites, which is a sign of higher number of NV centers and of much better quality of the reference sample, since the PL mechanism in the sample with single crystallites is damped by the grain boundary material. In all samples no NV^- center were detected.

A comparison of the PL and the Raman results (Fig. 95) shows that the main difference between the reference sample with an intensive PL signal from the NV centers and the others is the level of amorphous carbon in the grain boundaries. Probably these imperfections and their electronic levels interact with the electronic structure of the diamond nanocrystallites and damp the PL mechanism.

The amorphous phase with condensed sp^2-carbon rings will have a low band gap and its electronic levels could serve as some "escape levels" for the electrons excited to the levels of the NV centers: instead of radiative recombination they will fall back to their initial state by some non-radiative processes. Furthermore, an additional effect of such a process can be expected.

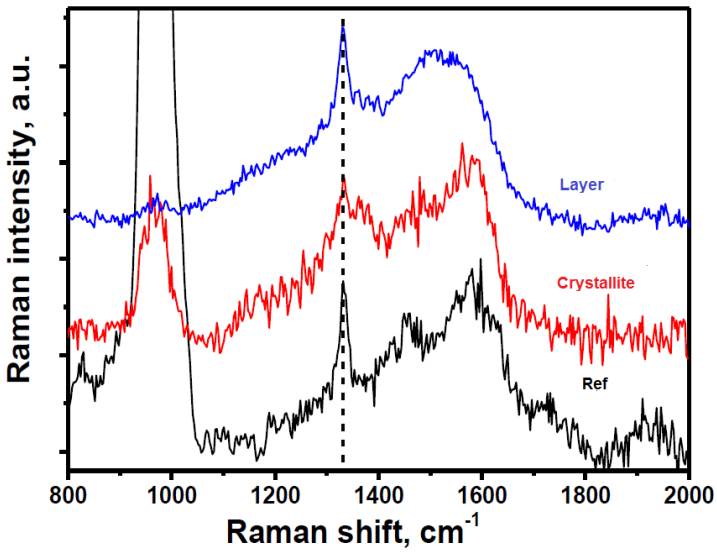

Fig. 95: Raman spectra from a reference sample, single crystallites and NCD layer

As reported in the literature [131], chemical control of the charge state of nitrogen-vacancy centers in diamond can be achieved by tailoring the surface termination. The samples under investigation in this work were prepared by chemical vapor deposition and are hydrogen-terminated. Simulations of the electronic band structure reveal band bending for the H-terminated diamond surface, inducing a p-type conductive surface layer due to the two-dimensional hole gas formed, leading to a depletion of electrons in the nitrogen-vacancies close to the surface favoring formation of predominantly NV^0 centers.

To overcome these problems the samples must be subjected after deposition to chemical cleaning and surface modification with, e.g. Piranha solution (H_2O_2:H_2SO_4) at elevated temperatures followed by O_2 microwave plasma treatment at 100 W input power and 0.7 mbar working pressure. As a result a replacement of the original hydrogen termination by an oxygen one is expected which should enhance the formation of negatively charged NV centers. After the cleaning procedure the samples were investigated with a confocal microscope described above. The room-temperature spectra revealed the presence of NV^- centers (zero-phonon line (ZPL) at 637 nm), together with NV^0 (ZPL at 575 nm) as well as SiV centers (ZPL at 737 nm), the latter most probably due to incorporation of Si atoms (stemming from the substrate) into the diamond lattice during the deposition (Fig. 96). In some of the PL spectra a dispersion of the peak position of the color centers was observed which

can be attributed to the shift of the characteristic zero-phonon lines in diamond nanocrystallites owing to their small size [132].

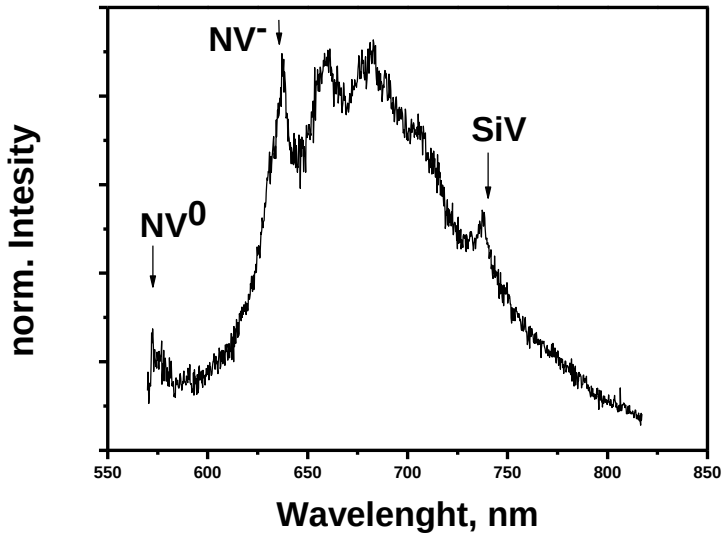

Fig. 96: PL spectrum from a sample with single crystallites after chemical cleaning and plasma treatment

After analyzing more than 35 PL spectra, statistics of the optical defects detected in the diamond single crystallites was performed (Fig. 97). The most defects are silicon vacancy centers (in 24 samples), followed by the neutral NV centers (in 21 samples). Not so presented are the NV^- centers (10) and surprisingly in some spectra peaks corresponding to nickel-nitrogen (NE8) defect centers at 797 nm [133] can be found. A small amount of nickel, stemming most probably from the nickel-chromium thermocouple is incorporated into the diamond lattice and combined with the substitutional nitrogen atom.

Several crystallites exhibiting strong fluorescence were further analyzed to establish the number of the color centers present in them. The antibunching from the crystallites measured showed $g^{(2)}$ =0.5 at τ = 0, indicating the presence of two or more color centers in each crystallite. The statistical distribution of the NV centers in crystallites with different sizes has been previously investigated; it was shown that the number of emitters per nanocrystallite increases with the crystal size and is higher than 1 for crystallites larger than 70 nm [118].

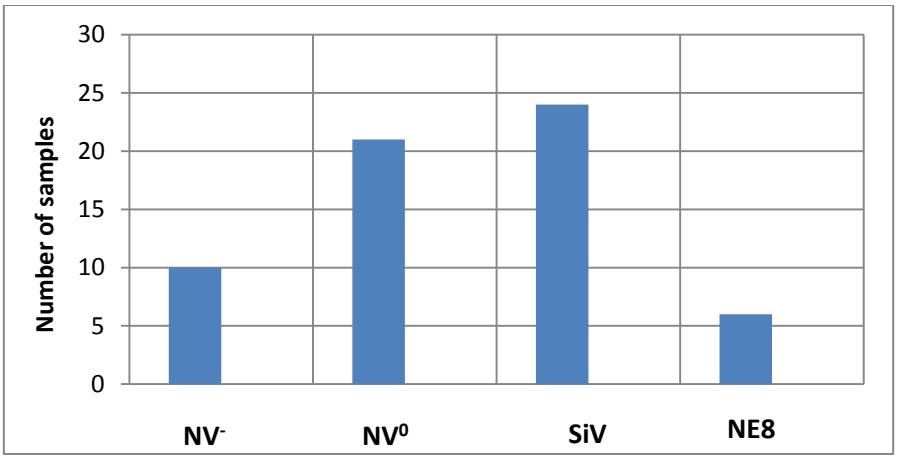

Fig. 97: Statistic of the color defects, presented in the diamond single crystallites

10.2. Investigations of NCD pillars

Finite-difference time-domain (FDTD) simulations have demonstrated that the coupling efficiency between a NV center and the waveguide mode of a diamond nanowire with a diameter of 200 nm is higher than 0.85 (if the polarization is perpendicular to the nanowire axis) [106].

In the current work nanocrystalline diamond pillars were fabricated, cleaned and treated with O_2 plasma in order to obtain NV^- centers instead of NV^0, as described in the previous chapters. Fluorescence mapping and photoluminescence spectroscopy have been used to characterize the optical properties of the created structures with different diameters - from 1 μm down to 50 nm.

10.2.1. Fluorescence mapping of NCD pillars

In a first step to characterize the optical properties of the NCD nanopillars they have been investigated by fluorescence mapping. Fig. 98 shows a map of an array of 10x10 pillars with a diameter of 1 μm.

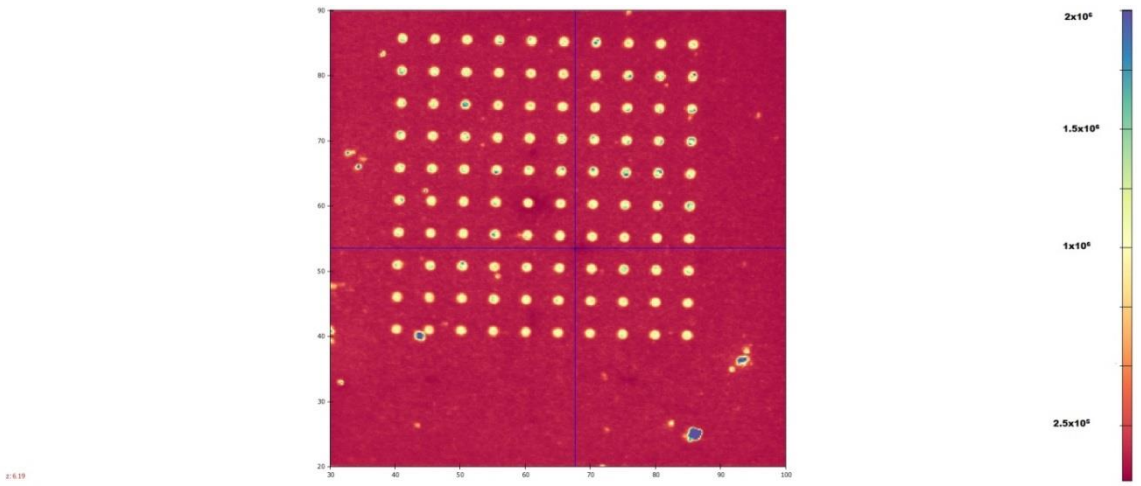

Fig. 98: Fluorescence mapping of an array of 1 μm NCD pillars

The fluorescence images of the arrays revealed bright spots that corresponded to the nanopillars (Fig. 98). The photon intensity of the brightest spots ($2.5x10^6$ counts per second at a pumping power of 1.7 mW) was about one order of magnitude higher than that of a bulk NCD film left unstructured as a marker. Investigating the fluorescence from the arrays with smaller diameters (Fig. 99) the photon intensity of the brightest spots from the NCD pillars increased with increasing the pumping power from 75 μW to 1.7 mW reaching $3.5x10^6$ cps for pillars with a diameter of 200 nm. The overall intensity was slightly lower for larger (1000 or 500 nm) or smaller (100 or 50 nm) diameters, which corresponds to the literature data, cited above.

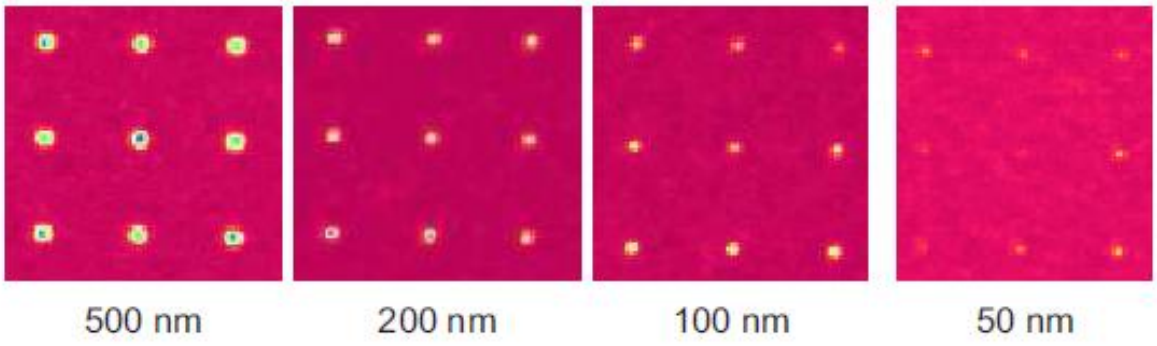

Fig. 99: Cut-offs of fluorescence maps of arrays of NCD nanopillars with different diameters

10.2.2. PL measurements of NCD pillars

Room-temperature PL spectra were taken from selected NCD pillars. Most of them

showed evidence for existence of NV centers, a typical spectrum is shown in Fig. 100.

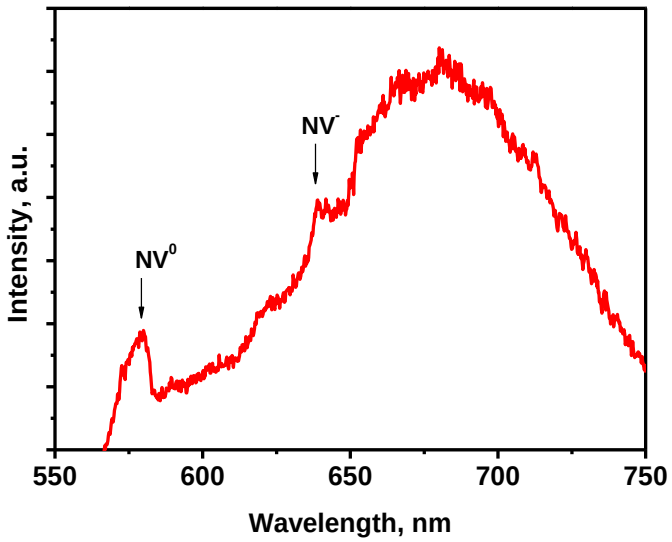

Fig. 100: PL spectrum from a single NCD pillar

The figure shows the typical peak for NV^0 center (ZPL) at 575 nm and for NV^- center at 637 nm. In order to check the homogeneity of the optical properties of the pillars, photoluminescence spectra have been taken from several pillars (1 *μ*m diameter) from a single array. The results are presented in Fig. 101.

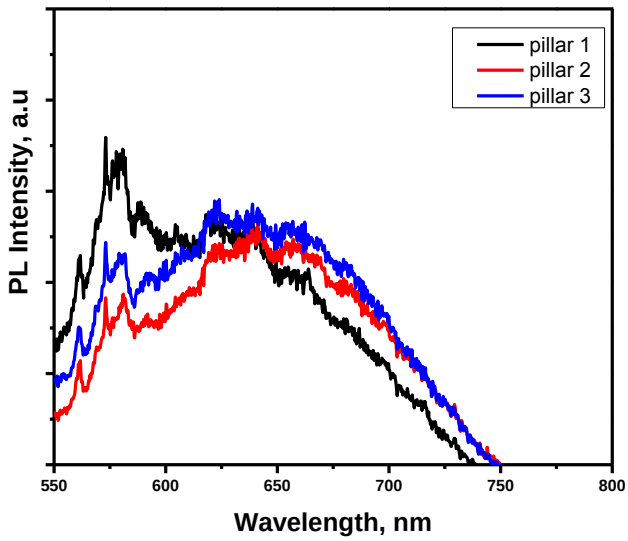

Fig. 101: PL spectra from three different NCD pillars (1 μm diameter) from one and the same array

It can be seen from the figure that all three spectra are quite similar thus proving the homogeneity of the optical properties of the pillars.

The second-order autocorrelation function $g^{(2)}(t)$ was measured (Fig. 102) using two avalanche photodiodes in a Hanbury-Brown - Twiss configuration. It was estimated to have a value of 0.9, which indicates the presence of more than one emitter (most probably between 8 and 10 emitters in a pillar).

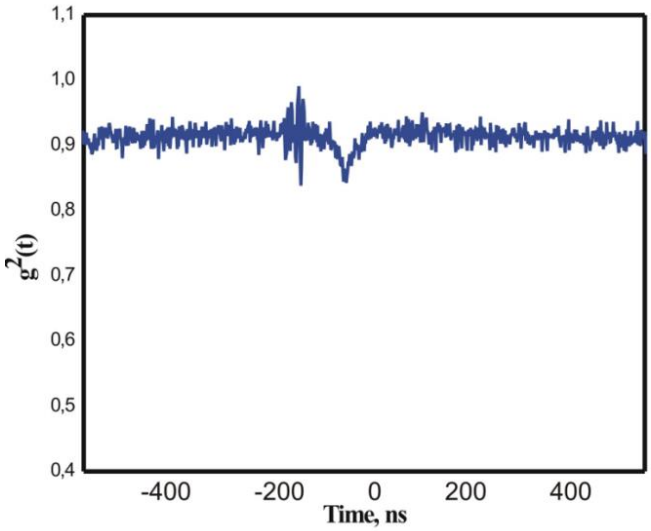

Fig. 102: Second-order autocorrelation function for NCD pillar

10.3. Investigation of UNCD pillars

Using the same etching procedure pillars from ultrananocrystalline diamond layers have been etched and optically characterized.

10.3.1. Fluorescence mapping of UNCD pillars

Fig. 103 shows a fluorescence map of an array of 10x10 UNCD nanopillars (d = 1 µm). But in contrast to the fluorescence map of the NCD pillars, only 55 out of 100 pillars show the expected bright spot in the map. The main reason is the destruction

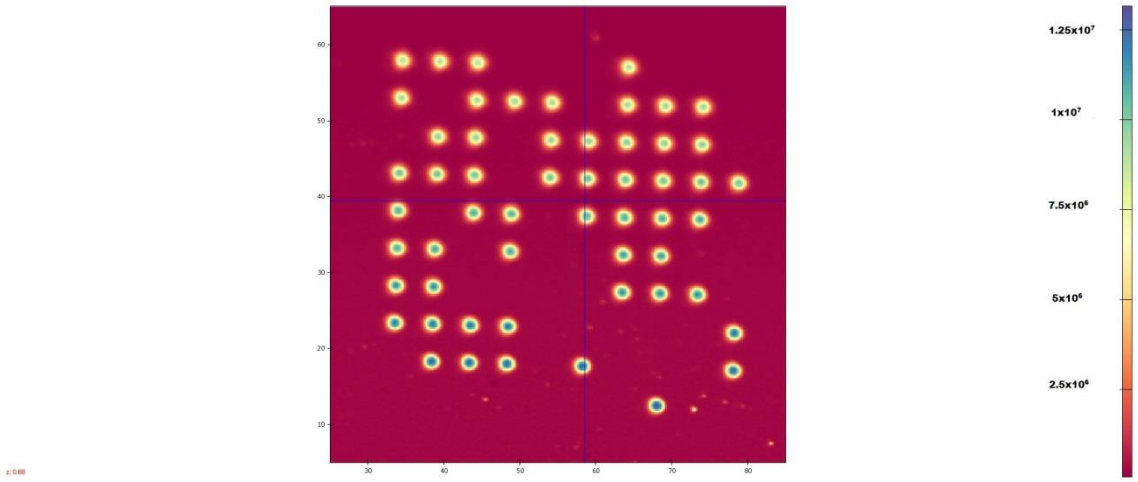

Fig. 103: Fluorescence mapping of an array UNCD pillars with diameter of 1 μm

of some pillars during treatment with oxygen plasma. However the photon intensity is even higher (around $1.25x10^7$ cps) compared to the NCD pillars, using the same pumping power. Also in the cut-outs of pillars with different diameters shown in Fig. 104 same pillars are missing.

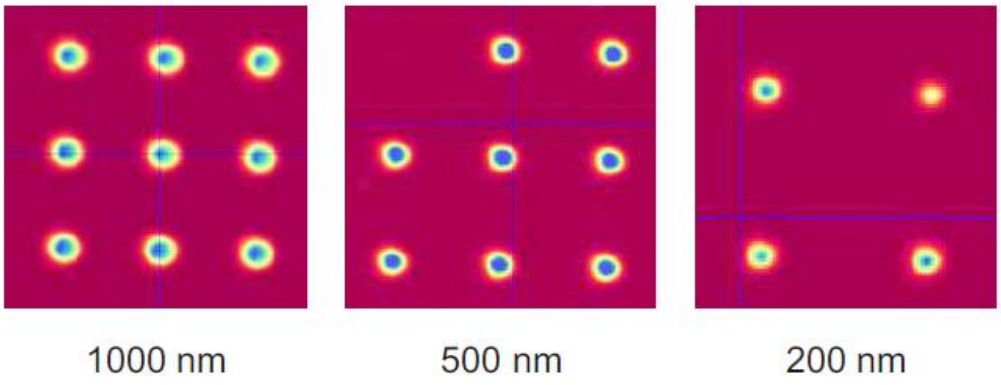

Fig. 104: Cut-offs of fluorescence maps of arrays of UNCD nanopillars with different diameters

10.3.2. PL measurements of UNCD pillars

The photoluminescence spectrum from a UNCD pillar is presented in Fig. 105. Unlike the PL spectrum of NCD pillar only the peak for NV^0 center is clear visible. The high amount of NV^0 especially in the UNCD samples could be explained by the increased

ratio of surface to volume atoms in such small crystallites that leads to a relatively high content of "active" surface electron traps per NV, like in the case of nanodiamonds, but also in our single diamond nanocrystallites (see above) [134]. But also in this case the presence of NV^0 centers can be assumed.

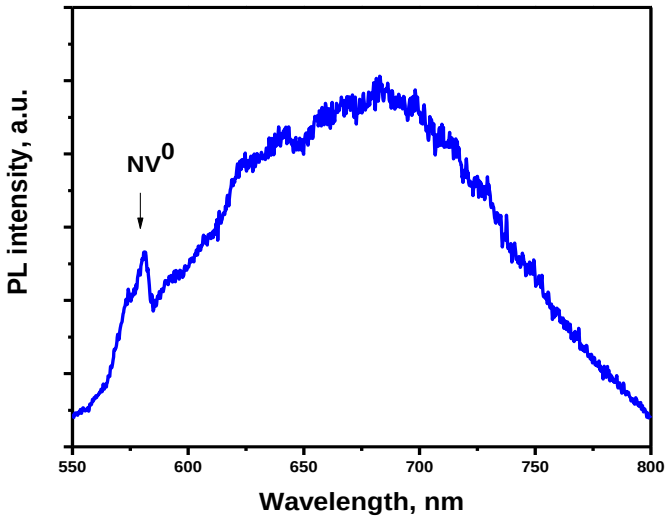

Fig. 105: PL spectra from UNCD pillar

11. CONCLUSIONS

In the present work the deposition of diamond by two techniques was demonstrated: hot-filament CVD for nanocrystalline diamond films and single diamond nanocrystallites and microwave plasma assisted CVD for ultrananocrystalline diamond layers. The obtained samples were thoroughly characterized with respect to their morphology, topology, structure and crystallinity by a number of techniques, like scanning electron microscopy, atomic force microscopy, Raman spectroscopy, X-ray photoelectron spectroscopy, etc. The NCD films are built up of diamond crystallites with a diameter up to few hundred nanometers grown from the substrate surface upwords, while the UCND films are composed on diamond nanocrystallites with a size up to 10 nm embedded in an amorphous carbon matrix with a fraction ration of both phases closed to unity.

The dependence of the properties of NCD and UNCD films on the substrate temperature was investigated. This task addressed the possibility to deposit diamond films on temperature sensitive substrates (such as low melting metals, microelectronic devices, III/V semiconductors, etc.). The quality of the NCD films suffered drastically changes lowering the substrate temperature from 900 ^{o}C down to 500 ^{o}C, while the quality of the UNCD layers did not change decreasing the temperature from 770 ^{o}C to 500 ^{o}C. From this investigation it can be concluded that for low temperature deposition the UNCD layers are a superior choice as their properties do not degrade to the same extent as those of NCD films. In order to obtain high quality NCD films the required substrate temperature should be in the range of 850 - 900 ^{o}C.

For the fabrication of diamond nanopillars electron beam lithography (EBL) followed by inductively coupled plasma reactive ion etching (ICP-RIE) with oxygen were implemented. Initially the etching conditions for diamond films were investigated and optimized by varying in broad ranges of the major process parameters, like RF power, ICP power, pressure, O_2 flow, etc. After establishing the optimized etching recipe, the etch mechanisms of NCD and UNCD films were investigated and compared. The differences observed were due to the different natures of the films, namely the grain size, the boundary material fraction, etc. In a following step,

diamond nanopillars with diameters between 1 μm and 50 nm were fabricated from both types of diamond films using two different hard masks: SiO_2 and gold. The application of Au as a hard mask showed several advantages with respect to the quality of the structured nanopillars.

Single diamond crystallites and nanopillars etched from NCD and UNCD films were optically investigated for the presence of nitrogen-vacancy (NV) centers embedded in them during the growth relying on the background nitrogen pressure in the chamber. Florescence mapping and photoluminescence measurements revealed the presence of NV centers in both types of pillars. There are, however, distinct differences between the NCD and the UNCD pillars. While the former contain the desired NV^- centers, the UNCD pillars contain only NV^0 centers. These results clearly demonstrate the possibility for fabrication of diamond nanostructures with NV centers embedded during the growth which can be candidates for applications in QIT.

REFERENCE

[1] J. Chung, J. Lin, Diamond Nanotechnology: Synthesis and Application, *Pan Stanford publishing Pte*. Ltd., 2010

[2] E. Frieden, The Chemical Elements of Life, *Scientific American*, p. 52, 1972

[3] R. Beckman, Abscheidung von Diamant aus der Gasphase, *PhD Thesis*, Kassel University, 1994

[4] F. Cotton, J. Wilkinson, Advanced Inorganic Chemistry, *Wiley*, 2007

[5] M. Latto, The Electrochemistry of Diamond, *PhD-Thesis*, University of Bristol, 2001

[6] H. Kroto, J. Heath, S. O'Brien, R. Smalley, C60: Buckminsterfullerene, *Nature*, vol. **318**, p. 162, 1985

[7] H. Latscha, H. Klein, Anorganische Chemie, *Springer*, 2007

[8] S. Mitura , K. Mitura , P. Niedzielski , P. Louda , V. Danilenko, Nanocrystalline diamond, its synthesis, properties and applications, *Journal of Achievements in Materials and Manufacturing Engineering*, vol. **16**, p. 9, 2006

[9] M. Dipalo, Nanocrystalline Diamond Growth and Device Applications, *PhD Thesis*, University of Ulm , 2008

[10] J. Angus, Y. Wang, M. Sunkara, Metastable growth of diamond and diamond-like phases, *Annual Reviews Material Science, vol.* **21**, p. 221, 1991

[11] J. Field, C. Freeman, Strength and fracture properties of diamond, *Philosophical Magazine A* , vol. **43**, p. 595, 1981

[12] R. Telling, C. Pickard, M. Payne, J. Field, Theoretical Strength and Cleavage of Diamond, *Physical Review Letters*, vol. **84**, p. 5160, 2000

[13] P. Bachmann, R. Messier, Emerging technology of diamond thin films, *Chemical and Engineering news*, vol. **15**, p.24, 1989

[14] A. Krüger, Neue Kohlenstoffmaterialien, *Teubner* , 2007

[15] A. Malave, Sensoren für Rastersondenmikroskopie auf Basis von polykristallinem Diamant, *PhD thesis*, Kassel University, 2004

[16] J. Olson, R. Pohl, J. Vandersande, A. Zoltan, T. Anthony, W. Bahnolzer, Thermal conductivity of diamond between 170 and 1200 K and isotope effect, *Physical Review B*, vol. **47**, p. 14850, 1993

[17] E. Wörner, C. Wild, W. Müller-Sebert, R. Locher, P. Koidl, Thermal conductivity of CVD diamond films: high-precision, temperature-resolved measurements, *Diamond and Related Mater*ials, vol. **5,** p.688, 1996

[18] P. May, Diamond thin films: a 21st-century material, *Philosophical Transactions of The Royal Society of London Series A - Mathematical Physical and Engineering Sciences*, vol. **358**, p. 473, 2000

[19] M. Seal, High technology applications of diamond in The properties of natural and synthetic diamond, edited by J. Fields, *Academic Press*, London, 1992

[20] J. Chelikowsky, S. Louie, First-principles linear combination of atomic orbitals method for the cohesive and structural properties of solids: Application to diamond, *Physical Review* B, Vol. **29**, p. 3470, 1984

[21] M. Gabrysch, Electronic properties of diamond, *PhD-Thesis*, University of Uppsala, 2008

[22] P. Chalker, C. Johnston, Thin film diamond sensor technology, *physica status solidi A-Applied Research*, vol. **154**, p. 455, 1996

[23] W. Wang, N. Fox, J. Steeds, S. Lin, J. Butler, Negative electron affinity observed in boron-doped p-type diamond films by scanning field emission spectroscopy, *Journal of Applied Physics*, vol. **80**, p. 6809, 1996

[24] C. Wang, A solid-state single photon source based on color centers in diamond, *PhD-thesis*, Ludwig-Maximilian University München, 2008

[25] the CVD diamond booklet, available at www.diamond-materials.com/download

[26] A. Kosevich, The Crystal Lattice: Phonons, Solitons, Dislocations, Superlattices, *WILEY-VCH Verlag GmbH & Co*., 2005

[27] M. Razeghi, Fundamentals of Solid State Engineering, *Springer Science + Business Media*, 2009

[28] W. Borhardr-Ott, Kristallographie: Eine Einführung für Naturwisenschaftler, *Springer*, 2009

[29] J. Morris Jr., Materials Science, Lecture notes, *Berkeley*

[30] W. Callister, "Fundamentals of Materials Science and Engineering," *John Wiley & Sons, Inc. Danvers*, 2005

[31] R. Robertson, J. Fox, A. Martin, Two types of diamond, Philosophical Transactions of the Royal Society A, vol. **232**, p. 463, 1934

[32] A. Zaitsev, Optical properties of diamond: a data handbook, *Springer*, 2001

[33]D. Steinmelz, Ni/Si-basierte Farbzentren in Diamant als Einzelphotonenquellen, *PhD thesis*, Saarbrücken, 2001

[34] A. Zaitsev, Vibronic spectra of impurity-related optical centers in diamond, *Physical Review B*, Vol. **61**, p. 12909, 2000

[35] F. Neugart, A. Zappe, F. Jelezko , C. Tietz ,J. Boudou, A. Krueger, J. Wrachtrup, Dynamics of Diamond Nanoparticles in Solution and Cells, *Nano Letters*, vol. **7**, p. 3588, 2007

[36] M. Doherty, N. Manson, P. Delaney, F. Jelezko, J. Wrachtrup , L. Hollenberg, The nitrogen-vacancy colour centre in diamond, *Materials Science* 2013, arXiv:1302.3288v1 [cond-mat.mtrl-sci] 14 Feb 2013

[37] F. Jelezko and J. Wrachtrup, Single defect centres in diamond: A review, *physica status solidi (a), vol.* **203**, p. 3207,2006

[38] G. Davies, Dynamic Jahn-Teller distortions at trigonal optical centres in diamond, *Journal of Physics C: Solid State Physics, vol.* **12** , p. 2551, 2007

[39] A. Gruber, A. Drabenstedt, C. Tietz, L. Fleury, J. Wrachtrup, C. von Borczyskowski, Scanning Confocal Optical Microscopy and Magnetic Resonance on Single Defect Centers, *Science*, vol. **276**, p. 2012, 1997

[40] C. Kurtsiefer, S. Mayer, P. Zarda, H. Weinfurter, Stable Solid-State Source of Single Photons, *Physical Review Letters*, vol. **85**, p. 290, 2000

[41] G. Balasubramanian, P. Neumann, D. Twitchen, M. Markham, R. Kolesov, N. Mizuochi, J. Isoya, J. Achard, J. Beck, J. Tissler, V. Jacques, P. Hemmer, F. Jelezko, J. Wrachtrup, Ultralong spin coherence time in isotopically engineered diamond, *Nature Materials,* vol. **8**, p. 383, 2009

[42] A. Gali, M. Fyta, E. Kaxiras, Ab initio supercell calculations on nitrogen-vacancy center in diamond: Electronic structure and hyperfine tensors. *Physical Review* B, vol. **77**, p. 155206, 2008

[43] J. Weber, W. Koehl, J. Varley, A. Janotti, B. Buckley, C. Van de Walle, an D.Awschalom, Quantum computing with defects, *Proceedings or the National Academy of Science*, vol. **107**, p. 8513, 2010

[44] F. Jelezko, P. Neumann, F. Remp, W. Schnitzler, K. Singer, F. Schmidt-Kaler, J. Wrachtrup, Ein Quantencomputer in Diamant, *Physkilisches Heft*, Ausgabe **5**, 2008

[45] F. Jelezko, Defekte mit Effekt, *Physik Journal* **7**, p.9, 2008

[46] C. Kurtsiefer, S. Mayer, P. Zarda, H. Weinfurter. Stable solid-state source of single photons, *Physical Review Letters*, vol. **85**, pp. 290, 2000

[47] J. Meijer, B. Burchard, M. Domhan, C. Wittmann, T. Gaebel, I. Popa, F. Jelezko, J. Wrachtrup, Generation of single color centers by focused nitrogen implantation, *Applied Physics Letters,* vol. **87**, p. 261909, 2005

[48] S. Pezzagna, B. Naydenov, F. Jelezko, J. Wrachtrup, J. Meijer, Creation efficiency of nitrogen-vacancy centres in diamond, *New Journal of Physics,* vol. **12**, p. 065017, 2010

[49] J. Boudou, P. Curmi, F. Jelezko, J. Wrachtrup, P. Aubert, M. Sennour, G. Balasubramanian, R. Reuter, A.Thorel, E. Gaffet, High yield fabrication of fluorescent nanodiamonds, *Nanotechnology*, vol. **20**, p. 235602, 2009

[50] J. Goss, R. Jones, S. Breuer, P. Briddon, S. Öberg, The Twelve-Line 1.682 eV Luminescence Center in Diamond and the Vacancy-Silicon Complex, *Physical Review Letters,* vol. **77,** p. 3041, 1996

[51] V. Vavilov, A. Gippius, A. Zaitsev, B. Derjaguin, B. Spitsyn,A. Aleksenko, –nIvestigation of the cathodoluminescence of epitaxial diamond films," Soviet Physics Semiconductors, vol. **14**, p. 1078, 1981

[52] I. Aharonovich, S. Castelletto, D. Simpson, C. Su, A. Greentree, S. Prawer, Diamond-based single-photon emitters, *Reports on Progress in Phys*ics, vol. **74**, p. 076501, 2011

[53] E. Neu, M. Fischer, S. Gsell, M. Schreck, C. Becher, Fluorescence and polarization spectroscopy of single silicon vacancy centers in heteroepitaxial nanodiamonds on iridium, *Physical Reviews B,* vol. **84**, p. 205211, 2011

[54] C. Wang, A Solid-State Single Photon Source Based on Color Centers in Diamond, *PhD thesis*, Ludwig-Maximilians-Universität München, 2007

[55] E. Neu, D. Steinmetz, J. Riedrich-Möller, S.Gsell, M. Fischer, M. Schreck, C. Becher, Single photon emission from silicon-vacancy colour centres in chemical vapour deposition nano-diamonds on iridium, *New Journal of Physics,* vol. **13**, p. 025012, 2011

[56] S. Pezzagna, D. Rogalla, D. Wildanger, J. Meijer, A. Zaitsev, Creation and nature of optical centres in diamond or single-photon emission—overview and critical remarks, *New Journal of Physics,* vol. **13**, p. 035024, 2011

[57] G. Blakey, The Diamond, *Paddington Press*, 1977

[58] F.Bundy, H. Hall, H. Strong, R. Wentorf, Man-made diamonds, *Nature*, vol. **176**, p. 51, 1977

[59] H. Spear, J. Dimushes, Synthetic diamond, *John Wiley & Son Inc*., 1994

[60] F. Bundy, Pressure vs. temperature phase and reaction diagram for elemental carbon, *Journal of Geophysical Research,* vol. **85**, p. 6930, 1980

[61] B. Spitsyn, B. Deryagin, USSR patent 339.134, 1956

[62] M. Prelas, G. Popovici, L. Begelow, Handbook of industrial diamonds and diamond films, *New York:Macel Dekker*, 1997

[63] M. Kamo, Y. Sato, S. Matsumoto, N. Setaka: Vapor Deposition of Diamond Particles from Methane, *Journal of Crystalline Growth,* vol. 62, p. 642, 1983

[64] R. Balmer, J. Brandon, L. Clewes, H. Dhillon, J. Dodson, I Friel, P. Inglis, T. Madgwick, M. Markham, T. Mollart, N. Perkins, D. Twitchen, A. Whitehead, J. Wilman, S. Woollard Chemical vapor deposition synthetic diamond: materials, technology and application, *Journal of Physics: Condensed Matter*, vol. **21**, p. 364221, 2009

[65] J. Herlinger, sp3's experience using hot filament CVD reactors to grow diamond for an expanding set of applications, *thin solid films*, Vol. **501**, p.65, 2006

[66] E.Sevillano, Low pressure synthetic diamonds, *Springer group*, p. 11, 1998

[67] K. Suzuki, A. Sawabe, H. Yasuda, T. Inuzuka, Growth of diamond thin films by dc plasma chemical vapor deposition , *Applied Physics Letters,* vol. **50**, p. 728, 1987

[68] P. Bachmann, D. Leers, D. Wiechert, Diamond Chemical Vapour Deposition, *Journal de Physique*, vol. **1**, p. 907, 1991

[69] J. Gracio, Q. Fan, J. Madaleno, Diamond growth by chemical vapour deposition, *Journal of Physics D: Applied Physics*, vol. **43**, p. 374017, 2010

[70] J. Angus, Synthetic Diamond: Emerging CVD Science and Technology, *New York Wiley*, p. 21, 1994

[71] M. Kamo, Y. Sato, S. Matsumoto, J. Setaka, Diamond synthesis from gas phase in microwave plasma, Journal of *Crystalline Growth,* vol. **62**, p. 642, 1983

[72] P. Bachmann, H. Hagemann, H. Lade, D. Leers, D. Weichert, H. Wilson, Diamond, SiC and nitride wide band gap semiconductors, *Material Research Society Symposium Proceedings,* vol. **339**, p. 267, 1994

[73] S. Matsumoto, M. Hino, T. Kobayashi, Synthesis of diamond films in a rf induction thermal plasma, *Applied Physics Letters,* vol. **51**, p. 737, 1987

[74] K. Kurihara, K. Sasaki, M. Kawarada, N. Koshino, High rate synthesis of diamond by dc plasma jet chemical vapor deposition, *Applied Physics Letters,* vol. **52** p. 437, 1988

[75] P. Bachmann, W. van Enckevort, Diamond deposition technologies, *Diamond and Related Materials*, vol. **1**, p. 1021, 1992

[76] T. Anthony, Metastable synthesis of diamond, *Vacuum*, vol. **41**, p. 1356, 1990

[77] W. Yang, J. Je, Effects of secondary pretreatments of substrate on the nucleation of diamond film, *Journal of Materials Research*, vol. **11**, p. 1787, 1996

[78] S. Bozeman, R. Stoner, J. Glass, Handbook of industrial diamonds and diamond films, *Marcel Dekker, Inc.*, p. 901, 1998

[79] S. Iijima, Y. Aikawa, K. Baba, *Applied Physics Letters*, vol. **57**, p. 2646, 1990

[80] P. Ascarelli, S. Fontana, Dissimilar grit-size dependence of the diamond nucleation density on substrate surface pretreatments, *Applied Surface Science,* vol. 64, p. 307, 1993

[81] W. Kulish, B. Sobish, M. Kuhr, R. Beckmann, Characterization of the bias nucleation process, *Diamond and Related Materials*, vol. **4**, p. 401, 1995

[82] O. Wiliams, Nanocrystalline diamond, *Diamond and Related Materials*, vol. **20**, p. 640, 2011

[83] J. Butler, Chemical vapor deposited diamond: Maturity and diversity, *The electrochemical Society*, 2003

[84] O. Williams, M. Daenen, J. Haen, K. Haenen, J. Maes, V. Moshchalkov, M. Nesládek, D. Gruen, Comparison of the growth and properties of ultrananocrystalline diamondand nanocrystalline diamond, *Diamond and Related Materials*, vol. **15**, p. 654, 2006

[85] W. Kulisch, C. Popov, On the growth mechanism of nanocrystalline diamond films, *physica status Solidi (a)*, No. **2**, p. 203, 2006

[86] W. Kulisch, C. Popov, Ultrananocrystalline diamond/amorphous carbon nanocomposite films, *New research on nanocomposite*, p. 115, 2008

[87] S. Koizumi, C. Nebel, M. Nesladek, Physics and applications of CVD diamonds, *Wiley Verlag*, p. 17, 2008

[88] K. Early, M. Schattenburg, H. Smith, Absence of resolution degradation in X-ray lithography for λ from 4.5nm to 0.83nm, *Microelectronic Engineering,* Vol. **11**, p. 317, 1990

[89] R. Jaeger, *Introduction To Microelectronic Fabrication*, 2 ed., *Auburn, Upper Saddle River - Prentice Hall*, 2002

[90] K. Jackson, W. Schroter, Handbook of Semiconductor Technology, *WILEY-VCH Verlag GmbH*, 2000

[91] Q. Luo, N. D'Angelo, R. Merlino, Shock formation in negative ion plasma, *Physics of Plasmas*, vol. **5**, p. 201, 1998

[92] R. Ahmad, Diamond Nanostructured Devices For Chemical Sensing Applications, *PhD-thesis*, University of London, 2011

[93] V. Rachenko, T. Kononenko, S. Pimenov, , Optical monitoring of nucleation and growth of diamond films, *Diamond and Related Materials*, vol. **2,** p**.** 904, 1993

[94] G. Ding, H. Mao, Y. Cai , Y. Zhang, X. Yao, X. Zhao, Micromachining of CVD diamond by RIE for MEMS applications, *Diamond and Related Materials*, vol. **14**, p. 1543, 2005

[95] G. Sandhu, Reactive ion etching of diamond*, Applied Physics Letters,* vol. **55**, p. 437, 1989

[96] I. Bello, M. Fung, W. Zhang, et al., Effects at reactive ion etching of CVD diamond *Thin Solid Films,* vol. **36**, p. 222, 2000

[97] R. Otterbach, U. Hilleringmann, Reactive ion etching of CVD-diamond for piezoresistive pressure sensors, *Diamond and Related Materials,* vol. 11, p. 841, 2002

[98] Q. Yang, T. Hamilton, C. Xiao, A. Hirose, A. Moewes, Plasma-enhanced synthesis of diamond nanocone films, *Thin solid films,* vol. **494**, p. 110, 2006

[99] C. Li, A. Hatta, Nanowhiskers formation by radio frequency Ar/O_2 plasma etching of aluminum coated diamond films, *Thin solid films,* vol. **515**, p. 4172, 2007

[100] L. Childress, R. Hanson, Diamond NV centers for quantum computing and quantum networks, *Material Research Society bulletin,* vol. **38**, p. 134, 2013

[101] M. Stoikou, Etching of CVD diamond surface, *PhD thesis*, Heriot-Watt University, 2010

[102] C. Vivensang, G. Turban, E. Anger, A. Gicquel, Reactive ion etching of diamond and diamond-like carbon films, *Diamond and Related Materials*, vol. **3**, p. 645, 1994

[103] Y. Ando, Y. Nishibayashi, K. Kobashi, T. Hirao, K. Oura, Smooth and high-rate reactive ion etching of diamond, *Diamond and Related Materials,* vol. **11**, p. 824, 2002

[104] S. Ilias, S. Gene, P. Moeller, V. Stambouli, Planarization of diamond thin film surfaces by ion beam etching at grazing incidence angle, *Diamond and Related Materials*, vol. **5**, p. 835, 1996

[105] J. Riedrich-Möller, L. Kipfstuhl, C. Hepp, E. Neu, C. Pauly, F. Mücklich, A. Baur, M. Wandt, S. Wolff, M. Fischer, S. Gsell, M. Schreck, C. Becher, One- and two-dimensional photonic crystal micro-cavities in single crystal diamond, *Nature Nanotechnology,* vol. **7**,p. 69, 2012

[106] B. Hausmann ,, M. Khan, Y. Zhang, T. Babinec , K. Martinick , M. McCutcheon , P. Hemmer , M. Lončar, Fabrication of diamond nanowires for quantum information processing applications, *Diamond and Related Materials,* vol. **19**, pp. 621, 2010

[107] B. Hausmann, T. Babinec, J. Choy, J.Hodges, S. Hong, I. Bulu, A. Yacoby, M. Lukin, and M. Lončar, Single-color centers implanted in diamond nanostructures, *New Journal of Physics,* vol. **13**, p. 045004, 2011

[108] A. Faraon, P. Barclay, C. Santori, K. Fu, R. Beausoleil, Resonant enhancement of the zero-phonon emission from a color center in a diamond cavity, *Nature Photonics,* vol. **5**, p. 301, 2011

[109] X. Jiang, K. Schiffmann, C.-P. Klages, Nucleation and initial growth phase of diamond thin films on (100) silicon, *Physical Review* B, vol. **12**, p. 50, 1994

[110] J. Arnault, L. Demuynck, C. Speisser, F. Le Normand, Mechanism of CVD diamond nucleation and growth on mechanically scratched Si(100) surfaces, *Europian Physical Journal* B, p. 327, 1999

[111] K.Reichelt, Nucleation and growth of thin films, *Vacuum*, vol. **38**, p. 1083, 1988

[112] BORALECTRIC heating elements for vacuum applications, http:///www.tectra.de/e/Heater.htm#BORALECTRIC (01.04.2000)

[113] S. Okoli, R. Haubner, B. Lux, Carborization of tungsten and tantalum filaments during low-pressure diamond depositon, *Surface and Coatings Technology,* No. **47**, p. 585, 1991

[114] A. Ferrari, J. Robertson, Resonant Raman spectroscopy of disordered, amorphous, and diamond like carbon, *Physical Reviews B,* vol. **63**, p. 121405, 2001

[115] R. Nemanich, J. Glass, G. Lucovsky, R. Schroder, Raman scattering characterization of carbon bonding in diamond and diamondlike thin films, *Journal of Vacuum Science Technolology A,* vol. **6**, p. 1783, 1988

[116] X. Xiao, J. Birrell, J. Gerbi, O. Auciello, J. Carlisle, Low temperature growth of ultrananocrystalline diamond, *Journal of Applied Physics*, vol. **96**, p. 2232, 2004

[117] T.MacCauley, D.Gruen, A.Krauss,Temperature dependence of the growth rate for nanocrystalline diamond films deposited from an Ar/CH_4 microwave plasma, *Applied Physics Lett*ers, vol. **73**, p. 1646, 1998

[118] J. Rabeau, A. Stacey, A. Rabeau, S. Prawer, F. Jelezko, I. Mirza, J. Wrachtrup, Single nitrogen vacancy centers in chemical vapor deposited diamond nanocrystals, *Nano Letters*, vol. **7**, p. 3433, 2007

[119] W. Kulisch, C. Popov, H. Rauscher, M. Rinke, M. Veres, Investigation of the initial growth of ultrananocrystalline diamond films by multiwavelength Raman spectroscopy, *Diamond and Related Materials,* vol. **20**, p.1076, 2011

[120] J. Asmussen, D. Reinhard, Diamond films handbook, Marcel Dekker Inc., 2002

[121] A. van der Drift, Evolutionary selection, a principle governed growth orientation in vapor deposited layers, *Philips Research Reports,* vol. **22**, p. 267, 1967

[122] C. Wild, R. Kohl, N. Herres, W. Müller-Sebert, P. Koidl, Oriented CVD diamond films: twin formation, structure and morphology, *Diamond and Related Materials,* vol. **3**, p. 373, 1994

[123] H. Maeda,K. Ohtsubo, N. Ohya,K. Kusakabe, S.Morooka, Determination of diamond [111] and[100] growth rate and formation of highly oriented diamond films by microwave plasma-assisted chamical vapor deposition, *Journal of Materials Research*, vol. **10**, p. 3115, 1995

[124] S. Szunerits, R. Boukherroub, Different strategies for functionalization of diamond surfaces, *Journal of Solid State Electrochemistry* , vol.**12,** p. 1205, 2008

[125] C. Nebel, B. Rezek, D. Shin, H. Uetsuka, N. Yang, Diamond for bio-sensor applications, *Journal of Physics D: Applied Physics, vol.* **40,** p. 6443, 2007

[126] D. Gruen, Nanocrystalline diamond films, *Annual Review of Materials Science,* Vol. **29**, p. 211, 1999

[127] J. Miller, Amines and thiols on diamond surfaces, *Surface Science*, vol. **439**, p. 21, 1999

[128] C. Nebel, B. Rezek, D. Shin, H. Uetsuka, and N. Yang,Diamond for bio-sensor applications, *J. Phys. D* , Vol.**40**, p. 6443, 2007

[129] J. Enlund, J. Isberg, M. Karlsson, F. Nikolajeff, J. Olson, D. Twitchen, Anisotropic dry etching of boron doped single crystal CVD diamond, *Carbon*, vol. **43**, p. 1839, 2005

[130] H. Choi, E. Gu, C. Liu, C. Griffin, J. Girkin, I. Watson, M. Dawson, Fabrication of natural diamond microlenses by plasma etching, *Journal of Vacuum Science Technology B, vol.* **23**, p. 130, 2005

[131] M. Hauf, B. Grotz, B. Naydenov, M. Dankerl, S. Pezzagna, J. Meijer, F. Jelezko, J. Wrachtrup, M. Stutzmann, F. Reinhard, J. Garrido, Chemical control of the charge state of nitrogen-vacancy centers in diamond, *Physical Reviews* B, vol. **83**, p. 081304(R), 2011

[132] Y. Shen, T. Sweeney, H. Wang, Zero-phonon linewidth of single nitrogen vacancy centers in diamond nanocrystals, *Physical Reviews* B, vol. **77**, p. 033201, 2008

[133] J. Rabeau, Y. Chin, S. Prawer, F. Jelezko, T. Gaebel, J. Wrachtrup , Fabrication of single nickel-nitrogen defects in diamond by chemical vapor deposition, *Applied Physics Letters*, vol. **86**, p. 131926, 2005

[134] L. Rondin, G. Dantelle, A. Slablab, F. Grosshans, F. Treussart, P. Bergonzo, S. Perruchas, T. Gacoin, M. Chaigneau, H.-C. Chang, V. Jacques, J.-V. Roch, Surface-induced charge state conversion of nitrogen-vacancy defects in nanodiamonds , *Physical Reviews* B*, vol.* **82**, p. 115449, 2010

PUBLICATIONS OF THE AUTHOR

1. W. Kulisch, C. Petkov, **E. Petkov**, C. Popov, P. N. Gibson, M. Veres, R. Merz, B. Merz, J. P. Reithmaier, Low temperature growth of nanocrystalline and ultrananocrystalline diamond films: A comparison, *physica status solidi (a),* vol. **209**, p.1664, 2012
2. **E. Petkov**, C. Popov, T. Rendler, C. Petkov, F. Schnabel, H. Fedder, S.-Y. Lee, W. Kulisch, J.P. Reithmaier, J. Wrachtrup, Investigation of NV centers in diamond nanocrystallites and nanopillars, *physica status solidi (b)* **250**, p. 48, 2013 – *featured on the journal cover and selected for special edition*
3. J. Evtimova, W. Kulisch, C. Petkov, **E. Petkov**, F. Schnabel, J.P. Reithmaier, C. Popov, Reactive ion etching of nanocrystalline diamond for the fabrication of one-dimensional nanopillars, *Diamond and Related Materials,* vol. **36**, p. 58, 2013
4. **E. Petkov**, T. Rendler, C. Petkov, F. Schnabel, J.P. Reithmaier, J. Wrachtrup, C. Popov, W. Kulisch,, Investigation of NV centers in Nano- and Ultrananocrystalline Diamond Pillars, *physica status solidi (a),* vol. **210**, p. 2066, 2013
5. C.Popov, **E.Petkov**, C.Petkov, F.Schnabel, J.P. Reithmaier, B.Naydenov, F.Jelezko, Quantum Information technolofy based on diamond: A step toward secure information transfer, Nanoscience Advances in CBRN Agents Detection, Information and Energy Security, edited by P.Petkov, D.Tsuilyanu, W.Kulish, C.Popov, *Springer*, 2014- submitted

SELBSTÄNDIGKEITSERKLÄRUNG

Hiermit versichere ich, dass ich die vorliegende Dissertation selbständig und ohne unerlaubte Hilfe angefertigt und andere als die in der Dissertation angegebene Hilfsmittel nicht benutzt habe. Alle Stellen, die wörtlich oder sinngemäß aus veröffentlichen oder unveröffentlichen Schriften entnommen sind, habe ich als solche kenntlich gemacht. Kein Teil dieser Arbeit ist in einem anderen Promotions- oder Habilitationsverfahren verwendet worden.

Kassel, 9.10.2014 ……

Emil Petkov

ACKNOWLEDGEMENTS

First of all I would like to thank Dr. Cyril Popov for the opportunity to work under his guidance and supervision, assisting with all kind of support, inspiration expertise and fruitful advice and discussion which they proffered throughout this investigation and preparation of the thesis.

I would like to thank Prof. Dr. Johann Peter Reithmaier for allowing me to work at the Institute of Nanostructure Technologies and Analytics.

Furthermore, I express great thanks to Dr. Wilhelm Kulisch for sharing his extraordinary theoretical knowledge and providing some excellent ideas relating to the improvement of the practical work.

I want to thank Dr. Miklos Veres, Hungarian Academy of Sciences for the Raman measurements, Dr. Neil Gibson**,** JRS, Ispra, Italy, for the XRD measurements, Dr. Rolf Merz IFOS, University of Kaiserslautern, Germany for the XPS measurements and Thorsten Rendler, University of Stuttgart for the optical measurements.

I am very greatful to our technicians, Miss Kerstin Fuchs and especially Mister Florian Schnabel for all their support for the etching of the diamond structures and preparing of pre-patterned substrates for site-controlled deposition.

All member of the Institute - I would like to thank for the great and friendly athmosphere.

Last but not least, I would like to thank my family for their support and love.